AD-A186 141 CHEMICAL REACTIONS IN TURBULENT MIXING FLOWS(U) 1/2
CALIFORNIA INST OF TECH PASADENA GRADUATE AERONAUTICAL
LABS P E DIMOTAKIS ET AL. 01 JUN 87 AFOSR-TR-87-1160
UNCLASSIFIED $AFOSR-83-0213 F/G 20/4 NL

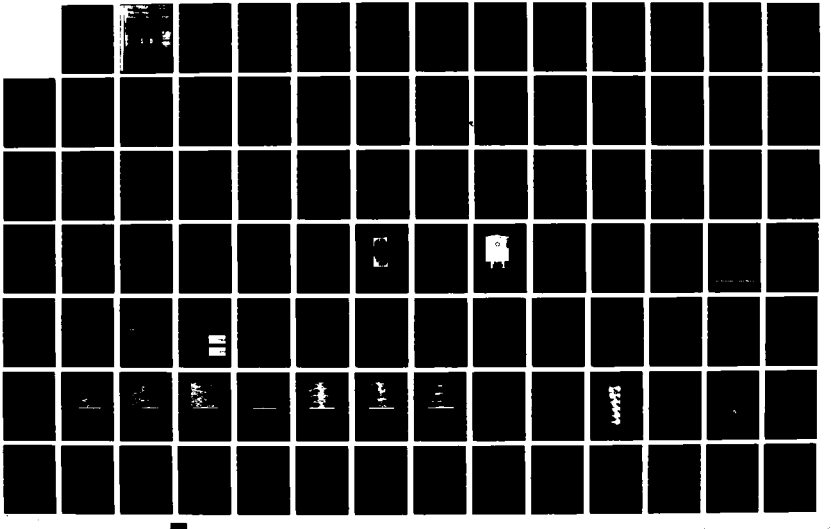

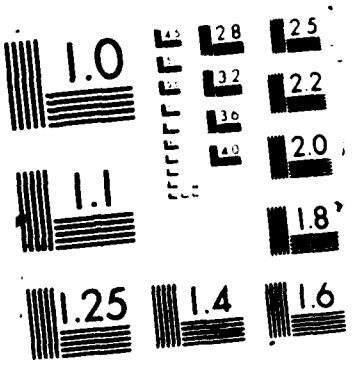
1.0
1.1
1.25
1.4
1.6
2.8
3.2
3.6
2.5
2.2
2.0
1.8

GRADUATE AERONAUTICAL LABORATORIES
CALIFORNIA INSTITUTE OF TECHNOLOGY

AFOSR-83-0213 Annual Report
for the Period Ending 15-Apr-87

CHEMICAL REACTIONS IN TURBULENT MIXING FLOWS

P. E. DIMOTAKIS, Professor, Aeronautics & Applied Physics

J. E. BROADWELL, Senior Scientist, Aeronautics

A. LEONARD, Professor, Aeronautics

Firestone Flight Sciences Laboratory

Guggenheim Aeronautical Laboratory

Karman Laboratory of Fluid Mechanics and Jet Propulsion

Pasadena

Unclassified

SECURITY CLASSIFICATION OF THIS PAGE

AD-A186 141

REPORT DOCUMENTATION PAGE

1a. REPORT SECURITY CLASSIFICATION: Unclassified	1b. RESTRICTIVE MARKINGS: None
2a. SECURITY CLASSIFICATION AUTHORITY	3. DISTRIBUTION/AVAILABILITY OF REPORT: Distribution unlimited; approved for public release
2b. DECLASSIFICATION/DOWNGRADING SCHEDULE	
4. PERFORMING ORGANIZATION REPORT NUMBER(S)	5. MONITORING ORGANIZATION REPORT NUMBER(S): AFOSR-TR- 87-1160
6a. NAME OF PERFORMING ORGANIZATION: California Institute of Technology; 6b. OFFICE SYMBOL (If applicable)	7a. NAME OF MONITORING ORGANIZATION: Air Force Office of Scientific Research
6c. ADDRESS (City, State and ZIP Code): Pasadena, CA 91125	7b. ADDRESS (City, State and ZIP Code): Bolling AFB, DC 20332-6448
8a. NAME OF FUNDING/SPONSORING ORGANIZATION: Air Force Office of Sci. Res.; 8b. OFFICE SYMBOL (If applicable): AFOSR/NA	9. PROCUREMENT INSTRUMENT IDENTIFICATION NUMBER: AFOSR-83-0213
8c. ADDRESS (City, State and ZIP Code): Bolling AFB, DC 20332-6448	10. SOURCE OF FUNDING NOS.

PROGRAM ELEMENT NO.	PROJECT NO.	TASK NO.	WORK UNIT NO.
61102F	2308	A2	

11. TITLE (Include Security Classification) (unclassified)
Chemical Reactions in Turbulent Mixing Flows

12. PERSONAL AUTHOR(S)
P. E. Dimotakis, J. E. Broadwell, A. Leonard

13a. TYPE OF REPORT	13b. TIME COVERED	14. DATE OF REPORT (Yr., Mo., Day)	15. PAGE COUNT
Annual Report	FROM Apr '86 TO Apr '87	1 June 1987	111

16. SUPPLEMENTARY NOTATION

17. COSATI CODES			18. SUBJECT TERMS (Continue on reverse if necessary and identify by block number)
FIELD	GROUP	SUB. GR.	
20	04		Turbulence, Shear Flow, Combustion
21	01		

19. ABSTRACT (Continue on reverse if necessary and identify by block number)

Work is continuing primarily in gas phase turbulent mixing and chemical reactions with important extensions to compressible (supersonic) shear layers. This work is divided into an experimental program, a theoretical and modelling program, a computational program and a diagnostics, instrumentation and data acquisition program. In the gas phase shear layer work, our investigations are concentrating on subsonic shear layer free stream density ratio effects, and a design effort in support of the planned extension of the hydrogen-fluorine shear flow facility to supersonic flows. The work on chemically reacting liquid shear layers has been published in its final form (Koochesfahani and Dimotakis 1986). In jet flows. the measurements of gas phase jet mixing, using laser Rayleigh scattering techniques developed for conserved scalar measurements down to diffusion space and time scales, are in progress. A first publication has just appeared in Combustion & Flame (Miake-Lye and Toner 1987) on an experiment completed with joint support from the Gas Research Institute,

20. DISTRIBUTION/AVAILABILITY OF ABSTRACT	21. ABSTRACT SECURITY CLASSIFICATION
UNCLASSIFIED/UNLIMITED ☒ SAME AS RPT. ☐ DTIC USERS ☐	Unclassified

22a. NAME OF RESPONSIBLE INDIVIDUAL	22b. TELEPHONE NUMBER (Include Area Code)	22c. OFFICE SYMBOL
Julian M. Tishkoff	(202) 767-4935	AFOSR/NA

DD FORM 1473, 83 APR EDITION OF 1 JAN 73 IS OBSOLETE.

Unclassified

SECURITY CLASSIFICATION OF THIS PAGE

in which digital imaging of soot in turbulent flames was used to describe the combustion flame sheets in methane flames.

Analytical/computational modeling efforts during this last year have included the development of a quantitative description of turbulent jet mixing and chemical reactions including finite Damköhler number effects, supersonic shear layer combustion studies of finite kinetic rate (Damköhler number) effects for the $H_2/F_2/NO$ and H_2/air systems, a new analytical model for turbulent shear layer mixing and chemical reactions, extensions of hydrodynamic stability calculations to include Mach number effects in supersonic shear layers. Finally, computational fluid dynamics studies have also proceeded using vortex methods as well as more fundamental studies using the machinery of non-linear systems dynamics.

GRADUATE AERONAUTICAL LABORATORIES
of the
CALIFORNIA INSTITUTE of TECHNOLOGY
Pasadena, California 91125

AFOSR-83-0213 1987 Annual Report

for the Period Ending 15-Apr-87

CHEMICAL REACTIONS in TURBULENT MIXING FLOWS

Principal investigators:

P. E. DIMOTAKIS, Professor, Aeronautics & Applied Physics

J. E. BROADWELL, Senior Scientist, Aeronautics

A. LEONARD, Professor, Aeronautics

1-Jun-87

ABSTRACT

Work is continuing primarily in gas phase turbulent mixing and chemical reactions with important extensions to compressible (supersonic) shear layers. This work is divided into an experimental program, a theoretical and modelling program, a computational program and a diagnostics, instrumentation and data acquisition program. In the gas phase shear layer work, our investigations are concentrating on subsonic shear layer free stream density ratio effects, and a design effort in support of the planned extension of the hydrogen-fluorine shear flow facility to supersonic flows. The work on chemically reacting liquid shear layers has been published in its final form (Koochesfahani & Dimotakis 1986). In jet flows, the measurements of gas phase jet mixing, using laser Rayleigh scattering techniques developed for conserved scalar measurements down to diffusion space and time scales, are in progress. A first publication has just appeared in Combustion & Flame (Miake-Lye & Toner 1987) on an experiment completed with joint support from the Gas Research Institute, in which digital imaging of soot in turbulent flames was used to describe the combustion flame sheets in methane flames.

Analytical/computational modeling efforts during this last year have included the development of a quantitative description of turbulent jet mixing and chemical reactions including finite Damköhler number effects; supersonic shear layer combustion studies of finite kinetic rate (Damköhler number) effects for the $H_2/F_2/NO$ and H_2/air systems; a new analytical model for turbulent shear layer mixing and chemical reactions; extensions of hydrodynamic stability calculations to include Mach number effects in supersonic shear layers. Finally, computational fluid dynamics studies have also proceeded using vortex methods as well as more fundamental studies using the machinery of non-linear systems dynamics.

1.0 INTRODUCTION

This project is concerned with mixing and chemical reactions in moderate to high Reynolds number, turbulent shear flows whose scope has been extended during this last year to cover the effects of compressibility on turbulence and turbulent mixing. It is directed and making significant progress towards addressing fundamental deficiencies in the conventional treatment and understanding of this subject.

The program is comprised of several complementary parts. In particular,

1. an experimental effort,

2. an analytical/computational modeling effort,

3. a computational fluid dynamics effort,

and

4. a diagnostics/data-acquisition effort, the latter as dictated by specific needs of our experimental program.

Our approach is to carry out a series of detailed studies in two well defined, fundamentally important flow fields: free shear layers and axisymmetric jets. The philosophy in effect being that these two flows encompass an important part of the generic properties and behavior of these flows. If the behavior in more complicated geometries is ever to be mastered, understanding of these two canonical flows needs to be recognized as an important milestone and proving ground of proposed models.

To elucidate molecular transport effects, experiments and theory concern themselves with both liquids and gases. A review of these issues appeared in the AIAA J. last June (Broadwell & Dimotakis 1986), which received a citation from the editorial staff of the AIAA J.

The gas phase studies are presently being extended to cover Mach number effects in shear layer mixing, i.e. the effects of compressibility in supersonic, high Reynolds number, reacting and non-reacting shear layers. Progress in these areas, realized since our last annual report (Dimotakis, Broadwell & Leonard 1986), is outlined below.

2.0 SHEAR LAYER MIXING & CHEMICAL REACTIONS

Turbulent, two-dimensional shear layer mixing and combustion is of primary interest in this effort. Studies in this area, published under the sponsorship of this program prior to the beginning of this reporting period (15 April 1986 - 15 April 1987), have concerned themselves with:

1. a simple model for turbulent shear flow mixing (Broadwell & Breideenthal 1982),

2. gas-phase mixing at low heat release (Mungal 1983, Mungal, Dimotakis & Broadwell 1984, Mungal & Dimotakis 1984), including Reynolds number effects (Mungal, Hermanson & Dimotakis 1985), and Damköhler number effects (Mungal & Frieler 1985),

3. a simple model for the entrainment ratio in a subsonic, two-dimensional shear layer (Dimotakis 1986),

4. gas-phase mixing at high heat release, including the effects of favorable pressure gradients (Hermanson 1985),

and

5. liquid-phase mixing and chemical reactions (Koochesfahani 1984, Koochesfahani, Dimotakis & Broadwell 1985, Koochesfahani & Dimotakis 1985)

Work published or in progress during the current reporting period is

outlined below.

2.1 Heat release effects

A paper (Hermanson, Mungal & Dimotakis 1987) has just appeared (AIAA J.), documenting part of the progress in this area. A first draft of the manuscript for the major publication derived from this effort (Hermanson 1985), intended for submission to the J. Fluid Mech., has been completed.

2.2 Stability analysis

A paper investigating the linear stability characteristics of the initial region of a two-dimensional shear layer, including the effects of the splitter plate wake as well as the effects of unequal free stream density, was presented at the 1987 AIAA Aerospace meeting (Koochesfahani & Frieler 1987). The important point of this paper was that when the effects of a possible velocity profile defect (arising from the splitter plate wake) are taken into account, it is found that the flow possesses two unstable modes. In particular, in addition to a "shear" mode that can be recognized as evolving from the classical Kelvin-Helmholz instability, a second "wake" mode is also present. For equal free-stream densities, the wake mode is not as unstable as the shear mode. For large values of the density ratio and for the case where the heavy fluid comprises the low speed stream ($\rho_2/\rho_1 > 1$), however, the wake mode can be considerably more unstable. There is evidence to suggest that, in that case, the importance of the wake mode is not confined to the initial region but extends over a large range of the flow. This paper (Koochesfahani & Frieler 1987) is reproduced as Appendix A of this report.

In an extension of this work, we are incorporating the effects of compressibility in this calculation. Earlier calculations (Gropengiesser 1970), as well as other investigations (Papamoschou 1986), suggest that such effects can be significant. The extension of this work to supersonic stability is undertaken as part of the on-going Ph.D. research of Ms. Mei Zhuang.

2.3 Density ratio effects

Considerable progress has been made in our experimental investigations of the effects of free stream density ratio in gas phase, subsonic shear layers. Specifically, using the results of chemical reactions at both high and low stoichiometric mixture ratios, i.e. $\phi = 1/8$ and $\phi = 8$, and paying particular attention to avoid finite Damköhler number effects, we have been able to determine the average high speed fluid mixture fraction in the molecularly mixed fluid (ξ_m) as a function of free stream density ratio, for density ratios ρ_2/ρ_1 in the range of 1/8 to 4. The new results clarified some unresolved questions that were raised in earlier investigations and are well correlated (in absolute value) with estimates computed using the simple dependence of the entrainment ratio on density ratio (Dimotakis 1986). See figure 1. We are investigating whether the small but increasing deviation as the density ratio increases is attributable to changes in the large scale flow structure, which would alter the entrainment ratio, or increasing contributions to $p(\xi)$, the probability density function (PDF) of the mixed fluid fraction ξ, from values of ξ close to unity, which may not have been adequately represented in the $\phi = 1/8$, 8 "flip" experiments. These new data also allow us to estimate the dependence of the molecularly mixed fluid mean number density profile across the layer, as a function of the free stream density ratio. The results are plotted in figure 2. The important conclusion is that this quantity remains essentially unaltered as the free stream density ratio is varied over a

wide range. Note that the peak values in this calculation are slightly depressed in the middle of the layer owing to the reduction of the total fluid density due to the heat release and need to be properly normalized with the corresponding mean number density profile to represent the mean mixed fluid mole fraction profile. The results of this calculation are depicted in figure 3.

This work is part of the on-going Ph.D. research effort of Mr. Cliff Frieler.

2.4 Damköhler number effects

The gas phase, subsonic low heat release Damköhler number experimental investigation, documented in the GALCIT Report FM85-01 by Mungal & Frieler (1985, reproduced also as appendix B in Dimotakis, Broadwell & Leonard 1986), has been accepted for publication in Comb. & Flame.

Pilot calculations of Damköhler number effects in supersonic shear layers are being performed, initially undertaken in support of the design effort for the supersonic shear layer facility. We subsequently decided that they are of general interest in their own right, and will be presented at the Joint Propulsion Meeting in San Diego this June (Hall & Dimotakis 1987). Briefly, the model calculations assume as a zeroth order flow/thermodynamic model that:

1. the chemical kinetic process evolves in a constant pressure "balloon" reactor, whose mass is increasing linearly with time (a consequence of the entrained reactant flux into the mixing layer),

2. the entrained fluid from each of the free streams is mixed and homogenizes at a (single-valued) composition corresponding to

the entrainment ratio,

and,

3. that it is entrained in a thermodynamic state contributing an energy flux from each of the free streams estimated by computing their enthalpy assuming that the entrained fluids are brought to stagnation conditions in the convected large scale vortex structure frame.

An important parameter that emerges from these calculations is the dimensionless ratio

$$\Omega_e = \frac{\dot{n}_{Ae}\,\tau_\chi}{n_A(0)}, \qquad (*)$$

which measures the relative importance of the entrainment flux in the chemical kinetic process. In this expression, $\dot{n}_{Ae}$ is the lean reactant species entrainment flux (moles/sec), τ_χ is the chemical time required to consume the lean reactant in a constant mass reactor, i.e. in the limit of small Ω_e, and $n_A(0)$ is the initial number of moles of the lean reactant species in the reactor, prior to the initiation of the entrainment process at $t = 0$. The latter quantity is intended to represent the effective amount of lean reactant that is rolled up in the first vortical structure, prior to the origin in time when the constant entrainment flux can be considered to have begun.

For $\Omega_e \ll 1$, the chemical kinetics evolve essentially as in a constant mass reactor, in which the reaction is initiated at $t = 0$ (with premixed reactants) and proceeds to equilibrium at constant pressure. For $\Omega_e \gg 1$, which is generally the fluid mechanically significant regime for high Reynolds number shear layers, the chemical kinetics evolution is different, reaching an asymptotic behavior that is independent of Ω_e for large values of that parameter. Sample calculations for the $H_2/F_2/NO$ chemical system for the two limiting

cases, i.e. $\Omega_e \ll 1$ (constant mass reactor; solid line), and $\Omega_e \gg 1$ (entrainment-dominated reactor; dot-dashed line), are depicted in figure 4. These calculations correspond to typical subsonic low heat release run conditions in the experiments of Mungal & Dimotakis (1984) and were performed using the CHEMKIN software library package (Kee et al 1980) and the $H_2/F_2/NO$ chemical reaction system, as described in Mungal & Frieler (1985). We note the much slower approach to equilibrium in the entrainment-dominated reactor; a consequence of the continuous dilution of the hot product mixture by the relatively cold entrained fluids.

Similar calculations were performed for a supersonic shear layer and a $H_2/F_2/NO$ reactant system, which indicate that (qualitatively) this system behaves quite predictably. In particular, as the entrained reactant concentrations and/or enthalpy are raised, the effective kinetic rate increases and the time required for the chemical reaction to be driven to completion decreases.

The H_2/air chemical system is also being studied in similar flow conditions for comparison purposes, as well as for its significance as a potential chemical system for hypersonic propulsion. We note, however, that for this system, while raising the static temperature (enthalpy) of the entrained reactants (preheating) decreases the time required for ignition (the beginning of any substantial heat release), as one would expect, it can also increase (possibly substantially) the time required for completion of the reaction. This is a consequence of the fact that, at the higher absolute temperatures attained under these conditions, a large fraction of the enthalpy in that system can be tied up in relatively small concentrations of minor but energetic species that, especially under the impeding influence of the cold entrained streams, reach their equilibrium concentrations rather slowly.

These calculations will be documented in the Joint Propulsion Meeting AIAA Paper (Hall & Dimotakis 1987).

2.5 Design effort for the supersonic combustion shear layer facility

As a consequence of the extension of the scope of this work to variable total enthalpy flows, made possible by co-funding under the AFOSR F49629-86-C-0113 URI Contract, the overall facility design had to be reviewed with this important new specification in mind. In particular, the design specifications for several critical items were modified. This, in turn, produced revised specifications for the high-pressure gas supply vessel and the fast-acting valve/pressure regulator (see Dimotakis, Broadwell & Leonard 1986, section 2.5). Additionally, two design concepts for the test section are being evaluated. These developments are briefly described below.

A final specifications document has been written for the high-pressure supply vessel (included as appendix B). This document has been sent to local manufacturers, who are now in the process of formulating official contract bids. Following receipt of the bids and on-site visits to potential vendors, the contract will be awarded shortly and that the finished tank should be delivered to Caltech by the end of this summer or early fall.

The stringent requirements placed on the pressure regulator (high pressure, high temperature, large flow rate, and fast response) have eliminated from our list of potential vendors all the commercial suppliers of conventional pressure regulators known to us. There is, however, reasonable hope that the Digital Valve (Digital Valve Corp.) will essentially meet our requirements. This valve consists of an array of typically 12 valve elements of different sizes. The sizes are arranged in a binary sequence. Each element is individually operated from a digital signal, thus in principle, within the resolution of one part per 2^{12} (4,096), any desired total-area-versus-time curve can be programmed into the valve. The valve model currently under consideration (2"-DIGICON-RC) meets the pressure specifications. The temperature specifications are being discussed with the manufacturer to

explore variations in the basic design permitting the accommodation of our temperature specifications†. We estimate that two such valves, operated in parallel (also increasing the resolution thereby), will have adequate flow capacity. There are additional questions, however, concerning the temporal resolution capabilities of the valve. The quoted response time of 75 msec for the opening/closing of each element made us apprehensive about the smoothness of the total-area-versus-time output and the resulting flow quality. Consequently, an analytical model of the valve dynamics was devised, in which the area change of a single element during the opening/closing cycle was represented by a smooth curve. Our analysis predicts that a very smooth output can be obtained when the valve configuration is updated at time intervals close to the response time. See figure 5. In summary, the prospects of using the Digital Valve are promising, provided the manufacturer can overcome the temperature limitations in the present design and that he (and we) confirm our timing predictions.

Finally, we are considering two candidate nozzle configurations for producing a variable exit Mach number in the range from 1.5 to 3.5 . In particular, we are evaluating the relative merits of a symmetric 2-D nozzle with replaceable contours, or an asymmetric 2-D nozzle with a sliding block. The former has the advantage of design simplicity and the disadvantage of the need to fabricate a nozzle with different contours for each different Mach number and gas (γ) combination. The latter offers the flexibility of a continuous Mach number range, with some (minor) compromises in flow quality, however, as well as some complications in the over-all test-section design and producibility. Additionally, the asymmetric nozzle needs to be about twice as long as the symmetric one, resulting in a splitter plate trailing-edge (high speed) boundary layer momentum thickness (θ_1) that will be roughly twice as thick. This is an important consideration, as the flow streamwise

† As of this writing, the high temperature (600°F) specification is causing some difficulties, as the stock item is fabricated with soft seals in the air cylinder actuators.

run (L) is more or less fixed by other constraints and we would like to operate at values of L/θ_1 that are as large as possible and, in particular, no less than 10^3, or so. We are presently acquiring and adapting computer flow codes to assist us in the design and relative evaluation of these nozzles. A decision as to which configuration will be implemented is expected in the next few months.

This work is part of the on-going Ph.D. research effort of Mr. Jeffery Hall, in collaboration with Dr. Dimitri Papamoschou and Mr. Cliff Frieler.

2.6 Liquid phase reacting and non-reacting shear layers

The archival documentation of our earlier efforts in this area has just appeared in the J. Fluid Mech. (Koochesfahani & Dimotakis 1986).

2.7 New shear layer mixing model

The approach adopted in the new model is that of viewing an Eulerian slice of the spatially growing shear layer, at a downstream station at x, and imagining the instantaneous interface between the two interdiffusing and chemically reacting fluids as well as the associated strain field imposed on that interface. It is recognized that both the Eulerian state and the local behavior of that interface are the consequence of the Lagrangian shear layer dynamics from all relevant points upstream of the station of interest at x. It is assumed, however, that this upstream history acts in such a manner as to produce a self-similar state at x, whose statistics can be described in terms of the local parameters of the flow. In particular, it is assumed that a Kolmogorov cascade process has been the appropriate description of the upstream dynamics, leading to the local Eulerian spectrum of scales and

associated strain rate field at x.

The justification for this approach is that while the large scale dynamics are all important in determining such things as the growth rate and entrainment ratio into the spatially growing shear layer, the predominant fraction of the interfacial area is associated with the smallest scales, which can perhaps be adequately dealt with in terms of universal similarity laws. The large scales, therefore, are viewed as feeding the reactants that are entrained at some upstream station into the smaller scale turbulence at the appropriate rate. These reactants subsequently get processed by the evolution of the cascade processes upstream to produce the local spectrum of scales at x (see discussion in Broadwell & Dimotakis 1986). This conceptual basis is also aided by the notion of a conserved scalar, according to which the state of diffusion and the progress of an associated chemical reaction, in the limit of fast (diffusion-limited) chemical kinetics, is completely determinable by the local (Eulerian) state of the conserved scalar (see, for example, Bilger 1980).

An important part of the proposed procedure is the normalization that is imposed on the statistical weight (contribution) of each scale λ to the total amount of molecularly mixed fluid and associated chemical product. This is done via the expected interfacial surface per unit volume ratio that must be assigned to each scale λ. When totalled over all scales, these statistical weights must add up to unity.

The results are first obtained conditional on a uniform value of the dissipation rate ε. An attempt to incorporate and assess the effects of the fluctuations in the local dissipation rate, i.e. $\varepsilon(\underline{x},t)$, is made by folding the conditional results over a probability density function for ε.

In a similar vein, a refinement of the entrainment ratio idea is incorporated, in which it is recognized that the large scale spacing ℓ/x is a random variable and that therefore, by the force of the arguments

in Dimotakis (1986), the entrainment ratio must also be treated as a random variable of the flow. Accordingly, the results are obtained conditional on a given value of the entrainment ratio E, and are subsequently folded over the expected distribution of values of E about its average value $\overline{E}$.

In the calculations, it is assumed that the molecular diffusivities for all relevant species are equal to each other, but not necessarily equal to the kinematic viscosity. Heat release effects and temperature dependence effects of the molecular transport coefficients are also ignored. This is appropriate for the liquid phase measurements of Koochesfahani & Dimotakis (1986), and may be adequate for the description of the gas phase measurements of Mungal & Dimotakis (1984) and the Reynolds number study of Mungal et al (1985). The issue of heat release effects on the flow was specifically addressed elsewhere (see Hermanson et al 1987). In computing the temperature corresponding to the heat released in the reaction, equal heat capacities are also assumed for the two fluids brought together within the mixing zone. While some of these assumptions were not necessary, they allowed calculations to be performed in closed form permitting, in turn, the examination of the dependence of the results on the various dimensionless parameters of the problem. The proposed procedure assumes that the relevant statistics of the velocity field are known (or can be estimated) and computes the behavior of the passive scalar process in response to that velocity field. Finally, the procedure is "closed" in that it yields the (absolute) chemical product volume fraction δ_P/δ in the shear layer at x, with no adjustable parameters.

The prediction for the chemical product thickness $\delta_{P1}(\phi)/\delta$, where δ_{P1} is given by

$$\delta_{P1}(\phi) = \frac{1}{c_{01}} \int_{-\infty}^{\infty} c_P(y,\phi)\, dy \ , \qquad (2)$$

where $c_P(y,\phi)$ is the chemical product concentration, c_{01} is the reactant

concentration in the high speed stream, δ is the total (1%) thickness of the layer and ϕ is the stoichiometric mixture ratio are depicted in figure 6. The data (circles) are from the gas phase measurements of Mungal & Dimotakis (1984). The correct prediction (in absolute value) is noteworthy.

The predictions for the chemical product mean volume fraction, δ_p/δ, where

$$\delta_p = \int_{-\infty}^{\infty} \frac{\Delta T(y,\phi)}{\Delta T_{flm}(\phi)}\, dy \ , \qquad (3)$$

$\Delta T(y,\phi)$ is the mean temperature rise profile, and where $\Delta T_{flm}(\phi)$ is the adiabatic flame temperature at the stoichiometric mixture ratio ϕ, are plotted (solid line) in figure 7 versus the stoichiometric mixture fraction, i.e.

$$\xi_\phi = \frac{\phi}{\phi + 1} \ ,$$

for the Mungal & Dimotakis (1984) data depicted in figure 6 (note that $\delta_{p1} = \xi_\phi \delta_p$). The corresponding predictions are also plotted (dashed line) for the liquid phase point of Koochesfahani & Dimotakis (1986), at $\phi = 10$ and a comparable Reynolds number. Note that the Schmidt number dependence of the chemical product volume fraction δ_p/δ is also predicted correctly.

Finally, the prediction for the Reynolds number dependence of δ_p/δ is depicted in figure 8 and compared with the gas phase measurements of Mungal et al (1985) and the liquid phase measurements of Koochesfahani & Dimotakis (1986).

Some of the features of this model and its predictions, which distinguish it from the model proposed by Broadwell & Breidenthal (1982), and as updated in the discussion in Broadwell & Mungal (1986),

are listed below. are:

1. There are no adjustable parameters in this model.

2. δ_p/δ, the volume fraction in the shear layer region occupied by chemical product tends to zero as the Schmidt number tends to infinity at fixed Reynolds number (there is no explicit procedure for computing this dependence in the Broadwell-Breidenthal model for large Schmidt numbers).

3. δ_p/δ is also predicted to tend to zero in the limit of infinite Reynolds numbers, albeit slowly (logarithmically). The corresponding limit in the Broadwell-Breidenthal model is finite (see discussion in section 3.5).

This work will be presented at the U.S. - France Joint Workshop on Turbulent Reacting Flows this July (Rouen, France) and will be issued in the interim as a GALCIT report (Dimotakis 1987).

3.0 TURBULENT JET MIXING & CHEMICAL REACTIONS

Parts of this work have been cofunded by the Gas Research Institute, the Office of Naval Research and the National Bureau of Standards.

3.1 Gas phase mixing at low to moderate Reynolds numbers

To increase the understanding of the mixing processes in gas phase turbulent jets, an investigation of the entire range of concentration length and time scales has been undertaken at low to moderate Reynolds numbers. In the first year of this effort a laser Rayleigh scattering diagnostic was developed and the design of an experiment to exploit the

power of this technique was begun. In the second year, the design was completed, the experiment was constructed and performance testing was begun. Last year was devoted to the resolution of problems identified by the performance tests and the improvement of some aspects of the experiment with new technologies. A few new runs were made at the full capabilities of the apparatus with some interesting results. A method of flow visualization and some new data processing software have also been developed.

In last year's report (Dimotakis, Broadwell & Leonard 1986, section 4.1), it was stated that the coflow became unsteady after about 15 seconds. This problem was attributed to a cooling trend in the coflow gas in the course of a run. Because the coflow gas enters at the top of the experiment, a cooler (denser) layer of gas was able to form over a warmer (lighter) gas. This configuration is gravitationally unstable to the formation of buoyancy currents. A feedback temperature control system was designed, fabricated and installed to address this problem. Nevertheless, the unsteady buoyancy currents in the test section were not entirely eliminated. The remaining problem was diagnosed to be a consequence of small isothermal density gradients, which could be established in the facility prior to the initiation of the run. A new purging procedure was subsequently adopted which solved this last problem. The coflow is now stable for approximately one minute, which is long enough to accommodate the scheduled runs.

Preliminary calculations had indicated that, with the advent of a new line of high quality photodiodes, the possibility of replacing the photomultiplier tube (PMT) as the photodetector should be considered. The photodiode has the advantage of higher quantum efficiency (0.6 to 0.7 in the wavelength range of interest), relative to that available from the PMT (typically 0.1). The disadvantage of a photodiode is that it does not amplify its signal (Gain ~ 1), as does the PMT (Gain ~ 10^4), and therefore must be mated to a very high quality, low noise (transimpedance) amplifier if it is to compete. A typical signal

current for this experiment, for example, would be about 0.3×10^{-9} A from a photodiode and about 0.3×10^{-6} A from the PMT. The design of the matched transimpedance amplifier was completed by Dr. Daniel Lang and a performance calculation was undertaken for the proposed matched photodiode/amplifier system. The results were promising enough to suggest that building and testing a prototype was warranted. Following a few modifications to decrease stray capacitance and increase bandwidth, the photodiode system performance was indeed proven better than the corresponding PMT system performance. The photodiode system is also a more attractive detector because it is inexpensive, mechanically tough and optically rugged. It is driven by a low voltage (+15 Volts), compared to the PMT (-800 Volts), which results in a safety advantage since possible sparks are of some concern when combustible gases are present in the measurement environment (most of the jet gases used in this study are hydrocarbons). These facts made the decision to replace the PMT system with that using the photodiode compelling. Figure 9 is a comparison plot of the measured power spectrum from each of the systems when illuminated by the Rayleigh scattered light from argon gas at 1 atmosphere pressure. The scattered light was collected from a 200 μm length of a collimated 15 Watt Ar^+ laser beam in both cases. As can be seen from these data, the spectrum below about 30 Hz, for both systems, is dominated by 1/f noise (from the laser). The main result to note is that from about 30 Hz to about 20 kHz, the bandwidth of interest for these studies, the photodiode system noise spectrum falls below that of the PMT system.

An effort was also made to update the existing data acquisition software to take full advantage of the increased A/D conversion capability, computing power, and memory available on the laboratory computer used for this experiment. In particular this allowed the length of a data set for each run to be comfortably increased by a factor of 2, to 2^{19} (~ 500,000) individual concentration measurements.

For this investigation, the power spectrum of concentration fluctuations is an important diagnostic of the turbulent state of jet mixing. In order to calculate a spectrum over the possible range of frequencies it was necessary to develop algorithms to calculate the high and low frequency parts of the spectrum separately. These routines were tested with some preliminary data and then used to compute the noise spectra (figure 9) mentioned above.

To ensure that the experimental apparatus is producing a "standard" jet, it is necessary to check that the half-angle of the cone which contains the jet fluid falls within the range of accepted values ($11^\circ \leq \alpha \leq 12.5^\circ$), i.e.

$$\frac{\delta(x)}{2x} = \tan\alpha$$

where $\delta(x)$ is the local jet diameter at the edge of the jet fluid containing region. This angle can be estimated experimentally from photographs of the jet flow. Because the gases used in this study are clear, shadowgraph photography was the obvious choice. In this case, the shadowgraphy relies on the same difference in the refractive index of the jet and reservoir gases exploited in the Rayleigh scattering measurements. A sample photograph is included as figure 10. The spreading half-angle for this jet is about 11.5°. The field of view is from x/d = 0 (top of photograph) to x/d = 40 (bottom of photograph) jet exit diameters. The jet gas is propylene, the reservoir gas is argon and the Reynolds number is 5,000. The slight non-uniformity in the background light level arises because the arc-lamp light source used does not produce a perfect spherically diverging beam.

With the coflow problems solved and the entire data acquisition system redesigned, reprogramed or upgraded, the high quality measurements that are focus of this work were begun. A power spectrum of the concentration fluctuations in the jet at x/d = 40 has been included as figure 11. The diagonal line has a slope of -5/3. The

frequency axis is normalized by the estimated local large scale time, estimated here by means of the expression

$$\tau_\ell = \frac{\delta}{U} ,$$

where $U = U(x)$ is the local mean jet velocity at the centerline. This is estimated to be about 0.6 seconds at this measuring station. A comparison with the noise spectra from the sensors shows that the concentration fluctuations in the jet are 3 to 4 orders of magnitude larger that the system noise. Recognizing that the turbulent cascade may be underdeveloped for this Reynolds number, a second and potentially more important observation is that the estimated Kolmogorov scale mean passage frequency, i.e.

$$f_K = \frac{U}{\lambda_K} ,$$

where the Kolmogorov scale λ_K is here estimated by,

$$\lambda_K = \frac{\delta}{2} Re^{-3/4}$$

and the observed "end" of the $-5/3$ spectral slope differ by almost a factor of 23 (at the Reynolds number of 5,000 for this run). This means that the smallest scalar diffusion scales ($Sc = 1$ here) are much larger than our design estimates. We consequently decided, so as to exploit the full capabilities of our diagnostics, to reconfigure the experiment so as to permit higher Reynolds numbers to be attained. This will involve increasing the volume flux from the coflow and designing and fabricating a new jet nozzle with a smaller exit diameter. The new nozzle should allow the jet Reynolds number to be increased to almost 25,000 while observing the strict spatial and temporal resolution constraints of the experiment.

We plan to complete the measurements and data analysis at the current Reynolds number (5,000), and then move to the new configuration to explore Reynolds number effects in the coming year.

This work is part of the on-going Ph.D. research effort of Mr. David Dowling.

3.2 High pressure jet combustion facility

The High Pressure Reactant Vessel is designed for studies of high Reynolds number turbulent reacting jets, at both reduced and elevated pressures. In addition to the capability of using conventional gaseous fuels, the vessel has been designed to handle more exotic reactants like fluorine, nitric oxide, and hydrogen. This capability will allow a systematic study of the effects of

1. stoichiometric mixture ratio,

2. jet/reservoir fluid density ratio,

3. heat release,

4. finite kinetic rate (Damköhler number),

as well as

5. buoyancy,

over a wide range of Reynolds numbers.

The High Pressure Reactant Vessel (HPRV) fabrication was completed and the vessel was assembled in the lab where it was helium leak tested and vacuum tested to our satisfaction. Figure 12 shows the vessel installed in the lab.

The gas delivery system will be modeled after the H_2/F_2 combustion shear layer delivery system. In order to ensure the safety of this design in the new facility, which will see much higher concentrations of fluorine at higher pressures than the shear layer facility, a materials test was performed at the TRW Chemical Laser Lab in Redondo Beach. The materials to be exposed to fluorine in the new lab were subjected to 5 times the highest concentration of fluorine we expect to see in the lab at the highest pressure. All materials survived the tests, indicating that we should proceed with our gas delivery design as planned. Most of the components of this delivery system have been purchased and construction of the control panel, schematically shown in figure 13, will begin soon.

Different diagnostic tools are being considered for the initial nonreacting cold runs and the ensuing reacting hot runs. Shadowgraphy flow visualization will be a first diagnostic. For the hot runs, the main (additional) diagnostic for the initial experiments will be cold wire thermometry, similar to the ones currently in use in the H_2/F_2 shear layer facility. Preliminary tests have also been conducted by Mr. Cliff Frieler using more sensitive wires, which are also characterized by considerably improved time/space resolution, of smaller diameter (0.6 μm, versus the 2.5 μm diameter wires presently in use in the shear layer experiments). The smaller wires are being fabricated by Mr. Earl Dahl. The amplifier circuits for these probes have been constructed and will allow 16 channels of high temporal/spatial resolution temperature to be measured. We hope to begin cold runs by the end of the summer. Subsequent experiments will also benefit from the diagnostics and instrumentation developments presently in progress under the guidance of Dr. R. Miake-Lye and Dr. D. Lang and sponsored, in part, by the AFOSR-85-0153 URI contract.

The design of this facility begun under the guidance of Dr. G. Mungal (presently at Stanford), primarily under funding from the Gas Research Institute. The work described here is part of the on-going

Ph.D. research effort of Mr. R. Gilbrech.

3.3 Laser scattering experiments in hydrocarbon flames

A paper was recently published in Combustion and Flame (Miake-Lye & Toner 1987, included as appendix C in this report) which describes our experimental studies of large buoyant diffusion flame using laser soot scattering. In that paper, arguments were presented justifying the use of soot as a marker for the combustion interface for the flame under study. In particular, we argue that the soot is localized in a thin layer close to and locally following the reaction interface surface.

Based on our r-t digital image data, we have calculated the soot intermittency (~ soot volume fraction), or fraction of time that soot is present, at each radial station. By determining the instantaneous flame boundary, we have also calculated the conditional soot intermittency, which we define to be the fraction of time that soot is present within the flame boundary at any radial station. The important result is the observation that the conditional soot intermittency is nearly constant across the flame. These results lead us to a picture of the flame made up of thin laminar diffusion flamelets distributed fairly uniformly within the puff-like large scale envelope of the flame. The flamelets are continuous laminar diffusion flames near the burner, but become increasingly convoluted and broken (non-contiguous) as the flame tip is approached.

Subsequent soot scattering experiments have concentrated on axially directed imaging in the same large buoyant diffusion flame. These experiments, which were proposed in the last annual report, were carried out at various fuel flow rates with the beam directed parallel to the axis of the burner at each of three radial locations. The puffing periodicity is evident in the reconstructed z-t images and the celerities of these structures can be measured from curve fits to the

processed digital image data.

Data analysis is in progress. Some of the software developed for the radial data analysis has been modified for the present investigation, new programs have been written (due to the different structure of the axial images), and software has also been written for use on a new image processing system. Work to date has begun to elucidate the accelerating flow region close to the burner, driven by the heat release and marked by the concomitant soot sheets. Not surprisingly, the structures persist longer in the z-t diagrams for higher fuel flow rates (consistent with longer flame lengths) and, further, the celerity of a structure at a given axial station depends on the fuel flow rate. Celerities are measured to range from 50 cm/s at $z/D = 0.2$ to 190 cm/s at $z/D = 1$ and beyond. Analysis should be completed soon and a report of these results will be written sometime during the current contract year.

In support of our ongoing efforts to understand flame structure, a feasibility experiment was performed using an additional flow visualization technique. This technique makes use of titanium tetrachloride ($TiCl_4$) which, in gas phase, reacts with water vapor to form TiO_2 particles (e.g. Roquemore et al. 1986), which scatter laser light strongly. The particles will be present anywhere in the flow where $TiCl_4$ and water vapor have mixed, so by adding $TiCl_4$ to the fuel or ambient air and water vapor to the same fluid or the other fluid, a variety of flow labeling schemes can be achieved. The results of such experiments can complement the information derived from soot scattering experiments.

The feasibility study was carried out with the 50 cm burner apparatus by including a partially filled $TiCl_4$ container in the fuel supply line. The fuel passed over the surface of the liquid $TiCl_4$, which introduced (an as yet unquantified amount of) $TiCl_4$ vapor into the fuel gas. When the $TiCl_4$ vapor encountered water vapor, either due to unreacting mixing with ambient air or upon combustion of the fuel, TiO_2

particles were formed. In a diffusion flame, soot particles are also often formed at the reaction interface, so the feasibility study was intended to determine whether the two sources of particles could be distinguished.

The burner was lit with a fuel flow rate corresponding to ~ 190 kW heat release, a value (the highest) used in our previous studies. The flame was run with and without the $TiCl_4$ seeding and an increase in the luminosity by a factor of 3 - 5 was apparent with $TiCl_4$. This was determined by noting the attenuation required to equalize exposures with and without the $TiCl_4$ seeding. The flame luminosity also changed color from the typical yellow color due to hot soot to an intense white color.

This feasibility study leads us to be cautiously optimistic about the prospects for using $TiCl_4$ as a flow visualization tool in our continuing flame structure experiments. It appears that when it is added to the fuel in the manner described above, there is a sufficiently large increase in the flame luminosity that the luminosity due to the soot will be a fraction (20 - 30%) of the total. This should permit the type of selective flow labeling that we envision as required for our ongoing experiments.

These studies were undertaken by Dr. R. Miake-Lye in collaboration with Dr. S. Toner.

3.4 Liquid phase jet mixing at small scales

Work is in progress to study the mixing interface and small-scale structure of turbulence in a liquid phase, axisymmetric, turbulent jet. The diagnostic method used is Laser Induced Fluorescence, which has several desirable attributes including the potential (for liquid phase fluorescence) of very high signal-to-noise ratio, high spatial resolution, and an intrinsic connection with the mixing/diffusion

process. Analysis of preliminary data has been undertaken using fractal and spectral methods.

The fractal processing algorithms developed are based on the "box-counting" scheme, which we have implemented in both one and two dimensions. Issues addressed in the fractal algorithms have included the effect of the thresholding process (which determines the boundary of the region to be "dimensioned"), the impact of finite record length, comparison of 1-D vs 2-D algorithms, and whether the turbulent jet interface is in fact describable by the notion of a characteristic fractal dimension. Results are relatively insensitive to the thresholding level and on whether one or two dimensional algorithms are used.

It was found that, at least within the range of (the small) scales examined, the jet does not seem to possess a characteristic fractal dimension. Additionally, end effects from finite record lengths can produce substantial noise for short records (i.e. 128 elements). The smallest scale examined is estimated to be a fraction of the Kolmogorov scale, while the width of the records was approximately a tenth of the jet diameter (consisting of 512 elements). While the scales used may be either too small (an unusual difficulty) or their range too narrow, and the Reynolds number (1,000 - 3,000) may perhaps be rather low, the lack of a characteristic fractal dimension is in conflict with the only other such account in the literature (Sreenivasan & Meneveau 1986), where the difficulties of end effects are not addressed at all.

These preliminary investigations have prompted us to consider additional experiments, tailored to the collection of data specifically suited for these techniques. The new experiments will be optimized for higher Reynolds numbers (- 20,000), which should be sufficiently large for more definitive conclusions, and with a design spatial/temporal resolution of the order of a few Batchelor (scalar diffusion) scales, a region never investigated in a laboratory jet at high Schmidt number, to our knowledge. We are hoping that the results from these experiments

will complement in many important ways the gas phase mixing measurements under way (section 3.1) and help clarify important issues in our understanding of turbulent jet mixing phenomena.

This work is part of the on-going Ph.D. research of Mr. Paul Miller.

3.5 Turbulent jet modeling efforts

During the past year, modeling efforts based on the ideas described in Broadwell & Breidenthal (1982) have focused in two areas:

1. attempts to clarify the connection of the model foundations to the classical ideas of Kolmogorov

and

2. the development, in quantitative and useable form, of an axi-symmetric jet model corresponding to that for the shear layer (Broadwell & Mungal 1986).

The first task has centered around the connection between kinetic energy dissipation and scalar mixing. While no definite conclusions have yet been reached, some progress can be reported. The calculation by Broadwell & Mungal (1986), of the fractional volume of molecularly mixed fluid in a shear layer, provides a link between the two processes. Roddam Narasimha and Anatol Roshko (private communications) conclude, somewhat tentatively, that in the limit of infinite Reynolds numbers, the fractional volume in which dissipation takes place, is finite. The counterpart (not quite analogously) in the Broadwell-Breidenthal model is that in this limit, the molecularly mixed volume fraction is finite - 0.3. Furthermore, in the same limit, the kinetic energy dissipation rate is, in the classical theory, independent of Re and the

corresponding assumption is made in the model for scalar mixing. These tentative ideas will be further pursued as they promise to provide a firmer theoretical basis for the model as well as to lead to new ideas about turbulence itself.

With regard to the role of Reynolds number, we have emphasized its influence on mixing in gases (Mungal, Hermanson & Dimotakis 1985) but of equal importance, from a fundamental point of view, is its lack of influence on mixing in liquids. Koochesfahani & Dimotakis (1986) confirm an earlier finding of Breidenthal (1981), that there is no change in reaction product in the Reynolds number range between about 2×10^4 and about 8×10^4 (Breidenthal's absolute measure of product has been shown to be in error, but there is no reason to doubt the trend, or lack thereof). Likewise, for high Re, turbulent jet flame length is empirically found to be independent of Re, again as predicted by the model. The practical inference to be drawn from these analyses is that the high Reynolds number asymptotic range for gases lies above ~ 10^6 and that, therefore, most (probably all) laboratory combustion experiments are influenced by explicit molecular effects. As we have emphasized (Broadwell & Breidenthal 1982 and Broadwell & Dimotakis 1986), conventional turbulent diffusion theories do not address these important effects.

The axi-symmetric jet model is described in the attached paper (appendix D), accepted for presentation at the US-France Joint Workshop on Turbulent Reactive Flows, 6-10 July 1986 (Rouen, France). It is suitable for engineering use, i.e. the computations are of practical length with realistic chemical kinetic systems. It will be employed to examine the "nitric oxide problem" in methane and hydrogen jets that has been discussed in earlier reports.

With regard to modeling supersonic combustion, there are reasons to hope that this model is applicable there also, at least roughly so. The Ph.D. thesis of Dimitri Papamoschou (1986) suggests the presence of large scale structures in the flow, the critical feature underlying the

model, and there is no a priori reason to doubt its applicability. The idea of homogeneously mixed fluid is presently being used as a design tool for the supersonic shear layer; the strained flames are not explicitly treated (see discussion is section 2.4). We are encouraged in this use by the fact that this form of the model provided valuable guidance throughout the supersonic chemical laser program, first described in Broadwell (1974). Other results from that program are likely to be helpful in the supersonic combustion study.

In summary, through the work of the past year, there is promise of showing that the model is consistent with the basic parts of classical turbulence theory. It has now been put in quantitative form for shear layers and jets, and provides a unified interpretation of our experimental observations for wide ranges of all the parameters that we have investigated. J. E. Broadwell is an invited lecturer on these topics at the NATO Advanced Summer Institute on: Disorder and Mixing to be held at the Institut D'Etudes Scientifiques de Cargèse, 12-27 June 1987.

4.0 COMPUTATIONAL EFFORT

We have tested several types of Lagrangian elements on a three-dimensional flow that features a strong interaction between vortex structures — the merging of two vortex rings. Figure 14a shows the merging as computed by a vortex filament method and, figure 14b, by a vortex stick method. In the filament method, tubes of vorticity are defined by a sequence of material points that move with the local velocity. This is an efficient representation for short times but has difficulties once the viscous reconnection of vortex lines becomes important. In the vortex stick method, vector elements of vorticity are used that move with the local velocity and are stretched and rotated in response to the local strain field. This method appears to have the flexibility and efficiency required to handle vortex merging in three

dimensions.

We are continuing our efforts to reduce the computational complexity of the vortex method, from N^2 to $N \log(N)$, where N is the number of computational elements. The presently investigated scheme, proposed by Appel, relies on using a monopole (center-of-vorticity) approximation for computing induced velocities over large distances and a binary free data structure to keep track of which vortices are sufficiently clustered to warrant the clustering dynamically. In a separate investigation of mixing and chaotic phenomena, a numerical and analytical study is in progress, preliminary results of which were recently reported at the Chaos 87 meeting in Monterey (Leonard, Rom-Kedar & Wiggins 1987). Using non-linear system dynamics methods, the entrainment, mixing transition and other dynamical properties of a simple vortex system were analyzed.

5.0 DIAGNOSTICS, INSTRUMENTATION & DATA ACQUISITION

5.1 Progress in low light level photodetection

This part of the work was described as part of section 3.1 .

5.2 Improved data acquisition rate

We have completed the first phase of our efforts to improve the maximum rate that we can record data into computer memory and/or computer disk to the following numbers.

a. Transfers to disk (sustained for a maximum of 80 MBytes) at 1.2 MBytes/s.

b. Transfers to computer memory for a maximum of 4 MBytes at roughly 3.5 MBytes/s.

c. Burst transfers to computer memory (for a maximum of 1 kByte per burst) at 5 MBytes/s.

The second part of our effort to increase these numbers further (in excess of 24 MBytes/s) is in progress. The design, based on the high speed VME bus, is nearly complete. Fabrication of interface boards to the new bus, designed for specific data acquisition applications, should be in progress by the end of the summer. Such data rates should permit real-time recording of two-dimensional digital image data, as well as high framing rate linear array data (as needed for the anticipated supersonic shear layer work).

This part of the effort was co-sponsored by the DoD/URIP contract AFOSR-85-0153 and is performed by D. Lang in collaboration with P. Dimotakis.

6.0 REFERENCES

BILGER, R. W. [1980] "Turbulent Flows with Nonpremixed Reactants", Turbulent Reacting Flows (Springer-Verlag, Topics in Applied Physics 44, 1980, Ed. P. A. Libby, F. A. Williams), 65-113.

BROADWELL, J. E. [1974] "Effect of Mixing Rate on HF Chemical Laser Performance", Applied Optics 13, 962-967.

BROADWELL, J. E. and BREIDENTHAL, R. E. [1982] "A Simple Model of Mixing and Chemical Reaction in a Turbulent Shear Layer", J. Fluid Mech. 125, 397-410.

BROADWELL, J. E. and DIMOTAKIS, P. E. [1986] "Implications of Recent Experimental Results for Modeling Reactions in Turbulent Flows", AIAA J. 24(6), 885-889.

BROADWELL, J. E. and MUNGAL, M. G. [1986] "The effects of Damkö̈hler number in a turbulent shear layer", GALCIT Report FM86-01.

DAHM, W. J. A. [1985] Experiments on Entrainment, Mixing and Chemical Reactions in Turbulent Jets at Large Schmidt Numbers, California Institute of Technology, Ph. D. thesis.

DAHM, W. J. A. and DIMOTAKIS, P. E. [1987] "Measurements of Entrainment and Mixing in Turbulent Jets", accepted for publication in the AIAA J.

DIMOTAKIS, P. E. [1986] "Two-Dimensional Shear-Layer Entrainment", AIAA J. 24(11), 1791-1796.

DIMOTAKIS, P. E. [1987] "Turbulent shear layer mixing with fast chemical reactions", US-France Workshop on Turbulent Reactive Flows, 7-10 July 1987 (Rouen, France), 9.1-106 (GALCIT Report FM87-01).

DIMOTAKIS, P. E., BROADWELL, J. E. and LEONARD, A. [1986] "Chemical Reactions in Turbulent Mixing Flows", AFOSR-83-0123 Interim Scientific Report (15-Jun-86).

GROPENGIESSER, H. [1970] "Study of the stability of boundary layers in compressible fluids", NASA TT-F-12, 786.

HALL, J. L. and DIMOTAKIS, P. E. [1987] "A simple model for finite chemical kinetics analysis of supersonic turbulent shear layer combustion", AIAA/SAE/ASME/ASEE Joint Propulsion Conference Colloquium on Supersonic Combustion, 29 June - 2 July 1987 (San Diego, California), AIAA Paper 87-1879.

HERMANSON, J. C. [1985] Heat Release Effects in a Turbulent, Reacting Shear Layer, California Institute of Technology, Ph. D. thesis.

HERMANSON, J. C., MUNGAL, M. G. and DIMOTAKIS, P. E. [1987] "Heat Release Effects on Shear Layer Growth and Entrainment", AIAA 23rd Aerospace Sciences Meeting 14-17 January 1985 (Reno, Nevada), AIAA J. 25(4), 578-583 (AIAA Paper 85-0142).

KOOCHESFAHANI, M. M. and DIMOTAKIS, P. E. [1985] "Laser Induced Fluorescence Measurements of Mixed Fluid Concentration in a Liquid Plane Shear Layer", AIAA 22nd Aerospace Sciences Meeting (Reno, Nevada), AIAA J. 23(11), 1700-1707 (AIAA Paper 84-0198).

KOOCHESFAHANI, M. M. and DIMOTAKIS, P. E. [1986] "Mixing and chemical reactions in a turbulent liquid mixing layer", J. Fluid Mech. 170, 83-112.

KEE, R. J., MILLER, J. A., and JEFFERSON, T. H. [1980] "CHEMKIN: A General Purpose, Problem-independent, Transportable, Fortran Chemical Kinetics Code Package", SANDIA Report SAND80-8003.

KOOCHESFAHANI, M. M. and FRIELER, C. E. [1987] "Inviscid Instability Characteristics of Free Shear Layers with non-Uniform Density", AIAA 25rd Aerospace Sciences Meeting, 12-15 January 1987 (Reno, Nevada), AIAA Paper 87-0047.

MIAKE-LYE, R. C., and TONER, S. J. [1987] "Laser Soot-Scattering Imaging of a Large Buoyant Diffusion Flame", Comb. & Flame 67(1), 9-26.

MUNGAL, M. G. [1983] "Experiments on Mixing and Combustion with Low Heat Release in a Turbulent Shear Flow", Ph. D. thesis, California Institute of Technology.

MUNGAL, M. G. and DIMOTAKIS, P. E. [1984] "Mixing and combustion with low heat release in a turbulent mixing layer", J. Fluid Mech. 148, 349-382.

MUNGAL, M. G. and FRIELER, C. E. [1985] "Chemical reactions in a turbulent mixing layer: The effects of the reaction rate coefficient - Part I", GALCIT report FM85-01 (31-Dec-85).

MUNGAL, M. G, HERMANSON, J. C. and DIMOTAKIS, P. E. [1985] "Reynolds Number Effects on Mixing and Combustion in a Reacting Shear Layer", AIAA J. 23(9), 1418-1423.

PAPAMOSCHOU, D. [1986] "Experimental Investigation of Heterogeneous Compressible Shear Layers", Ph. D. thesis, California Institute of Technology.

ROQUEMORE, W. M., TANKIN, R. S., CHIU, H. H., and LOTTES, S. A. [1986] "A Study of a Bluff-body Combustor Using Laser Sheet Lighting", Experiments in Fluids 4, 205-213.

SREENIVASAN, K. R. and MENEVEAU, C. [1986] "The Fractal Facets of Turbulence", J. Fluid Mech. 173, 357-386.

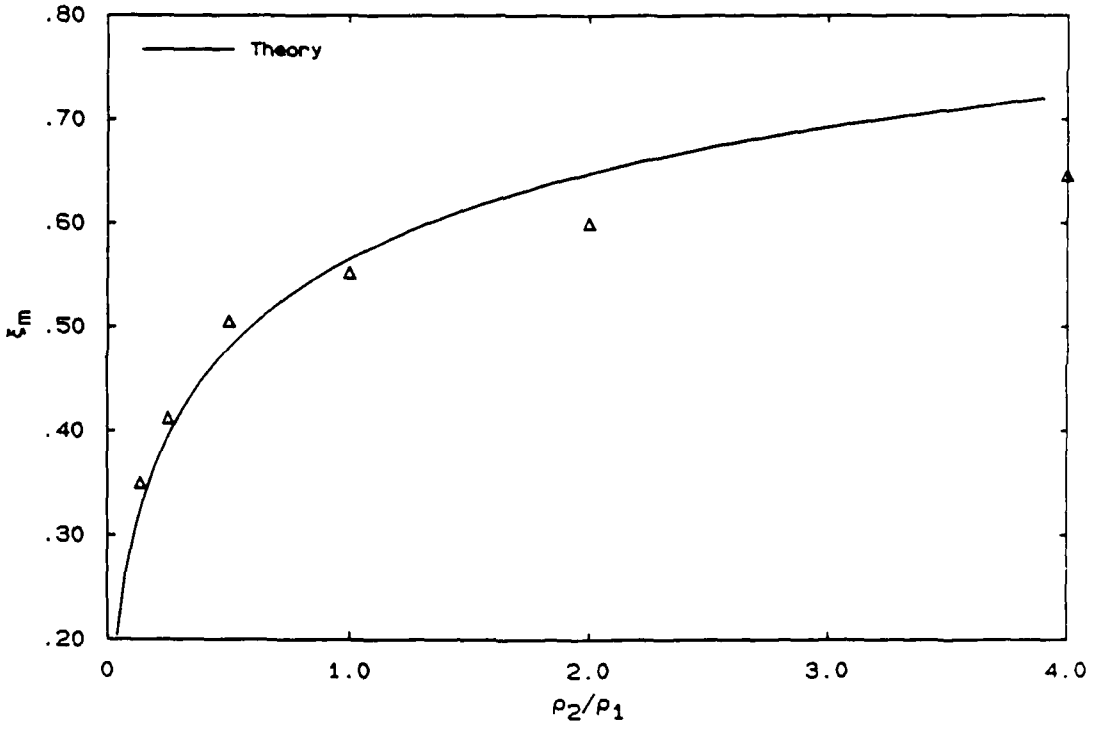

FIGURE 1. Mean mixed fluid mixture fraction (ξ_m) as a function of the free stream density ratio ρ_2/ρ_1 ($U_2/U_1 \approx 0.4$).

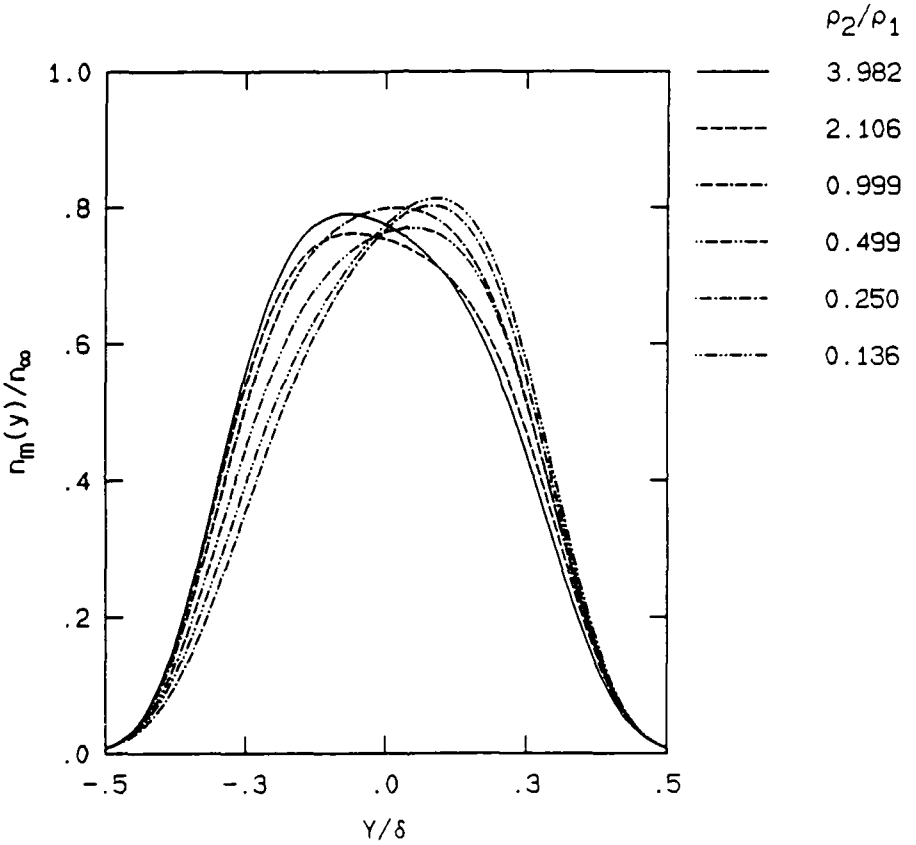

FIGURE 2. Mixed fluid mean number density profiles, for several free stream density ratios ρ_2/ρ_1. Data normalized by the free stream number density.

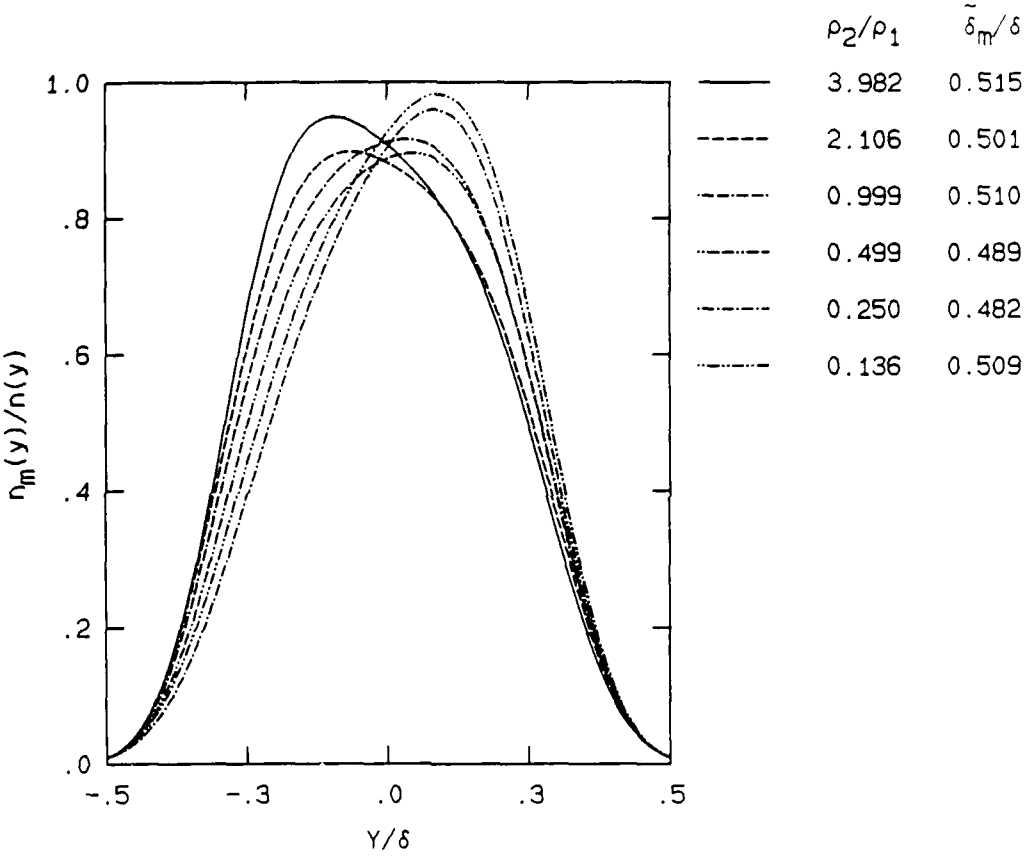

FIGURE 3. Mixed fluid mole fraction profiles, for several free stream density ratios ρ_2/ρ_1. $\tilde{\delta}_m = \int n_m(y)/n(y)\, dy$ (molecularly mixed fluid mean mole fraction).

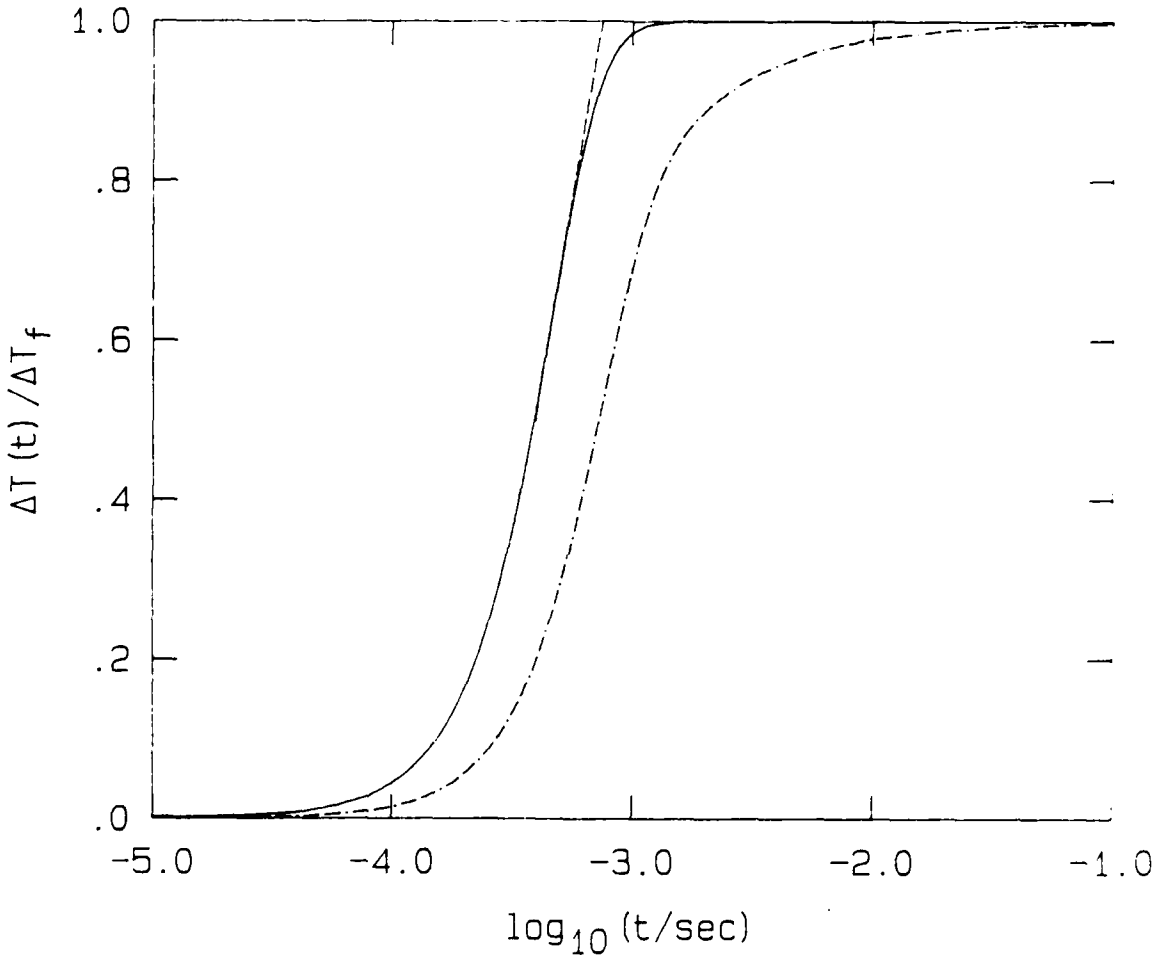

FIGURE 4. Low heat release, $H_2/F_2/NO$ system reactor kinetics. Solid line for constant mass reactor. Dot-dashed line for entrainment-dominated reactor. Intercept of maximum slope (dashed) line with $\Delta T(t)/\Delta T_f = 1$ at $t = \tau_\chi$. High speed stream: 8% H_2, 0.03% NO, 91.97% N_2 @ $T_1 = 293$ K & $M_1 = 0.063$. Low speed stream: 1% F_2, 99% N_2 @ $T_2 = 293$ K & $M_2 = 0.025$.

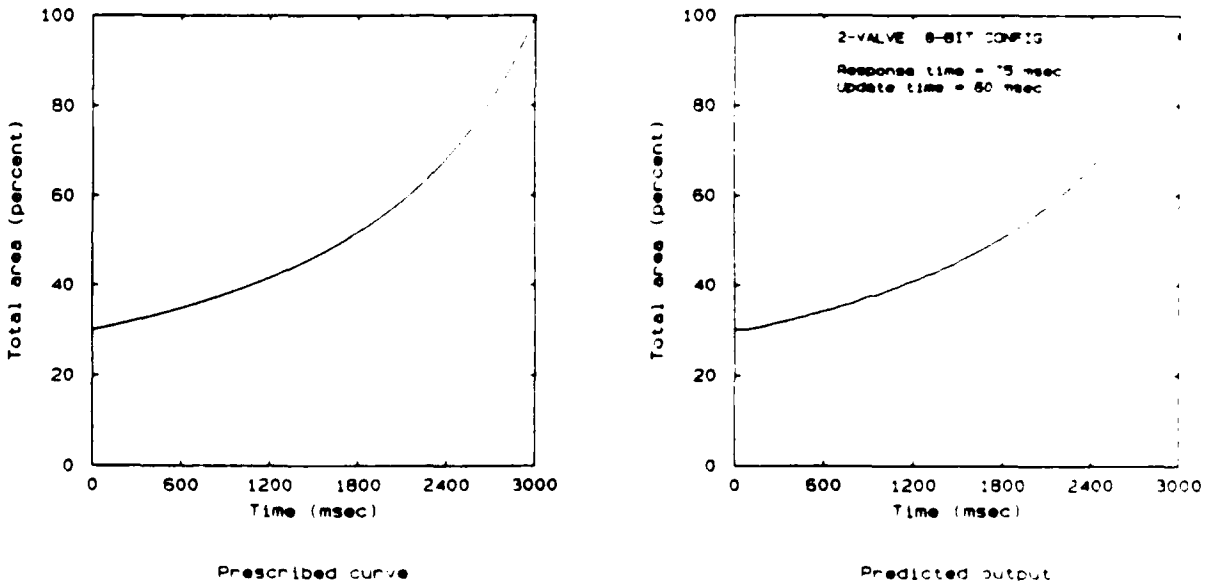

FIGURE 5. Calculated performance of an 8-bit (256 element) digital valve.

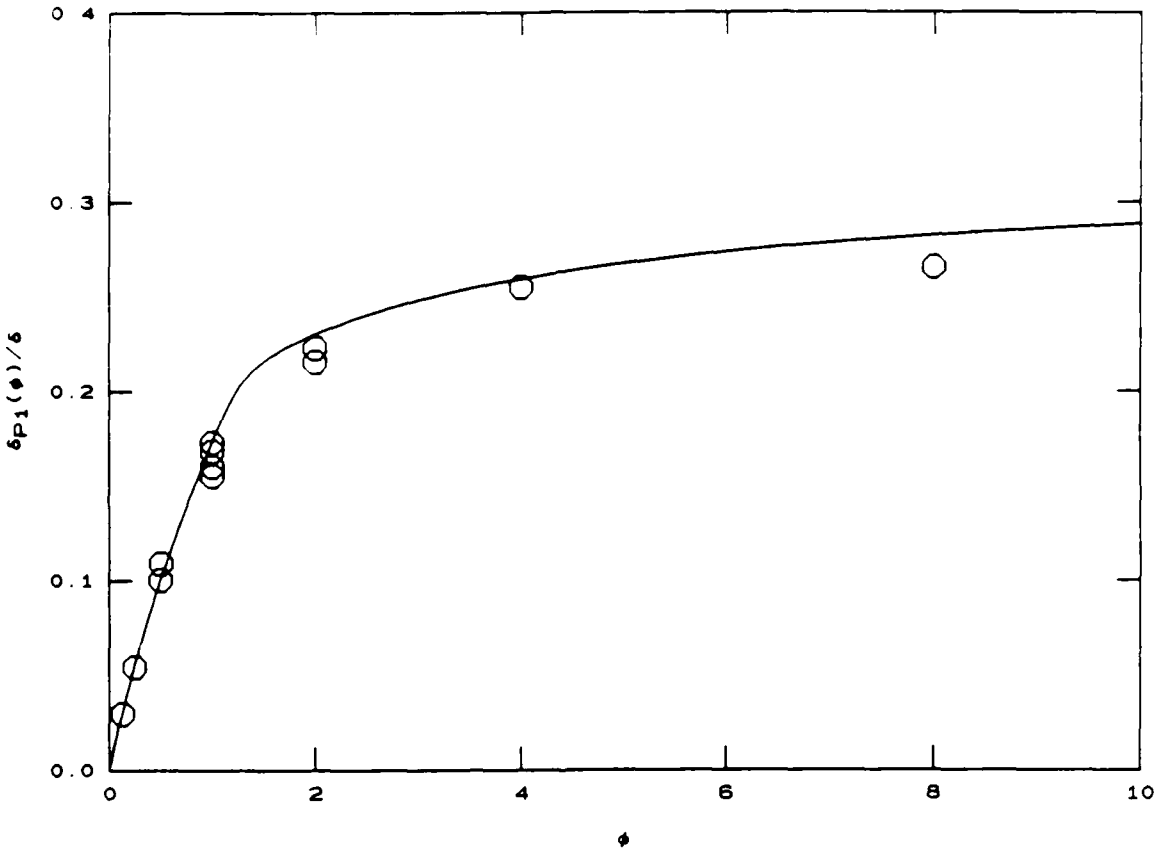

FIGURE 6. Shear layer mixing model (Dimotakis 1987) predictions for gas phase $\delta_{P1}(\phi)/\delta$ chemical product thickness. Data from Mungal & Dimotakis (1984).

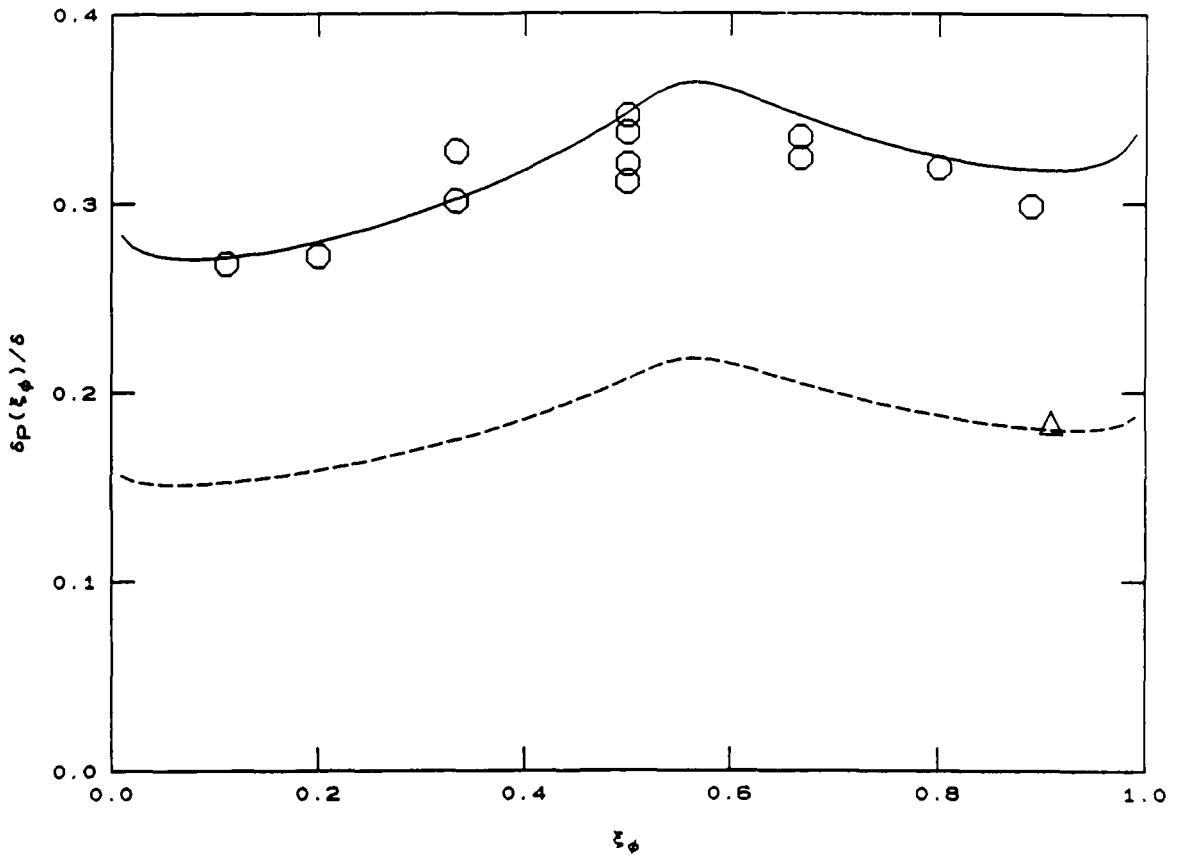

FIGURE 7. Shear layer mixing model (Dimotakis 1987) predictions for $\delta p/\delta$ chemical product volume fraction. Circles from Mungal & Dimotakis (1984) gas phase data. Triangle from Koochesfahani & Dimotakis (1986) liquid phase data at comparable Reynolds number.

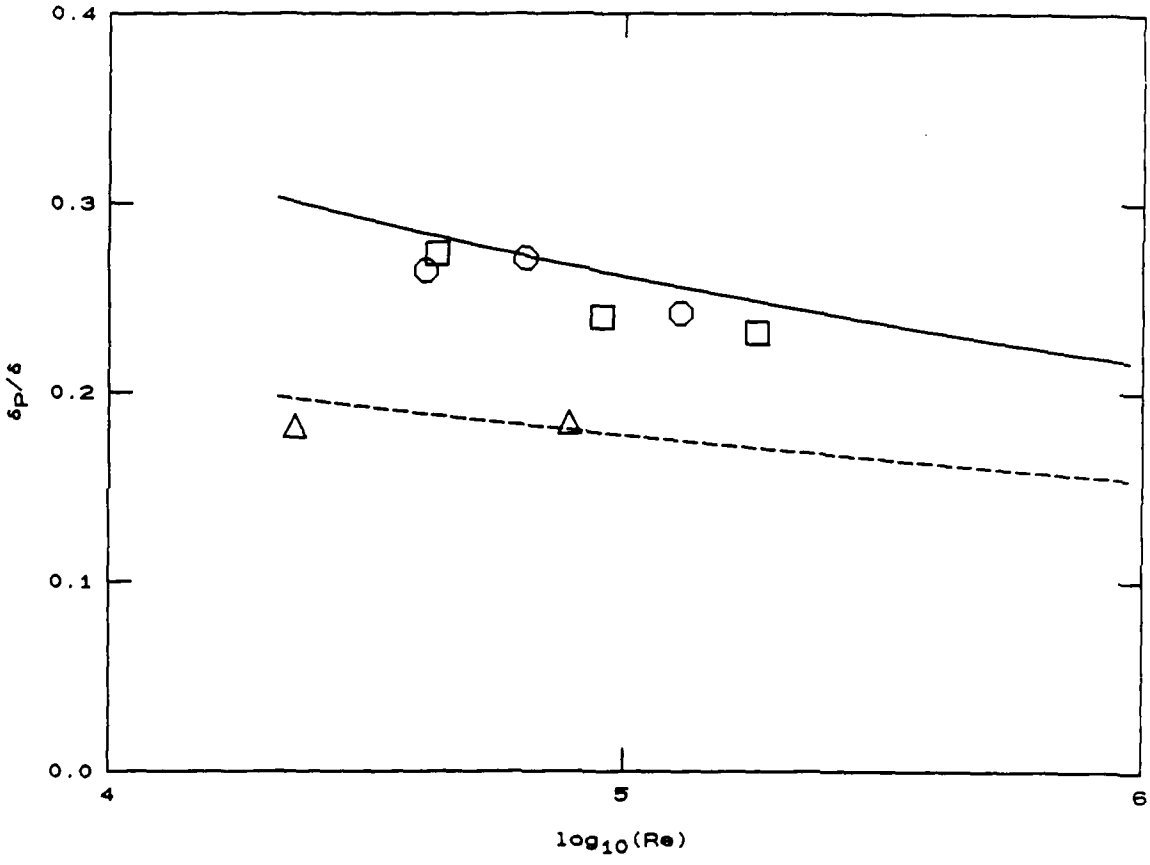

FIGURE 8. Shear layer mixing model (Dimotakis 1987) predictions for dependence of δ_p/δ chemical product volume fraction on Reynolds number. Circles and squares from gas phase measurements of Mungal et al (1985). Triangles from liquid phase measurements of Koochesfahani & Dimotakis (1986).

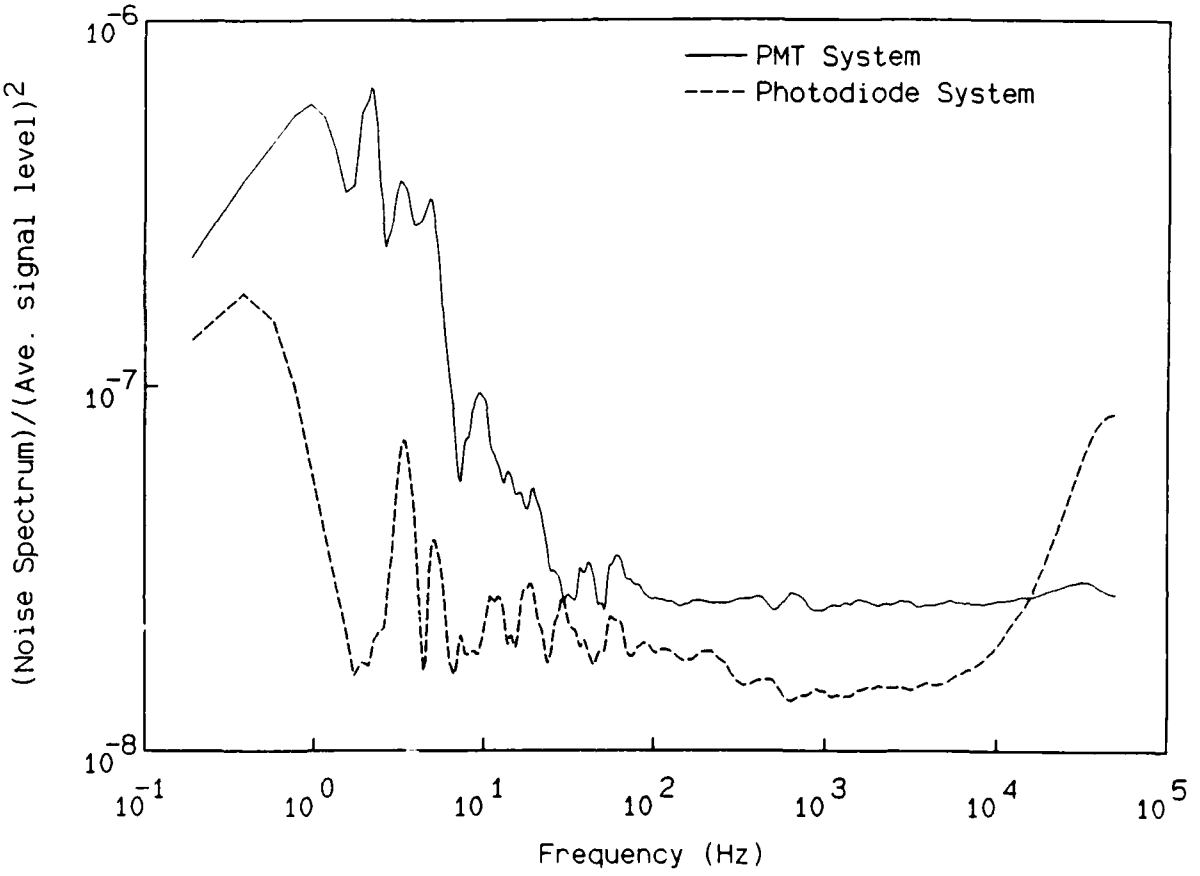

FIGURE 9. The power spectra of the noise from the PMT and Photodiode systems when illuminated by the Rayleigh scattered light from pure argon (15 W Ar^+ laser power).

FIGURE 10. A shadowgraph image of the first 40 diameters of the jet at a Reynolds number of 5,000.

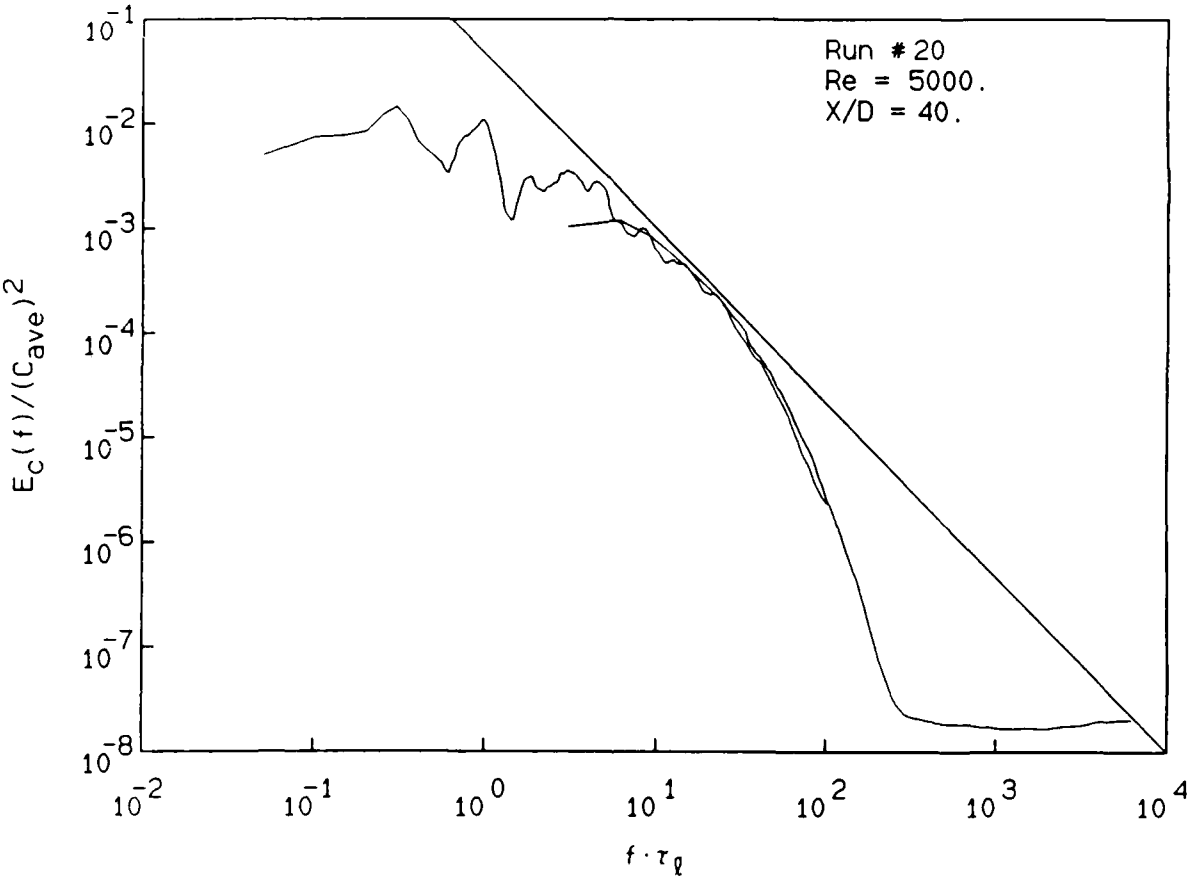

FIGURE 11. Concentration fluctuations power spectrum, 40 diameters downstream on the jet centerline at a Reynolds number of 5,000 ($f_{K\,\tau_\ell} = 1,200$).

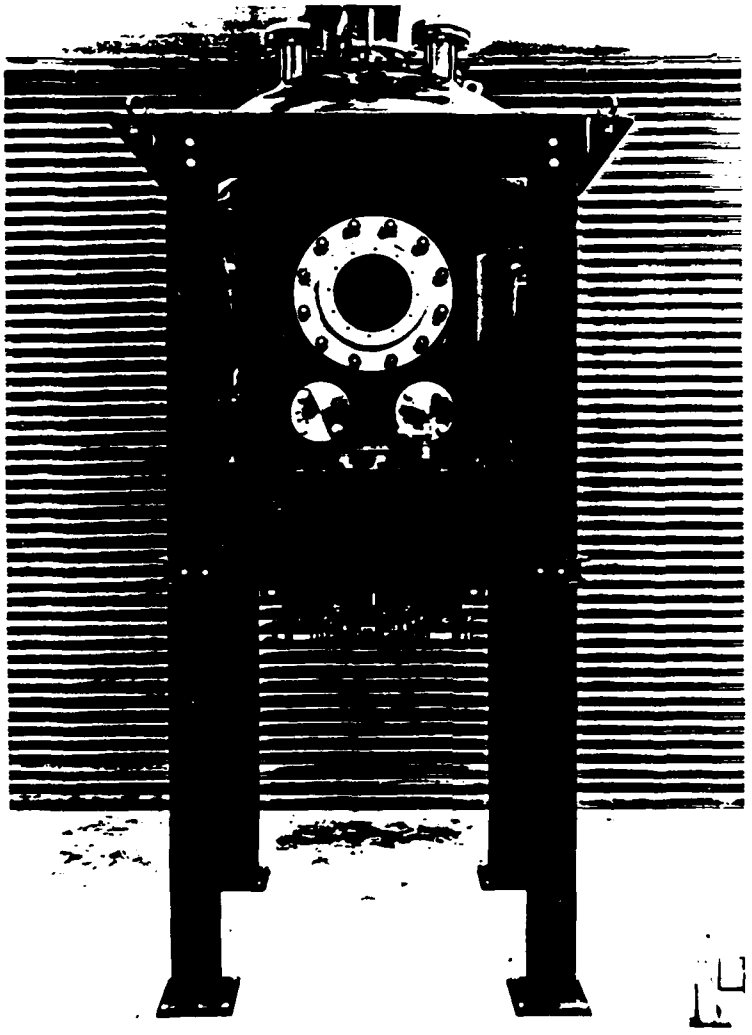

FIGURE 12. High pressure reactant vessel (see section 3.2).

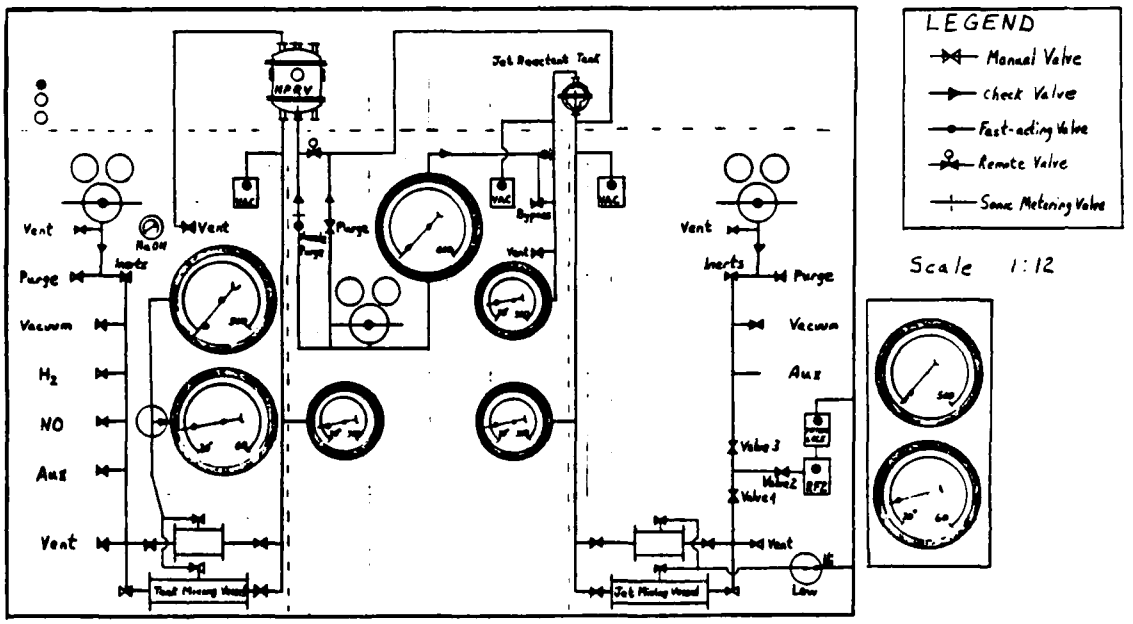

FIGURE 13. High pressure combustion facility control panel schematic.

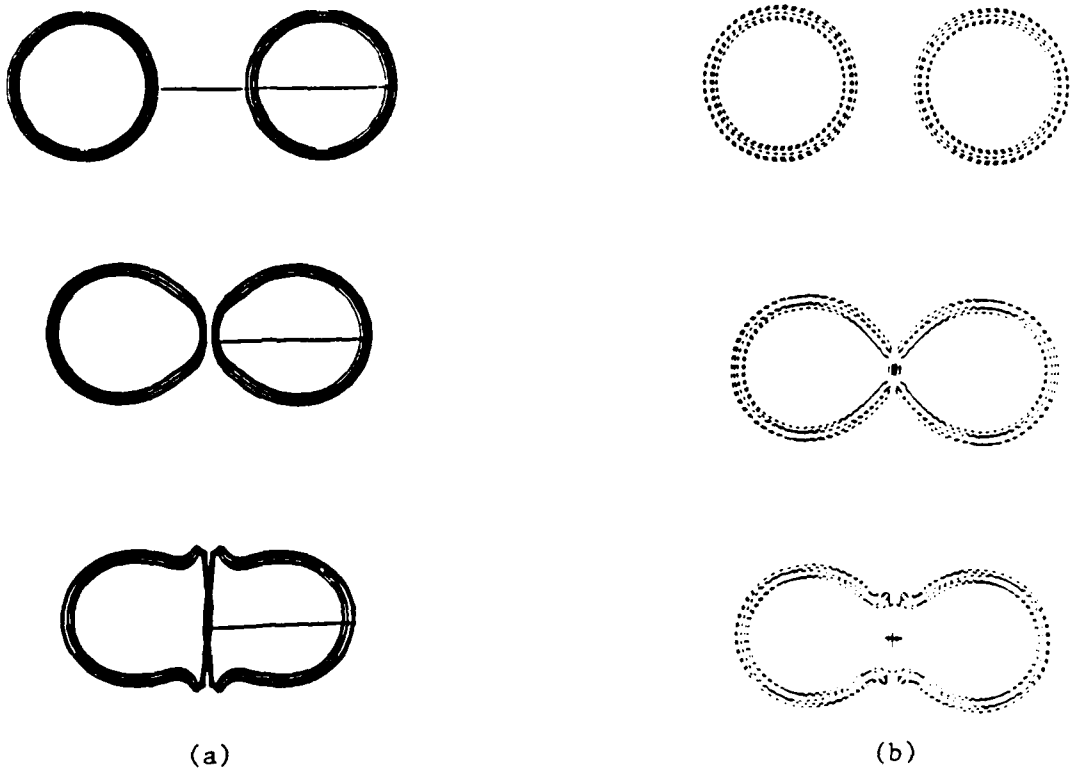

FIGURE 14. Computation of vortex ring merging. (a) vortex filaments, (b) vortex sticks.

Appendix A

AIAA'87

AIAA-87-0047

Inviscid Instability Characteristics of Free Shear Layers with Non-Uniform Density

M.M. Koochesfahani and C.E. Frieler
California Institute of Technology
Pasadena, CA

AIAA 25th Aerospace Sciences Meeting

January 12-15, 1987/Reno, Nevada

INVISCID INSTABILITY CHARACTERISTICS OF FREE SHEAR LAYERS WITH NON-UNIFORM DENSITY

M. M. Koochesfahani* and C. E. Frieler#

California Institute of Technology
Pasadena, California

Abstract

The linear spatial instability characteristics of both uniform and non-uniform density plane mixing layers were investigated taking into account the wake component of the initial velocity profile. Two unstable modes were found. In the shear layer mode, the growth of the unstable disturbance leads to the usual Kelvin-Helmholtz roll-up pattern, whereas in the wake mode, roll-up patterns resemble those in wake flows. It was found that the shear layer mode dominates the wake mode when the density is uniform across the layer. The wake mode, however, can become comparable or even stronger than the shear layer mode if the density of the low-speed stream is larger than that of the high-speed stream. Experimental evidence in support of these findings is provided.

Introduction

The inviscid linear instability of two-dimensional two-stream plane mixing layers has been studied extensively in the past. In the case of uniform density, Michalke[1] investigated the single-stream shear layer, while the effect of the velocity ratio in two-stream mixing layers was considered by Monkewitz & Huerre[2]. Maslowe & Kelly[3] studied stratified (non-uniform density) shear layers and showed that density variations can be destabilizing. In all these studies, the mean velocity profile has been assumed to be monotonically increasing from the value on the low-speed stream to that on the high-speed stream and usually the hyperbolic tangent form is used. It should be noted, however, that under experimental conditions the initial mean velocity profile almost always has a wake component due to the boundary layers on the two sides of the splitter plate. The effect of the wake component has only recently come into consideration with the investigations of Miau[4] and Zhang et al.[5] for the uniform density case.

The purpose of the present work is to study the instability characteristics of both uniform and non-uniform density plane shear layers, whose initial velocity profiles include a wake component. The inviscid, linear, parallel-flow stability analysis of spatially growing disturbances is utilized to numerically calculate the range of unstable frequencies and wave-numbers. The flow patterns resulting from the amplification of the instability are examined by calculating the streaklines and are compared with the experimental flow visualization pictures.

Formulation of the Problem

We consider the general case of a two-stream plane shear layer with U_1, ρ_1 as the free-stream velocity and density on the high-speed stream and U_2, ρ_2 as the corresponding quantities on the low-speed side of the layer. All of the quantities used here are normalized with the average velocity $(U_1+U_2)/2$, average density $(\rho_1+\rho_2)/2$ and the local layer thickness δ as the length scale. Since we are not aware of any exact solutions for the initial evolution of non-uniform density mixing layers with a wake component, we assume that the mean velocity and density profiles have the following forms. The mean velocity profile is composed of the usual hyperbolic tangent profile plus a wake component (due to the splitter plate) represented by a Gaussian distribution and has the form

$$U(y) = 1 + \lambda_U \tanh(y) - W e^{-y^2} \qquad (1)$$

where $\lambda_U = (U_1-U_2)/(U_1+U_2)$ and W is the normalized wake deficit. The mean density profile has a hyperbolic tangent profile and is given by

$$\rho(y) = 1 + \lambda_\rho \tanh[(y-y_s)/\sigma] \qquad (2)$$

where $\lambda_\rho = (\rho_1-\rho_2)/(\rho_1+\rho_2)$ and y_s and σ adjust the lateral position and thickness of the density profile relative to the velocity profile.

The disturbance stream function is written in the form

$$\psi = \phi(y)\, e^{i(\alpha x - \beta t)} \qquad (3)$$

where $\alpha = \alpha_r + i\alpha_i$ is the complex non-dimensional wave-number and β is the non-dimensional frequency

* Present address: Department of Mechanical Engineering, Michigan State University, East Lansing, Michigan 48824. Member AIAA.
# Graduate Student, Aeronautics.

which is taken as pure real for the present spatial calculations. In the case of two-dimensional incompressible flow with negligible buoyancy effects (i.e. gravity is ignored), it can be shown that the disturbance eigenfunction ϕ satisfies the equation

$$\phi'' + (\rho'/\rho)\,\phi' - \left[\alpha^2 + \frac{U'' + \rho' U'/\rho}{U-\beta/\alpha}\right]\phi = 0 \qquad (4)$$

where $(\,)'$ corresponds to d/dy. The equation above reduces to the Rayleigh equation when the density is uniform. A "shooting" technique was used to solve this eigenvalue equation with the boundary conditions

$$\phi(y \to \pm\infty) = e^{\mp\alpha y}. \qquad (5)$$

Equation 4 was integrated from both sides toward $y = 0$ and the matching of ϕ and ϕ' at this point yielded the spatial growth rate, $-\alpha_i$, of unstable disturbances and the corresponding wave-number, α_r, versus frequency β.

The flow patterns resulting from the amplification of the instability were determined from streakline calculations. The procedure for this calculation, which is essentially the same as that used by Michalke[1], is outlined below. The perturbation velocities are given by

$$u(x,y,t) = \text{Real}\{\partial\psi/\partial y\},$$
$$v(x,y,t) = \text{Real}\{-\partial\psi/\partial x\}, \qquad (6)$$

where ψ is given by equation 3 and ϕ is known from the solution of equation 4 for a specific set of eigenvalues (α, β). The motion of each fluid particle is then given by

$$dx/dt = U(y) + \epsilon\, u(x,y,t),$$
$$dy/dt = \epsilon\, v(x,y,t), \qquad (7)$$

with the initial conditions $x(t=0) = x_0$ and $y(t=0) = y_0$. In equation 7, $U(y)$ is the undisturbed mean profile (equation 1) and ϵ is a measure of the initial magnitude of the disturbance. For the streaklines shown in the present work, x_0 was selected to be zero with $\epsilon = 0.0005$. Calculations were made by integrating equation 7, at different starting y locations, forward in time using the Euler method.

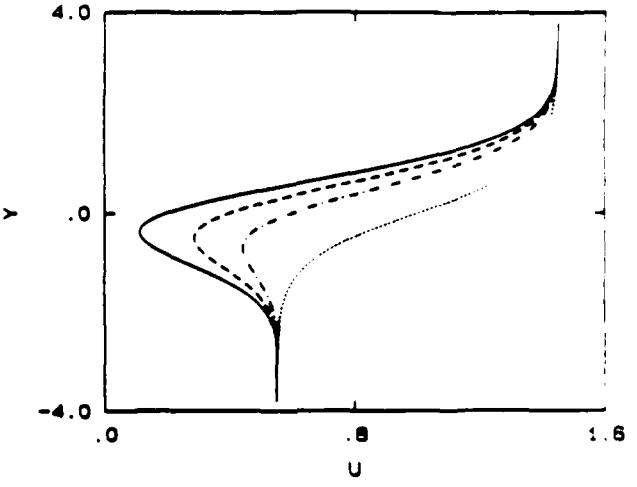

Fig. 1 Mean velocity profiles for different values of W, $\lambda_u = 0.45$ ($U_2/U_1 = 0.38$). ····· W = 0, tanh profile; ----- W = 0.4; ----- W = 0.6; —— W = 0.8.

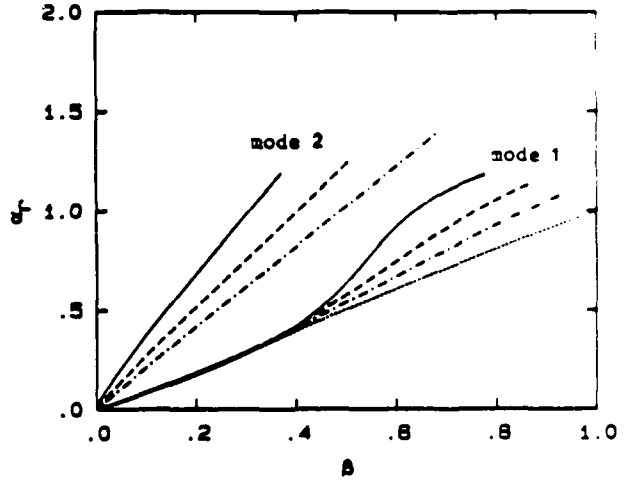

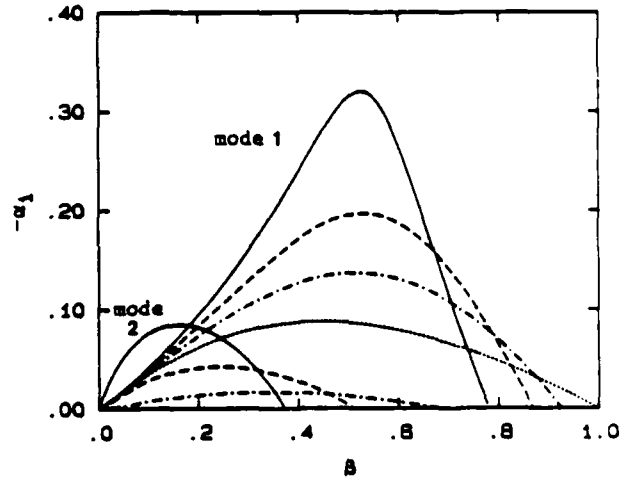

Fig. 2 Instability characteristics of the mean profiles in figure 1, uniform density. For legend see figure 1.

Results and Discussion

Uniform Density

The spatial instability characteristics of the shear layer with a wake component were calculated for a fixed velocity ratio as a function of the depth of the wake deficit (see the mean velocity profiles in figure 1). These profiles can be thought of as representing the evolution of the mean profile due to viscous diffusion. Starting near the splitter plate tip, a profile with a large wake deficit develops, as it convects downstream, into one with no wake component. The main result, shown in figure 2, is that when the wake component is present, there are <u>two</u> unstable modes as opposed to one in the case of the hyperbolic tangent profile. Consistent with previous results[5], as the wake deficit increases, the neutral point of mode 1, the stronger mode, moves to lower frequencies and its maximum amplification rate increases. We point out that the existence of mode 2, the weaker mode, has been known from the work of Miksad[6]. His results, however, were based on temporal stability calculations. Note, from figure 2, that in the limit of zero wake component, mode 1 approaches the tanh profile solution while mode 2 vanishes.

The set of profiles in figure 3 were used to calculate the behavior of the solution in the limit of unity velocity ratio, namely the case of pure wake. Results shown in figure 4 indicate that, in this limit, the two modes of instability still persist. In the limit of pure wake, examination of the eigenfunctions (not shown here) revealed that modes 1 and 2 approach the "sinuous" and "varicose" modes, respectively, of wake instability (e.g. see the wake stability solutions of Mattingly & Criminale[7]).

Streaklines were calculated in order to examine the flow patterns that would result from the amplification of the unstable disturbance in each of the two modes (see the previous section for details). Calculations were performed only for the case of maximum amplification rate. The integration proceeded until the first structure roll-up appeared. The results are illustrated in figures 5 and 6. We emphasize that the calculated streaklines are only intended to provide a qualitative description of shear layer roll-up patterns. Non-parallel flow and nonlinear effects are absent in these results.

The flow patterns in the case of the tanh profile, figure 5, are similar to those calculated by Michalke[1] (for U_2=0 shear layer) and show the familiar roll-up of the shear layer into a vortex. Figure 6 depicts the streaklines for the two modes

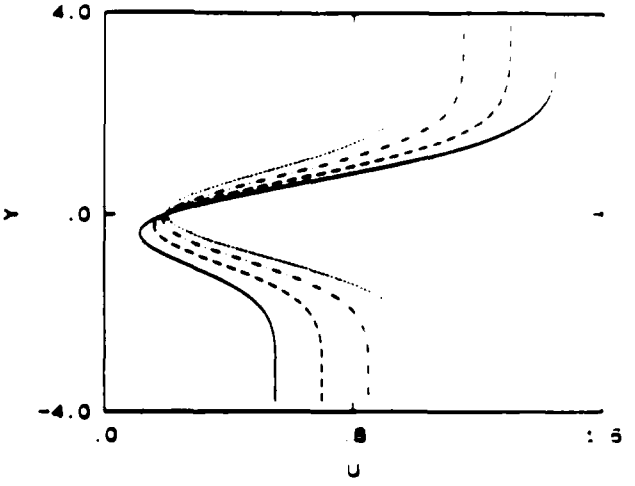

Fig. 3 Mean velocity profiles for different values of λ_u, W = 0.8.
···· λ_u = 0.0, pure wake; ----- λ_u = 0.15;
---- λ_u = 0.30; —— λ_u = 0.45.

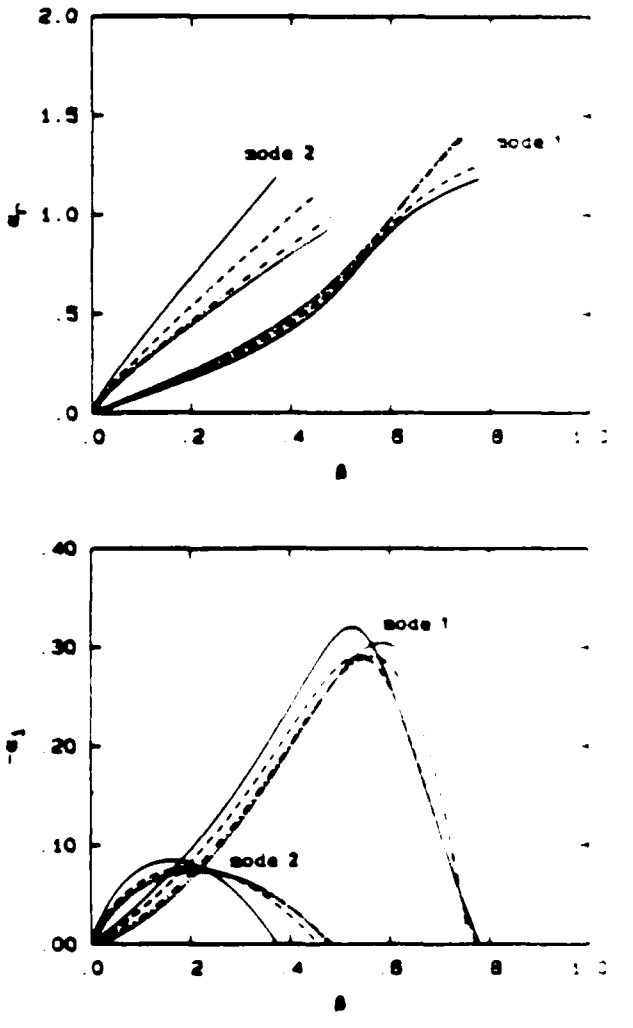

Fig. 4 Instability characteristics of the mean profiles in figure 3, uniform density. For legend see figure 3.

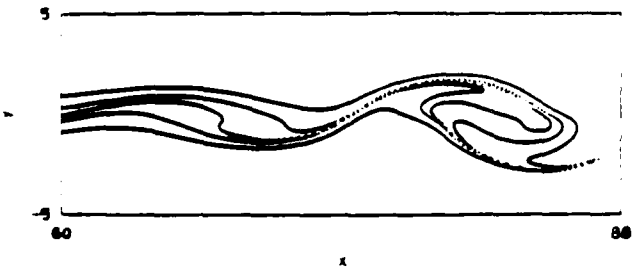

Fig. 5 Streaklines for uniform density tanh profile, $\lambda_\theta = 0.45$.

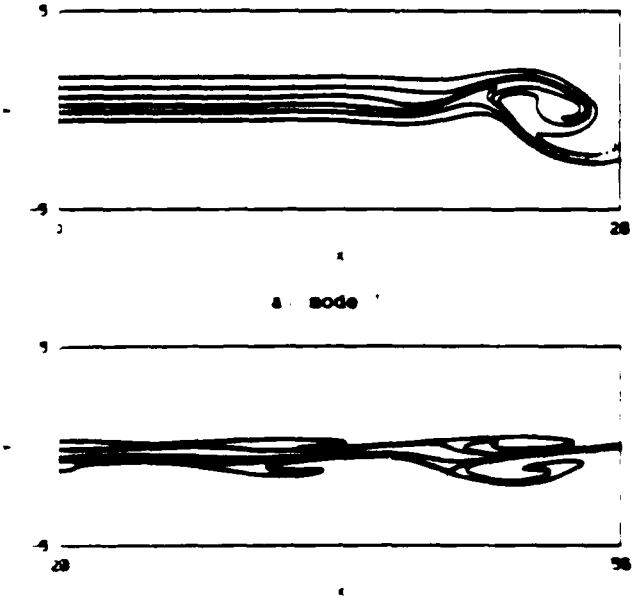

a. mode 1

b. mode 2

Fig. 6 Streaklines for uniform-density shear layer with wake component, $\lambda_\theta = 0.45$, $d = 0.8$.

of instability when the wake component is present. We note that the amplification of mode 1 leads to the usual Kelvin-Helmholtz type shear layer roll-up, whereas the mode 2 roll-up patterns resemble a wake flow. We, therefore, refer to modes 1 and 2 as the "shear layer" and "wake" modes, respectively. The wake mode, in the uniform density case, is very difficult to observe experimentally since its amplification rate is much less than that of the shear layer mode through most of the unstable frequency range (see figure 2).

Non-Uniform Density

In investigating the effect of non-uniform density, a specific velocity profile with $\lambda_\theta = 0.45$, $U_2/U_1 = 0.38$, and a wake deficit of $d = 0.8$ was selected. We are particularly interested in the case of low-speed stream having the higher density. The density profile was

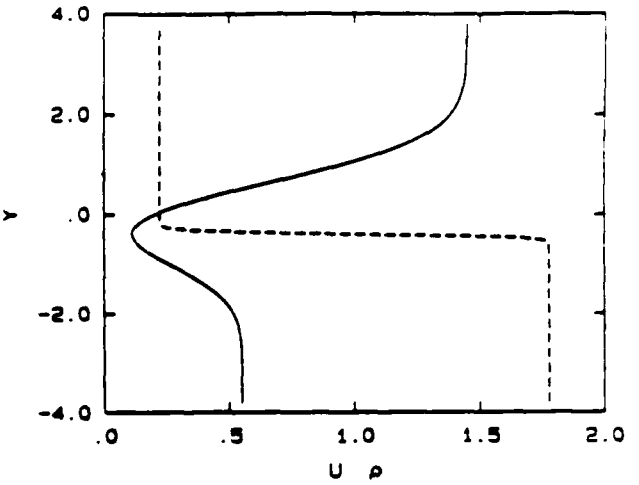

Fig. 7 Mean velocity and density profiles, $\lambda_U = 0.45$, $\lambda_\rho = -0.78$ ($\rho_2/\rho_1 = 8$), $1/\sigma = 16$.

arranged to have its inflection point at the minimum of the velocity profile and its thickness much smaller (in equation 2, $1/\sigma = 16$) than that of the velocity profile, see figure 7. These conditions are expected to hold in the initial region of the flow near the splitter plate tip. The qualitative features of the results are not sensitive to these conditions as long as the density profile is "reasonably" thin relative to the velocity profile. See also the next section. Calculations were performed for $\rho_2/\rho_1 = 8$ ($\lambda_\rho = -0.78$). The case of high-density high-speed stream ($\rho_2/\rho_1 = 1/8$, $\lambda_\rho = +0.78$) was also calculated for comparison.

The most important result, see figure 8, is that when the high density is on the low-speed side, the two instability modes have similar amplification rates. In fact, the normally weak wake mode in the case of uniform density, now has a slightly larger growth rate than the shear layer mode. The corresponding streaklines (at maximum amplification rate) for these two modes, figure 9, again illustrate the shear layer and wake type roll-up patterns. We also note, from figure 8, that having the high density on the high-speed stream does not alter the relative significance of the two instability modes compared to the uniform-density shear layer.

The findings described above imply that, depending on the spectrum of the disturbances in the flow and the extent of the persistence of the wake component in the downstream region, a shear layer of non-uniform density may not roll up like the usual Kelvin-Helmholtz structures but more like a wake. These results also suggest that, under the right flow conditions, both shear layer and wake modes of instability may exist simultaneously and interact with each other.

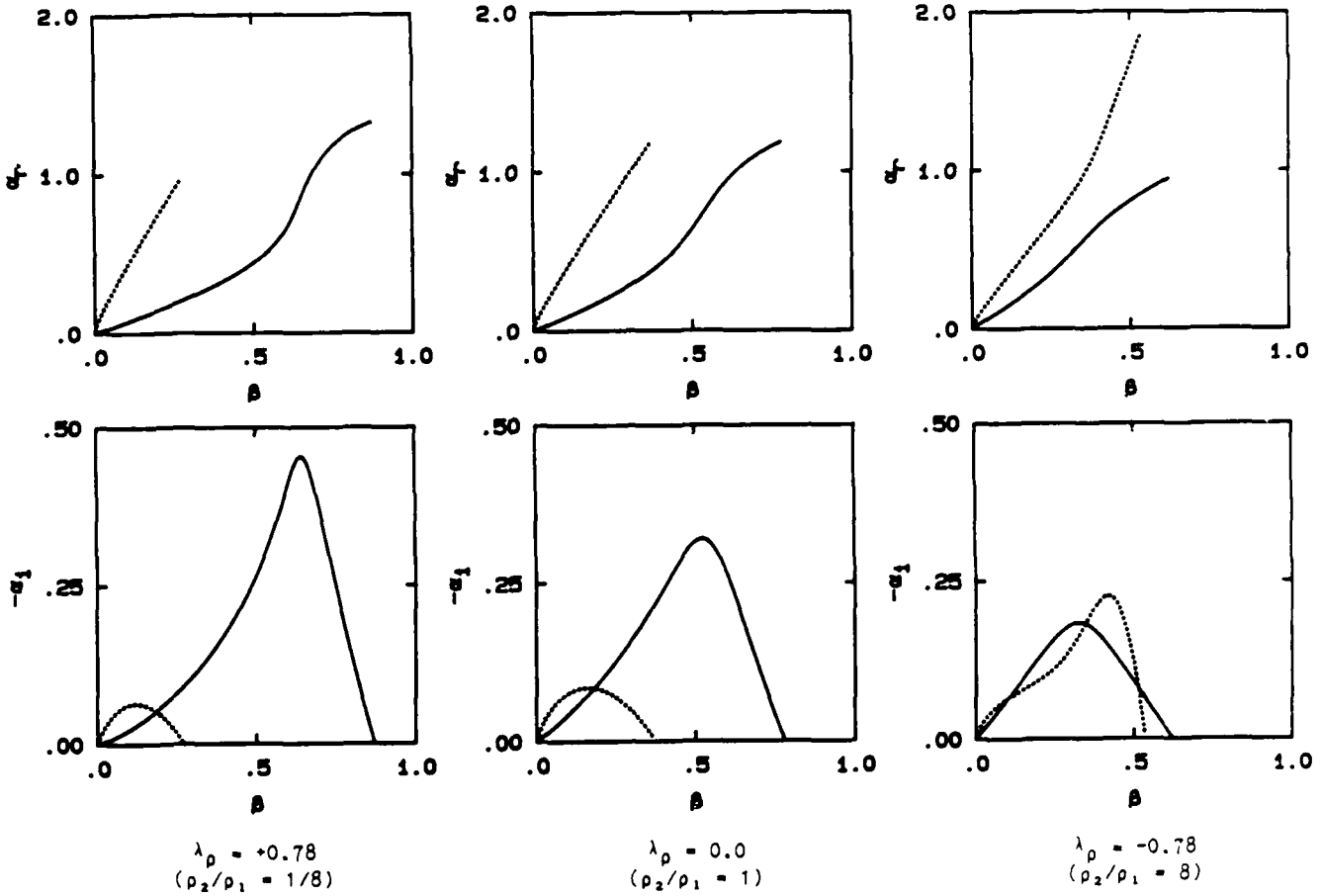

Fig. 8 Instability characteristics for non-uniform density.
—— shear layer mode, ····· wake mode

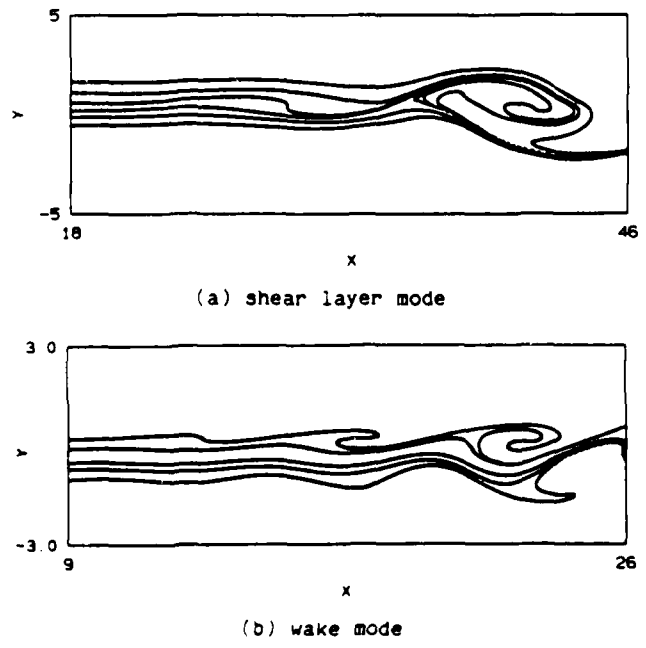

Fig. 9 Streaklines in non-uniform density shear layer with wake component, λ_ρ = -0.78 (ρ_2/ρ_1 = 8).

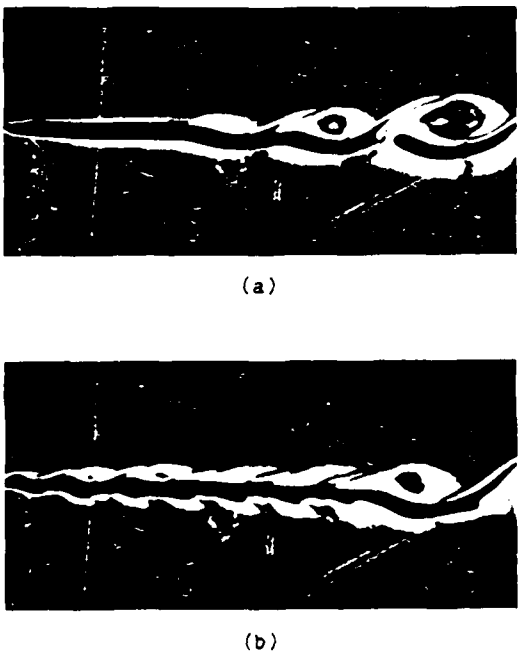

Fig. 10 Schlieren photographs of the shear layer mode (a) and the wake mode mode (b). Flow is from left to right with high-speed stream on top (U_2/U_1 = 0.38, ρ_2/ρ_1 = 10).

Since the shear layer and wake modes can be equally strong when the low-speed stream has the high-density fluid, an attempt was made to experimentally observe these modes. A shear layer ($U_2/U_1 = 0.38$) between a high-speed stream of Helium and low-speed stream of Argon ($\rho_2/\rho_1 = 10$) was forced acoustically. The flow visualization by Schlieren photography, figure 10, shows that both shear layer and wake modes can be generated in a two-stream mixing layer. Note that the wake mode pattern, in figure 10(b), appears to approach that of the shear layer mode toward the right side of the photograph. This is to be expected, since as the flow moves downstream the wake component of the velocity profile ultimately vanishes and only the shear layer instability mode remains.

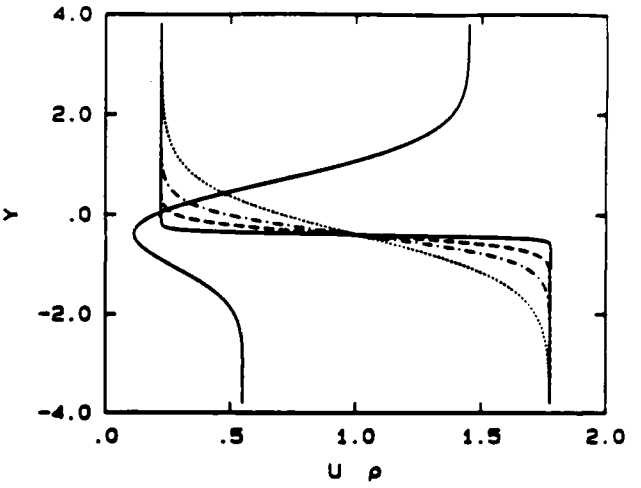

Fig. 11 Mean velocity and density profiles for different values of σ, $\lambda_u = 0.45$, $W = 0.8$, $\lambda_\rho = -0.78$ ($\rho_2/\rho_1 = 8$).
····· $\sigma = 1$; ----- $\sigma = 1/2$; -·-·- $\sigma = 1/4$; —— $\sigma = 1/16$.

Effect of the Density Profile Thickness

The case of uniform density can be considered to be equivalent to that of non-uniform density with a very large (in fact, infinite) thickness relative to the mean velocity profile. A question, then, remains as to how a weak wake mode in a uniform-density shear layer transforms into one equally strong as the shear layer mode when the high-density fluid is carried on the low-speed side. To shed some light on this question, the instability characteristics of the non-uniform density shear layer were calculated as a function of the density interface thickness (i.e. σ was varied in equation 2). The mean velocity and sample density profiles are shown in figure 11. The results, see figure 12, illustrate that the density profile thickness must be smaller than a certain value before the wake mode becomes dominant. For these particular profiles, for example, it is required that the thickness of the density profile be at least 2.9 times smaller than the thickness of the velocity profile. On the other hand, when the high-density fluid is on the high-speed side, regardless of the density profile thickness (lowest value calculated was $\sigma = 1/16$), the shear layer mode of instability was found to be always dominant.

An interesting feature in figure 12 is that the appearance of a strong wake mode, between $\sigma = 1/2.8$ and $1/2.9$, seems to be a resonance phenomenon. This "repelling" of two otherwise

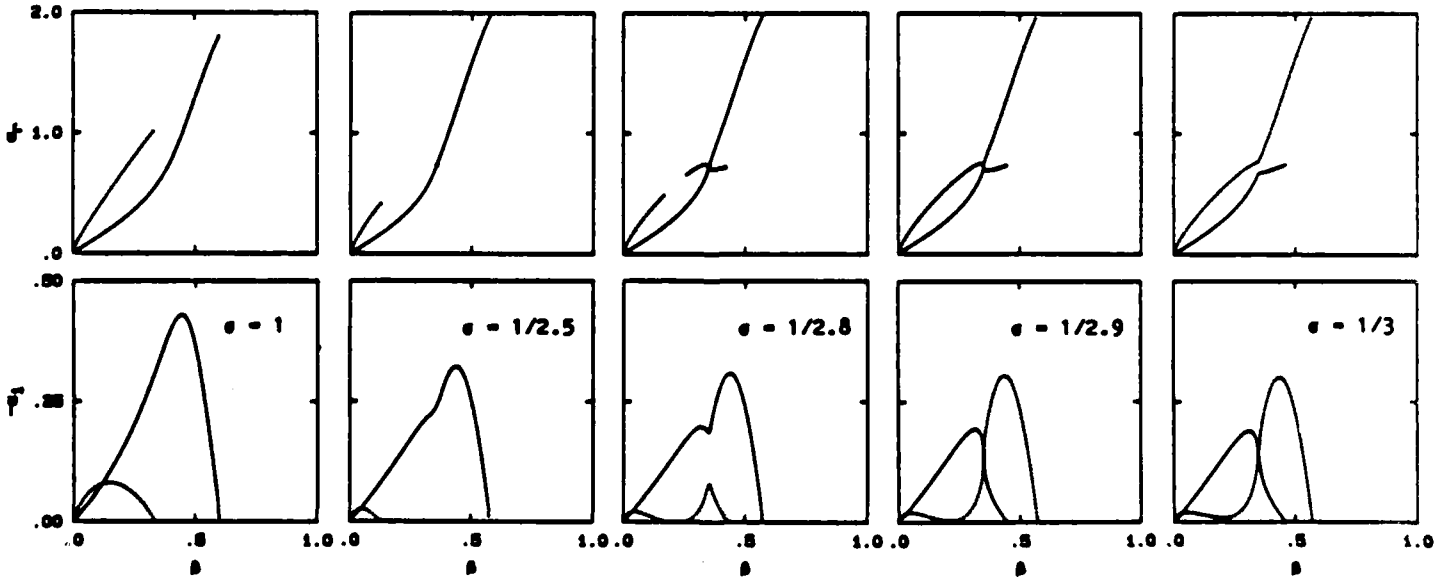

Fig. 12 Effect of the density profile thickness on the instability characteristics, $\lambda_u = 0.45$, $W = 0.8$, $\lambda_\rho = -0.78$ ($\rho_2/\rho_1 = 8$).
—— shear layer mode, ····· wake mode

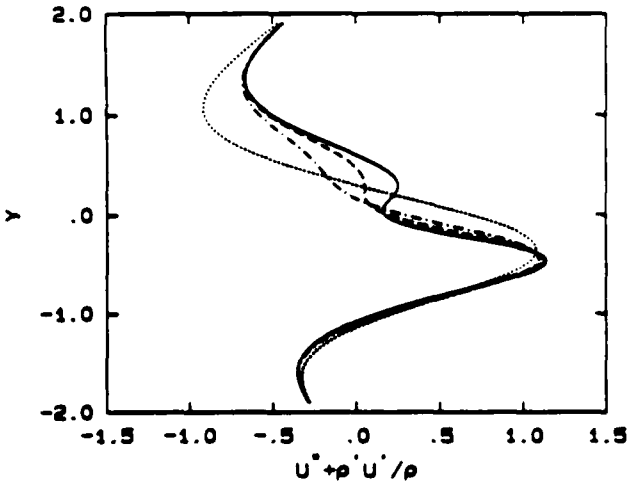

Fig. 13 Shape of $(U'' + \rho'U'/\rho)$ profile for different density profile thicknesses.
····· $\sigma = 1$; -·-·- $\sigma = 1/2$; ----- $\sigma = 1/2.5$; —— $\sigma = 1/3$.

identical eigenvalues is thought to be similar to the "Eckart" resonance[8], which is the quantum-mechanical analog of the problem of two potential minima and the penetration of the potential barrier between them. In comparison with the Eckart resonance phenomenon, it seems that the behavior of the term $(U'' + \rho'U'/\rho)$ in equation 4, in particular the presence of two maxima in its profile, is the determining factor. A plot of this term as a function of σ, see figure 13, shows the appearance of two maxima close to the value of σ where the resonance occurs (see figure 12).

Conclusions

The instability characteristics of uniform and non-uniform density plane shear layers were investigated. The mean velocity profile included a wake component in order to take account of the effect of the boundary layers on the two sides of the splitter plate. The range of unstable frequencies and wave-numbers and the flow patterns resulting from the amplification of the instability were calculated using the inviscid, linear, parallel-flow, spatial stability analysis.

It was found that the shear layer with a wake component has two unstable modes. The growth of the unstable disturbance, in the shear layer mode, results in the usual Kelvin-Helmholtz roll-up patterns, while in the wake mode, the flow patterns resemble a wake structure. When the density is uniform, the amplification rate of the wake mode is dominated by that of the shear layer mode. If the low-speed stream carries the high-density fluid, however, the two modes can become comparable in amplification rate. The opposite arrangement with the high-density fluid on the high-speed side behaves similar to the uniform density case in that the shear layer mode remains the dominant mode. Schlieren flow visualization pictures of a shear layer between a high-speed stream of a light gas (Helium) and a low-speed stream of a heavy gas (Argon) confirmed that both modes of instability could be excited experimentally. For the wake mode to become dominant, the thickness of the density profile, relative to the velocity profile thickness, must be smaller than a certain value. The onset of a strong wake mode, as the density profile thickness is reduced, appears to exhibit a resonance phenomenon. It is believed that this behavior is similar to the "Eckart" resonance.

Acknowledgements

We are greatly indebted to Professor Toshi Kubota who is an unofficial co-author of this paper. He always had the answers to our questions and the time to discuss ideas. Also, the constant interest in this problem by Professor Paul Dimotakis and the late Professor Lester Lees is much appreciated. This work was supported by the Air Force Office of Scientific Research Grant No. AFOSR-83-0213.

References

1. Michalke, A., "On Spatially Growing Disturbances in an Inviscid Shear Layer.", J. Fluid Mech. 23(3), 1965, pp. 521-544.

2. Monkewitz, P. A. and Huerre, P., "Influence of the Velocity Ratio on the Spatial Instability of Mixing Layers.", Phys. Fluids 25(7), 1982, pp. 1137-1143.

3. Maslowe, S. A. and Kelly, R. E., "Inviscid Instability of an Unbounded Heterogeneous Shear Layer.", J. Fluid Mech. 48(2), 1971, pp. 405-415.

4. Miau, J-J., "An Experimental Study on the Instability of a Mixing-Layer with Laminar Wake as the Initial Condition.", Ph.D. thesis, Brown University, 1984.

5. Zhang, Y-Q, Ho, C-H. and Monkewitz, P., "The Mixing Layer Forced by Fundamental and Subharmonic.", LAMINAR-TURBULENT TRANSITION, Proc. IUTAM Symp., Novosibirsk, USSR, July 9-13, 1984, Springer-Verlag, pp. 385-395.

6. Miksad, R. W., "Experiments on the Nonlinear Stages of Free-Shear-Layer Transition.", J. Fluid Mech. 56(4), 1972, pp. 695-719.

7. Mattingly, G. E. and Criminale, W. O., "The Stability of an Incompressible Two-Dimensional Wake.", J. Fluid Mech. 51(2), 1972, pp. 233-272.

8. Eckart, C., "Internal Waves in the Ocean.", Phys. Fluids, 4(7), 1961, pp. 791-799.

Appendix B

Caltech Pressure Vessel 26-May-87 Specifications

The following represents a listing of the Caltech Pressure Vessel Specifications:

1. The internal tank volume must be in the range of 1.2 m^3 to 1.3 m^3 (42 ft^3 to 44 ft^3).

2. The working pressure range is vacuum to 10^7 Pa (vacuum to 1500 psi).

3. The working temperature range is 273 K to 615 K (32^oF to 650^oF).

4. The working gases are (dry) H_2, NO, N_2, He, Ar.

5. The tank material is carbon steel. The preferred type is SA516-70.

6. The tank geometry is cylindrical with 2:1 semi-elliptical end caps (refer to the attached sketch for clarification).

7. One of the end caps shall be removable. This will require a flanged connection as depicted in the attached sketch.

8. Nominal access to the tank is via two 0.1 m (4.0 in) diameter weld neck flanges, one at either end.

9. The outer diameter of the tank is 0.91 m (3.0 ft).

10. The maximum flange face to flange face height of the tank is 2.75 m (9.0 ft).

11. The interior of the tank shall be packed in the following manner: Vertical rolls of aluminum mesh screen shall fill the cylindrical portion of the tank, except for the cross-section occupied by a central alignement tube and necessary clearances between the packing rolls and the internal tank walls.

12. The aluminum rolls are to be supported by three stainless steel grates, one at either end and one in the middle. These grates are to be bolted to mounting rings which are in turn welded to the inner wall of the tank.

13. Caltech will supply the aluminum screen and the central alignment tube. The tank manufacturer will be responsible for the packing supports and the overall assembly.

14. The tank is to be mounted vertically on top of a skirt. The skirt must have four 0.45 m (18 in) circular holes cut into it aligned in a cross fashion. The skirt will have a connecting

ring welded to its bottom which is suitable for bolting the tank assembly to the floor. The height of the centers of these holes is to be agreed upon at the time of manufacture.

15. The exterior of the tank is to be wrapped with 12 electrical heating tape elements. Separate electrical connector pairs shall be provided for each element through the insulation (see below). Two thermocouples will be mounted for each heating element (for a total of 24) on the tank exterior wall, with electrical connection pairs again made accessible through the insulation material. Caltech will provide the heating tape elements and thermocouples, which will be selected in consulation with the tank manufacturer. Total heating power shall be in the range 8 kW to 10 kW.

16. The exterior of the tank is to be insulated in such a fashion that there are no exposed surfaces. The outside temperature of the insulation shall not exceed ambient room temperature by more than 10 K ($18^{o}F$) when the tank interior is at its maximum temperature of 615 K ($650^{o}F$).

17. The tank assembly will be stress relieved.

18. The interior of the tank is to be sandblasted clean after stress relieving.

19. The hydro test is to be conducted in the prescence of Caltech representatives and will follow a mutually agreed upon procedure.

20. After final assembly, the tank is to be purged with nitrogen and shipped with a slight nitrogen atmosphere overpressure.

21. The tank manufacturer shall be responsible for shipping costs to Caltech.

22. The tank is to be certified by the manufacturer according to the ASME code and any applicable local codes. In particular, this certification must cover:

    a. tank operation at the specified temperature and pressure range, and

    b. the use of hydrogen as a working gas at the specified maximum temperature.

    In addition,

    c. the tank, the skirt support structure and the mounting provisions shall be certified by the manufacturer to one and a half times the local earthquake code specifications.

Any deviations from these specifications should be agreed upon prior to the submission of bids.

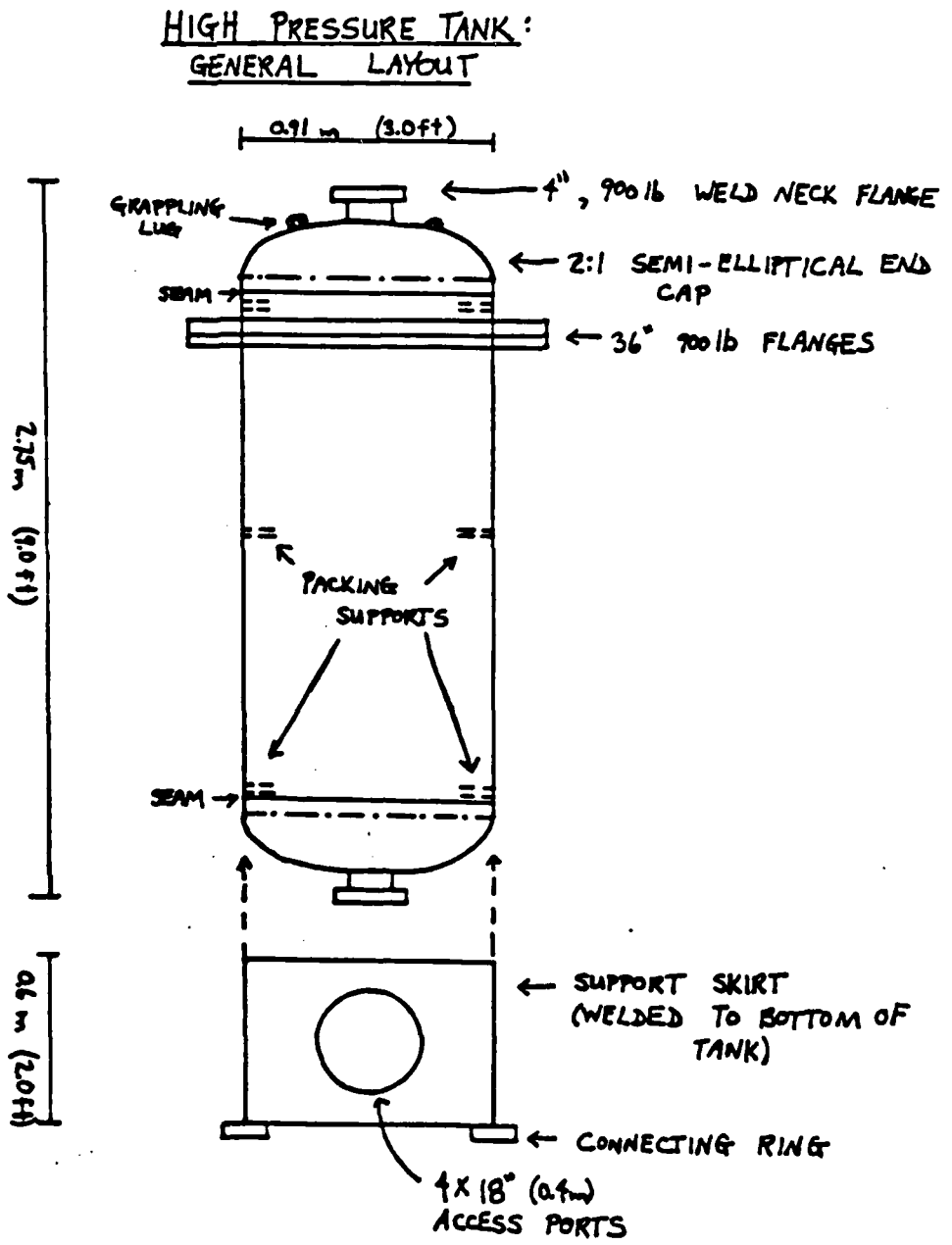

Appendix C

COMBUSTION AND FLAME 67: 9–26 (1987)

Laser Soot-Scattering Imaging of a Large Buoyant Diffusion Flame

RICHARD C. MIAKE-LYE

Graduate Aeronautical Laboratories, California Institute of Technology, Pasadena, CA 91125

and

STEPHEN J. TONER

Department of Mechanical Engineering, California Institute of Technology, Pasadena, CA 91125

A novel diagnostic technique, which makes use of laser light scattered by soot particles, was used in an effort to identify the flame sheets within a natural gas diffusion flame. Soot particles, inherently created and consumed in the flame, were used as the scattering medium, which obviated the need for externally supplied seed material. Since no foreign material was added to the flame, the current technique can be considered truly nonintrusive. The soot distribution within a large buoyant natural gas diffusion flame is argued to be a reasonable marker of the flame sheets. Measurements made in 47.4–190 kW natural gas flames stabilized on a 0.5 m diameter burner show that the flame sheets are highly wrinkled and convoluted surfaces. The flame sheets are distributed fairly uniformly within the instantaneous volume of the flame, based on images of the associated soot, and the instantaneous flame volume is devoid of soot for 40–60% of the time. When soot is present, it is observed as thin sheets which become narrower in regions where the average strain rate is estimated to be greater.

INTRODUCTION

The complex internal flow field produced by a large diffusion flame in the region in which rapid heat release occurs is not yet well understood. Visual studies of the flame luminosity have been useful in studying some phenomena, such as the flame height and the unsteady "puffing" characterizing many of these flames [1, 2]. However, these methods do not allow visualization of the often complex internal flows which are relevant to the entrainment rate and heat release rate in the flame, nor do they suggest a sufficiently detailed model required for calculation of radiant flux to the fuel beds. More recently, laser lighting has been used effectively to study flows in which combustion is an important feature [3]. In these cases, particles are used as markers for the fuel, oxidizer, or products. The particles may be created or destroyed in the reaction, or may be unaffected by the combustion region. These methods require either upstream seeding or auxiliary chemical reactions to produce the particles.

The purpose of the current investigation was the demonstration of the laser soot-scattering technique as a useful tool in studying the structure of the flame and the location and nature of the instantaneous combustion interfaces. Since soot that is created and consumed in the flame itself is used as the scattering medium, no extraneous seeding or chemistry is required. The technique has been applied in a study of large buoyant

Published by Elsevier Science Publishing Co., Inc.
52 Vanderbilt Avenue, New York, NY 10017

0010-2180/87/$03.50

diffusion flames with the intent of elucidating the complex internal structure of the large vortical pufflike features that dominate the heat release region of these flames.

QUALITATIVE DESCRIPTION OF THE FLAME

The flame studied in this investigation models liquid pool fires and related buoyant flames by a bed of glass beads with fuel supplied by the injection of natural gas. The associated flow is highly unsteady and buoyancy-dominated, and the heat release regions of the resulting flames are made visible by soot formed in the combustion processes. The transition between laminar and turbulent flows and the operational distinction between unsteady laminar flows, which contain highly wrinkled laminar flames, and turbulent flows is often obscure; a body of data does not yet exist from which a convincing set of criteria can be developed to define the laminar-to-turbulent transition in these flames.

For flames with a height-to-source diameter ratio (Z_f/D) greater than 1.0 and for which the initial momentum flux is negligible compared with the buoyancy force, the flame surface pinches in periodically toward the axis of symmetry just above the origin of the flame and produces a distinct structure in the flame. This structure has the appearance of a large irregular donut-shaped vortex ring, which rises slowly above the source and defines the top of the flame when the fuel it contains burns out. In a flame with a large height-to-diameter ratio, several of these structures are present at any given time, and for flames with a height-to-diameter ratio of two to three, only one structure is visible at a time. For flames with height-to-diameter ratio less than one, the process cannot be seen in the visible flame, but does appear in the shadowgraph images of the rising plume of hot products. For the flames in the present study, $1 < Z_f/D < 3$.

The puffing process has been the subject of numerous investigations, e.g., Thomas et al. [1], and recent reviews are given in Zukoski et al. [4], Beyler [5], and Cetegen et al. [6]. The dominant frequency appears to scale as $\sqrt{g/D}$, for a wide range of diameters and fuels. Here g is the gravitational constant and D is the burner diameter. The fluctuations are most marked when the flame height-to-diameter ratio, Z_f/D, is between one and three, and the amplitude of the fluctuations decreases markedly as Z_f/D increases from 3 to 20.

The large size of the structures and the speed at which they evolve suggest that they play an important part in fixing the entrainment and heat release in the lower part of the flame.

There have also been a number of studies of the radiation flux produced by buoyancy-controlled diffusion flames. With the exception of a technique developed by Markstein [7], these experiments are based on absorption and emission measurements of the flame made along a line of sight through the flame, and thus do not give any information concerning the structure of the interior of the flame. Markstein's technique uses a probe which had a resolution of about 60 mm. In contrast, the present technique is nonintrusive and can be used to give qualitative data for a cubical resolution element with a dimension of 1–2 mm on a side. However, it will not give the quantitative data required to determine flame radiation that Markstein's intrusive probe will give.

DESCRIPTION OF APPARATUS

A 50 cm diameter burner was used to deliver natural gas fuel to the flame. The fuel passed through a 4 cm deep porous bed of 2 mm spherical glass beads whose surface was made flat and flush with the outer metal edge of the burner. The sides of the burner were vertical and extended to the floor located an adjustable distance from the burner surface, but always maintained at greater than one burner diameter distance in order to minimize ground interference.

The burner was located in the center of a 2.4 m^2 area enclosed on the sides by a double layer of aluminum screen used to reduce the strength of flow disturbances present in the laboratory air. The screens were 2.4 m high and above them was a 2.4 m^2 hood which removed the exhaust gases from the laboratory.

A schematic of the optical arrangement is shown

in Fig. 1. A 3 W Ar^{++} laser beam (514.5 nm) was passed through a steering and focusing apparatus which allowed accurate alignment to the axis of the line segment in the flame that was to be imaged and permitted the imaged segment to be translated vertically with a high degree of parallelism. A spherical lens collimated the beam to a long thin waist within the flame and a polarization rotator maximized the scattered intensity in the viewing direction. The r-direction is taken along the line from the periscope to the beamstop and the z-direction is taken vertically from the face of the burner, with the center of the burner face defined as the origin.

The collection optics for the scattered light consisted of a heat reflecting filter, one of several narrow band interference filters, an imaging lens, and a linear solid-state camera. This camera used a (RETICON) 1024 element photodiode array to image the illuminated line segment up to 586 times per second. The interference filter was used to pass only that light within a narrow band (1–10 nm at 514.5 nm) centered at the wavelength of the incident laser light. Given the narrow bandwidths of these filters, very little luminosity was passed through to the camera.

Because the flow evolved significantly as it passed the measurement station (i.e., relative velocities within a structure were comparable to the celerity of the structure), the distinction between an r–t diagram and an r–z "snapshot" was especially important.[1] Structures were in the process of changing dramatically as they crossed the measured line segment so that the signature they left on an r–t diagram was quite distorted relative to their appearance at an instant in time. To make a correspondence between the r–t data and an instantaneous view, a high-speed movie camera was synchronized to photograph two perpendicular views of the flame luminosity simultaneously with the photodiode array images (117 frames per second or one movie frame for every 2.5 or 5 photodiode scans). The scattered laser radiation could not be observed consistently in the high-speed movie films, although the imaged axes could be discerned.

A computerized data acquisition system based on a DEC PDP 11/23 CPU was used to coordinate data collection. The photodiode array was interfaced to this system through a high-speed A/D converter designed and built at Caltech. This computer data acquisition system has been described previously [8].

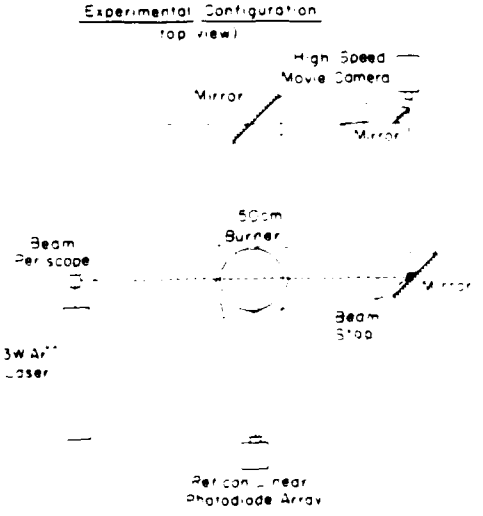

Fig. 1. The ~1 mm diameter beam from a 3 W Ar^{++} laser (514.5 nm line) was directed through the buoyant diffusion flame above the 50 cm burner. A segment of the beam was imaged on a linear photodiode array (1024 elements) clocked at 300 or 600 kHz. Simultaneous high-speed (117 fps) movies incorporating two orthogonal views of the luminous soot could be taken in synchrony with the linear array data. The z direction was vertical and the r direction was parallel to the burner diameter.

[1] Both an r–t diagram and a "snapshot" can be viewed as a two-dimensional slice through an inherently four-dimensional object (three spatial dimensions plus time). A snapshot captures two spatial dimensions, while an r–t diagram captures one spatial dimension and time. The two representations offer different (reductional) views of the entire object and only in the context of a given set of questions can either be considered superior. A movie or a two-dimensional electronic imaging time series offers a three-dimensional (two spatial plus time) view and clearly contains more information than either two-dimensional view if the spatial and temporal resolutions are comparable in all cases. In the present investigation neither a snapshot nor any other two-dimensional imaging of the soot scattering was possible with the present illumination source (3 W Ar^{++} laser), given the high background due to the flame luminosity and due to the drop in intensity in forming a sheet of light. A much higher power laser or a pulsed laser and a fast-shuttered detector would be required to overcome this experimental difficulty.

RESULTS AND DISCUSSION

Data were collected at various z/D values, from 0.1 to 2.0, and for various values of the heat releases, from 47.4 to 190 kW, as shown in Table 1. Inlet Richardson numbers for the fuel based on the burner diameter, $(\Delta\rho gD)/(\rho U^2)$, varied from about 100,000 at the lower heat rates to 5000 at the higher rates. The Reynolds numbers at the inlet ranged from 100 to 600, but increased downstream as the velocities increased due to buoyancy. For each entry in Table 1 marked with ×, four sets of r–t diagram data wre collected at a 600 kHz clocking rate. One of these four data sets was collected in synchrony with the high-speed movie for each entry. For the entries marked with an asterisk, an additional data set was also collected at a 300 kHz clocking rate synchronized with the high-speed movie. The slower clocking rate allowed nearly three times more data to be collected due to computer data acquisition limitations, albeit at a lower temporal resolution.

For the 600 kHz data, core memory limited the data collection to 384 scans of 512 pixels. This amounted to 0.66 s of data collection. All 1024 pixels were read out; only the central 512 were recorded for $z/D < 0.5$, while every alternate pixel (again 512 total) was recorded for $z/D \geq 0.5$. For the 300 kHz data, core memory was not a limitation since the data could be written directly to disk at this speed, so that 1024 scans of 512 pixels (or more) could be accommodated. Thus these data sets represent 3.5 s of data collection. Since the fire puffs at about 2 Hz, the higher clocking rate data correspond to about one puffing cycle, while the slower clocking rate data correspond to about seven cycles.

TABLE 1

Flame Lengths and Axial Measurement Stations[a]

Q	47.4	67.0	95.0	134	190	kW
Flame Lengths						
Z_f/D	1.3	1.6	1.75	2.3	2.82	
Axial Position						
z/D						
0.1	×*	×	×*	×	×*	
0.2	×*	×	×*	×	×*	
0.35	×*	×	×*	×	×*	
0.5	×*	×	×*	×	×*	
0.75	×*	×	×*	×	×*	
1.0	×	×	×*	×	×*	
2.0				×*	×*	

[a] The experimental conditions that were studied are indicated in the table. The columns are headed by the heat release rate (or fuel flow rate) in kW. The rows are labeled with the z/D values. For all the cases marked with an "×" four sets of 0.67 s duration r–t data at 600 kHz clocking rate were collected. One set was taken in synchrony with a high-speed movie. For those entries marked with an asterisk 3.5 s of 300 kHz clocking rate data were also taken in synchrony with a high-speed movie. The 300 kHz data sets were image processed and, for the entries in the 190 kW column, digital images are shown in Figs. 2–8. The nondimensional flame length, Z_f/D, based on 50% intermittency of the flame, is given for each heat release rate studied.

In Fig. 3, four sections through the image are

Flame lengths [6], Z_f/D, for various heat releases studied here are also shown in Table 1. These flame lengths are based on 50% intermittency of the flame. The data presented in this paper correspond to the highest heat release values collected with a 300 kHz clocking rate. Except for the major difference of flame length (Z_f/D) as seen in Table 1, the results presented are representative of all heat release values where Z_f/D consistently reached the given axial station, i.e., $z < Z_f$.

Figures 2–8 show r–t diagrams for a heat release of 190 kW and for z/D values of 0.1, 0.2, 0.35, 0.5, 0.75, 1.0, and 2.0 taken with a 300 kHz clocking rate. Darker regions indicate larger values of scattered intensity, although no effort has been made to interpret this intensity quantitatively since both the particle size distribution and their number density affect the scattered intensity.

In Fig. 2, vertical lines indicate the locations of the pixels corresponding to the center of the burner and the burner edge. (These lines were added to the image digitally after processing the data.) The same optical geometry was used for Figs. 2–4. In Figs. 5–8, a different optical geometry that imaged more than a full diameter of the burner was used. The two outer edges of the burner are marked for this geometry in Fig. 5 by vertical lines added in the same manner as those in Fig. 2.

LASER SOOT-SCATTERING IMAGE

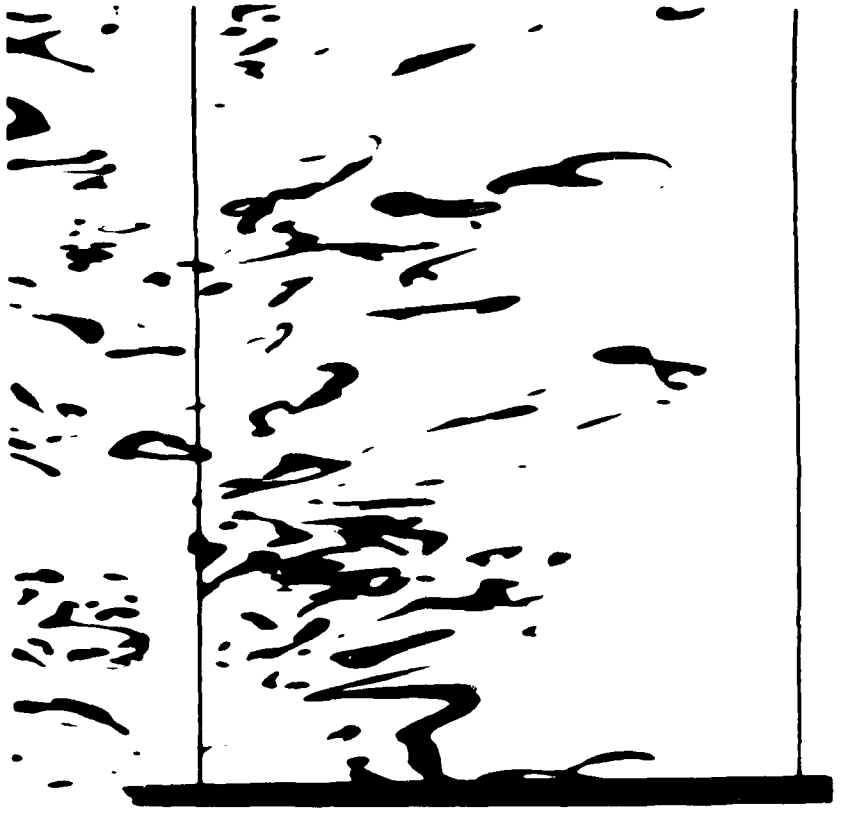

Fig. [illegible] The image photographed from a digital image processing monitor showing [illegible] with a clocking rate of [illegible] kHz and a line reading rate of [illegible] kHz. The total 1024 scans are displayed, representing [illegible] the earliest time at the top. The [illegible] lines indicate the position of the center and one edge of the burner, separated by [illegible] the bottom. A gray scale is also indicated, [illegible] increasing intensity.

represented by lines, two oriented horizontally and two vertically. These sections are plotted in Figs. 9a–9d. The vertical lines are shown in Figs. 9a and 9b as intensity versus time records of pixels 205 and 350, located at z/D = [illegible] and z/D = [illegible], respectively, for the first [illegible] scans of 1024 of the array. The horizontal lines correspond to Figs. 9c and 9d and are single intensity versus position scans of the array. Fig. 9c is scan 200; Fig. 9d is scan 350.

These sections elucidate the thin sheetlike structure of the soot distribution at z/D of [illegible], represented in Fig. 8. Figures 2–8 demonstrate that this convoluted sheet structure is present through z/D of 0.5 and perhaps beyond. The experimental resolution begins to affect the image at z/D = [illegible] (see below). It is apparent from these [illegible] diagrams that most [illegible] of the soot is contained in thin, convoluted sheets that exist throughout the region occupied by the flame.

In the [illegible] diagrams and the sections shown in Fig. 9, it appears that the nature of the soot sheets does not depend on radial position in the flame. That is, the soot sheet thickness and curvature are quantitatively the same toward the center and toward the edges. The primary difference between the center and edges of the flame is the frequency of occurrence of soot sheets, which is larger near the center and goes to zero at the edges. The frequency of occurrence is defined as the [illegible]

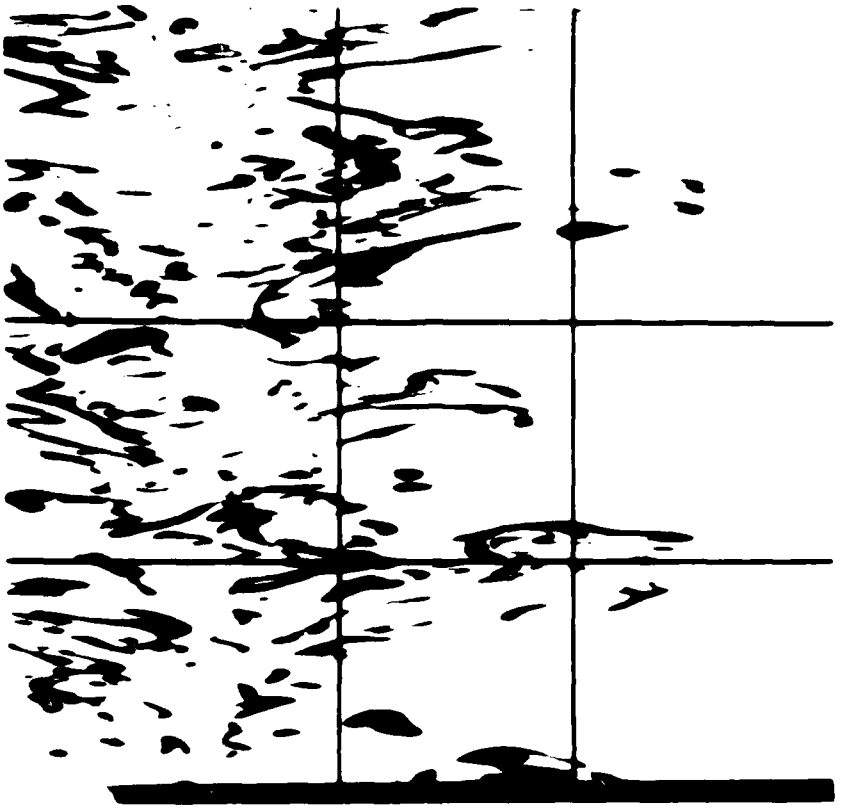

Fig. . As Fig. . for z/D = 0.20

intermittency, which allows a more quantitative analysis of these ideas and will be discussed below.

As previously stated, the high speed movies offer a complementary view of the flame structure. The movie camera images the luminous soot over the whole flame, not just the soot intersecting the laser beam. Also the movie captures most the flame region at an instant in time, so that the flame structure can be seen directly in (r, z) space. A sequence of high speed movie half frames for the z/d = 0.5, (90 kW, 300 kHz) data set is shown in Fig. . The corresponding r/z diagram is Fig. 5.

The puffing behavior of the flame is evident in both the r/z diagrams and in the high speed movies. Near the burner a strong 2 Hz periodicity is evident in the r/z data, although individual separated puffs have not formed at this stage. At z/D of 0.25 and beyond, distinct puffs can be observed. By integrating across r and plotting the resulting average intensity as a function of time, the 2 Hz periodicity can be easily displayed graphically as is illustrated in Fig. . This type of plot clearly shows that the puffing is a quasi-periodic phenomenon, and that the period of the cyclic behavior is variable within some range. The mean frequency, f, of the puffing depends little if at all on the heat release rate and has a nondimensionalized value of $f\sqrt{D/g} = 0.5$.

The r/z diagrams are of interest from several points of view, not the least of which is the demonstration of the imaging soot scattering technique as a useful probe of flame structure. The interpretation of these data is fairly straightforward, although some caveats may be in order. The first of these is that the interpretation of the absolute intensity of the scattered radiation has not been established. As was mentioned above, both the number density of particles and their size distribution determine the scattering intensity

Fig. 4. As Fig. 2 for $z/D = 0.35$.

Thus, without measuring or otherwise evaluating one of these parameters, there is ambiguity in the interpretation of the intensity. An unambiguous measurement would require a more sophisticated technique using either two-color or multiangle scattering at each pixel location.

The most interesting and instructive aspect of the r–t data is their structure. As will be argued below, this structure is reflective of the behavior of the flame sheet surface and as such it tells much about the structure of the flame. This structure evolves with z/D and is quasi-periodic in time at each z/D. The flame structure only depends weakly on the heat release rate (fuel flow rate) over the range studied, even though the overall length of the flame, Z_f, does depend on the fuel flow rate (see Table 1).

The structure of the soot distribution can be tied to that of the flame sheet by several arguments. In a photographic study where the luminous soot and the laser-illuminated soot were observable simultaneously (data not shown), there was no evidence of laser-illuminated soot in a region where there was no luminous soot. This is interpreted to mean that there is no appreciable cold (nonluminous) soot in the flame. This suggests that the soot is located primarily close to the hot combusting flame sheet.

Certainly the formation of soot requires the high temperatures found near the diffusion flame. If one were to suppose that soot were to survive and move away from the flame surface, it might cool radiatively and show up as nonluminous soot—which was not observed. Further, and perhaps more significantly, soot surviving away from the burning regions would show up in the r–t diagrams, coexisting with other products in the large heated regions of the flame at larger z/D stations. This is also not observed, nor is any significant amount of soot released by the flame as a whole.

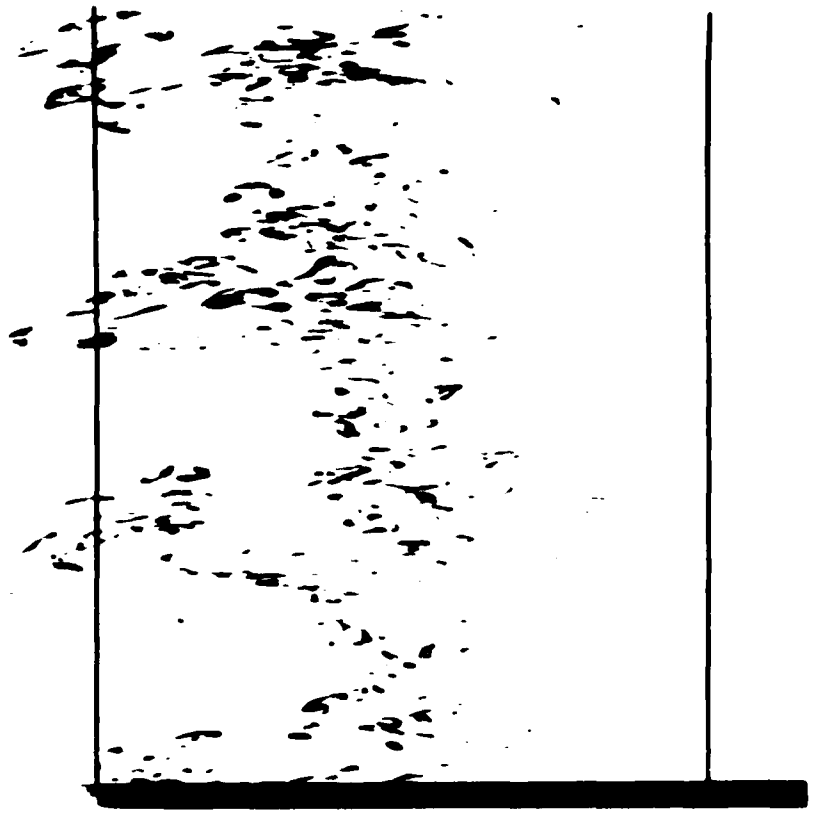

Fig. 5. As Fig. 2 for $z/D = 0.50$, except here the vertical lines indicate the two edges of the burner (separated by 50 cm). The right edge of the figure is indistinct due to the angular cutoff of the interference filter. The angular "window" was positioned slightly offcenter to ensure that at least one edge of the flame was seen clearly.

From these lines of evidence, we argue that for this buoyant natural gas flame, the soot location approximately marks the flame sheet surface. The correspondence is approximate however, since the soot is formed on the fuel side of the flame sheet, before the fuel encounters oxygen and, further, the soot bearing region is probably larger than the reaction zone [9, 10] (see Fig. 12). Thus, the soot distribution is probably wider than the flame sheet itself in a direction normal to the flame sheet surface and is slightly displaced to the fuel side in the same direction. The wider soot distribution will not misrepresent the structure of the flame, however, if the soot burns completely before it approaches another flame sheet. That is, the soot width must be small compared to the Kolmogorov scale, but not necessarily small compared to the flame sheet thickness, for the soot distribution to be useful as a marker of the flame sheet surface. The difference in thickness of the two surfaces must nevertheless be kept in mind.

Thus, where there is soot, there is a flame sheet, but the converse is not necessarily true. It is possible that in an appropriate straining field, the flame temperature could drop below that required to form soot but not so low as to extinguish the flame [11]. Alternatively, the effects of strain may be to diminish the time available for soot nucleation and growth to proceed [12]. In any case, our data do not allow us to ascertain whether there is combustion without soot formation in this flame, but there are clear indications of breaks in the soot distribution for z/D of 0.35 and greater. The strain rate increases with the velocity as z/D

Fig. 6. As Fig. 5 for $z/D = 1.75$.

increases, so this may possibly be viewed as a straining out of at least the soot production. Whether the entire flame is strained out at the same places is not addressed by this technique.

With the view that the soot structure and the flame sheet structure have a close correspondence, it is interesting to reconsider Figs. 2–8. Near the burner at $z/D = 0.1$ and 0.2 (Figs. 2 and 3), the structure is a continuous, convoluted surface. The soot thickness, which is presumably an upper bound for the flame sheet thickness as discussed above, is on the order of 5 mm. This estimate was obtained from the minimum widths of the soot sheets in the r direction in the r–t images. At about $z/D = 0.35$, discontinuities begin to appear (Fig. 4) and the structures become more discontinuous with increasing z/D, although the spatial resolution of our measurements may be inadequate at or beyond $z/D = 0.75$. The soot thickness is on the order of 2 mm at $z/D = 0.35$. The spatial resolution is about 1 mm, so that as the soot thickness approaches 1 mm it should become impossible to observe all the details of the soot structure. This is consistent with the observed lack of resolution at and beyond $z/D = 0.75$.

One initially surprising feature of the soot structure is that the contorted and for large z/D broken surface does not fill a larger fraction of the space occupied by the flame. Photographs and movies of the luminous soot radiation, which integrate all luminous soot along the line of sight, lead one to conclude wrongly that the soot approaches a more or less uniformly volume filling distribution. In fact the opposite seems to be the case in the r–t diagrams, where the soot distribution is made up of flamelet-like fragments which occupy the region within the outer boundaries of the flame. They are distributed approximately uniformly on average but individually are sharply localized.

[illegible] illumination [illegible] through the [illegible] soot distribution and the fraction of time that soot [illegible] present can be measured [illegible]. The average fraction of time that soot [illegible] present at a given location [illegible] defined as the soot intermittency [illegible]. [illegible] the total time that the intensity from a given region exceeds some low threshold value [illegible] divided by the total measurement time. This [illegible] plotted [illegible] Figs. [illegible] were [illegible] and 4 [illegible] the [illegible] and [illegible] experiments [illegible] that [illegible] value [illegible] about [illegible] near the center [illegible] that the value decreases toward the edges [illegible] the burner. [illegible] into account the fact that the soot thickness [illegible] upper bound [illegible] the flame sheet thickness [illegible] concludes that the fraction of time that flame sheets are present might be considerably [illegible].

[illegible] the threshold value used to determine the presence [illegible] the magnitude of the [illegible]

soot intermittency [illegible] features. By raising the threshold [illegible] each diameter [illegible] the soot [illegible] lowering the [illegible] soot intermittency. But insofar as the soot sheets [illegible] throughout the flame [illegible] raising the threshold [illegible] the flame. This argument [illegible] where the measurement [illegible] the soot sheets.

The soot intermittency [illegible] with the diagrams [illegible] flame [illegible] presumably following the [illegible] edges. Near the burner [illegible] sheets [illegible] complicated [illegible] with [illegible] burner [illegible]

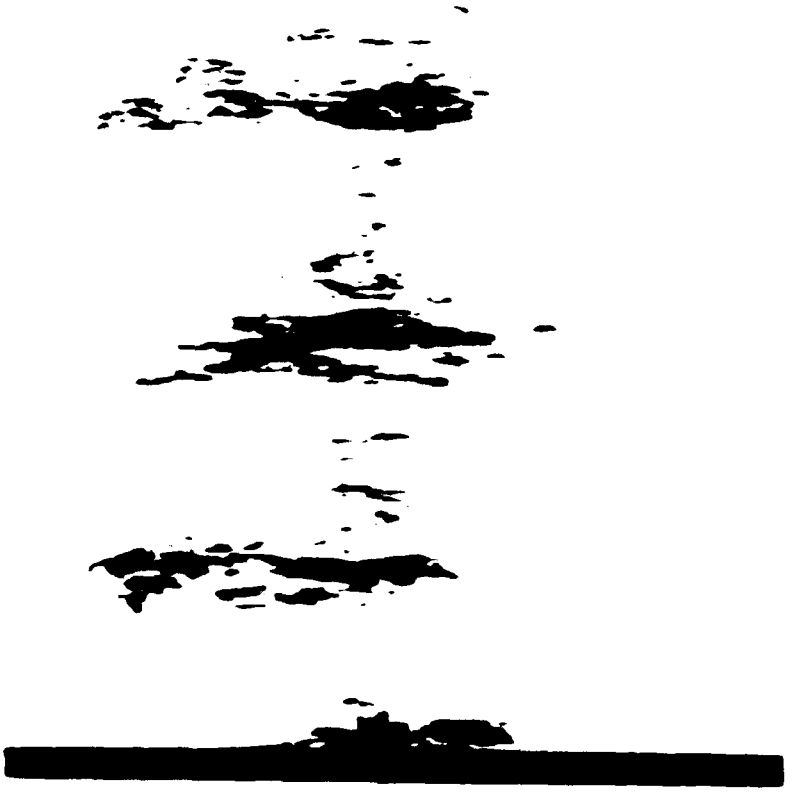

Fig. 4. As Fig. 3 (D = 2.5).

he sheets and their radius of urvature The adius of urvature i on the order of the Kolmo gorov length cale The Reynolds number ranges from about 600 near the burner to about 6000 near D based on rude estimates of the enterline velocity the flame diameter and the hot gas kinematic viscosity The overall envelope becomes a simple puff shape at about D S and his puffing occurs at the predominant f equency The puffs at larger values of D are made up of less continuous soot sheets distrib ted more or less uniformly within the outlines of he puff shape

The uniformity of the soot distribution is demonstrated in Figs 3 and 4 upper curves where conditional soot intermittency is plotted This conditional soot intermittency is defined as the intermittency of the soot measured within the boundaries of the whole flame It was calculated by first determining the horizontal edges of the soot distribution in the data set for each time frame using the low threshold value to distinguish the rightmost and leftmost positions at which soot was present Then for each pixel the fraction of time the pixel contained soot was divided by the fraction of time that the pixel was contained between the rightmost and leftmost extents of the soot distribution determined on a frame by frame basis For the values of heat release rate and D examined here the conditional soot intermittency is nearly the same as the previously defined soot intermittency near the center of the flame since the center of the flame is always within the edges of the flame and the flame is continuously present near the center Toward the edges however the flame edge moves in and out whether there exist distinct puffs or not and the conditional soot intermittency is substantially greater than the simple soot intermittency due to the fully developed effect of the puffing behavior

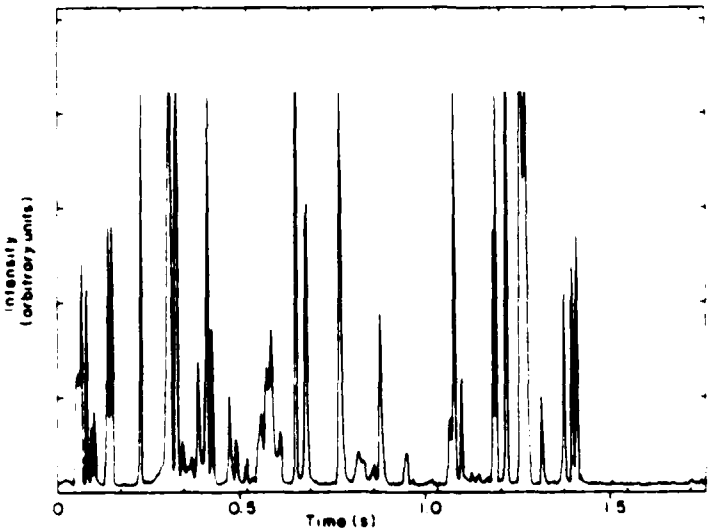
Intensity
(arbitrary units)
0
0.5
1.0
1.5
Time (s)

Fig. 9a.

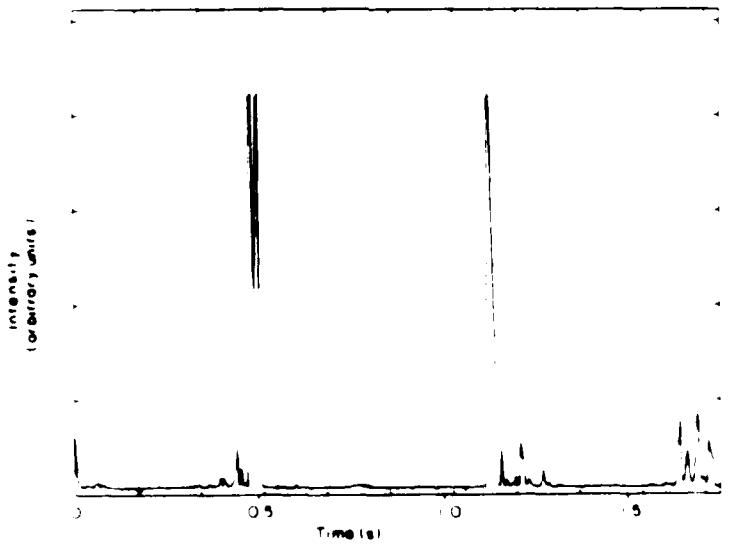
Intensity
(arbitrary units)
0.5
1.0
Time (s)

Fig. 9b

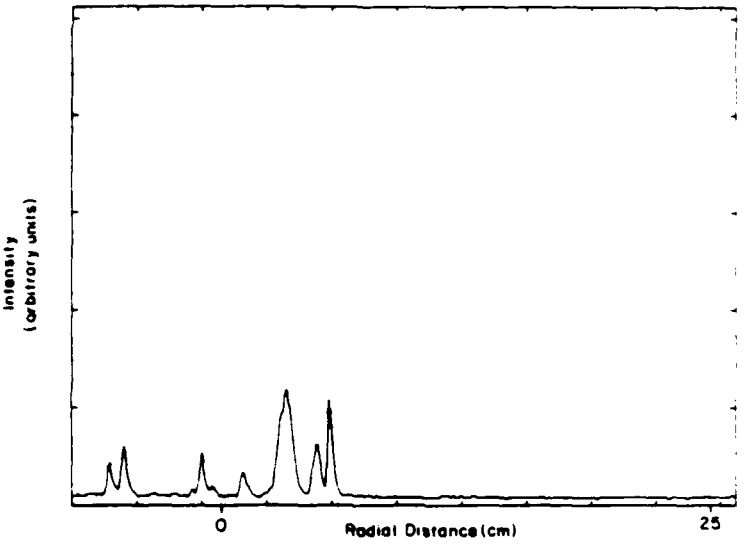

Fig. 9c.

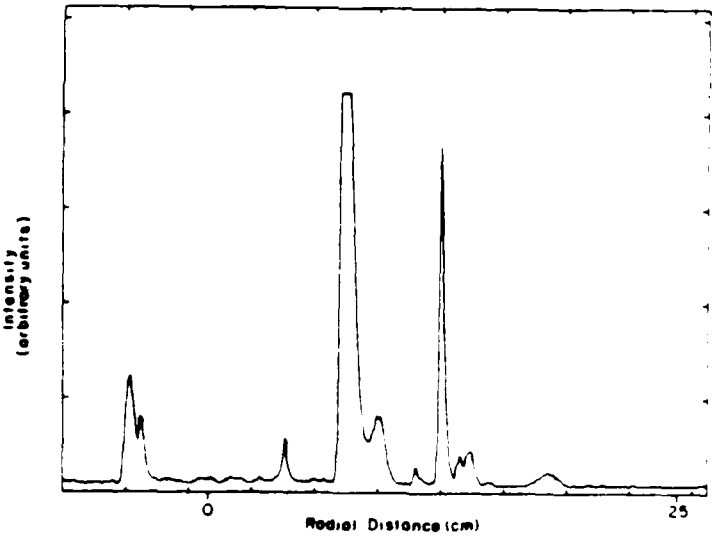

Fig. 9d

Fig. 9. Plots a and b are intensity versus time histories of pixels 205 (r/D = 0.118) and 350 (r/D = 0.312) for z/D = 0.20 shown in Fig. 3. The data shown are 512 time points (of the total 1024) corresponding to 1.7 s of data collection time or 3.5 puffing cycles. Plots c and d are single intensity-versus-position scans of the photodiode array for frames 200 and 350, respectively. The full width of the frame corresponds to 34.3 cm, with the left edge of the frame 7.8 cm to the left of the burner center (pixel 117).

Fig. 10. High speed movie photographs taken in synchrony with the acquisition of r–t data are shown. The photographs presented are negatives of the right image of the two images recorded and are every tenth frame of a series taken at 117 frames per second (spanning 0.43 s). In each photograph the view shown is a mirror image representation of the r–z view where the r-direction is as used in the r–t data presented.

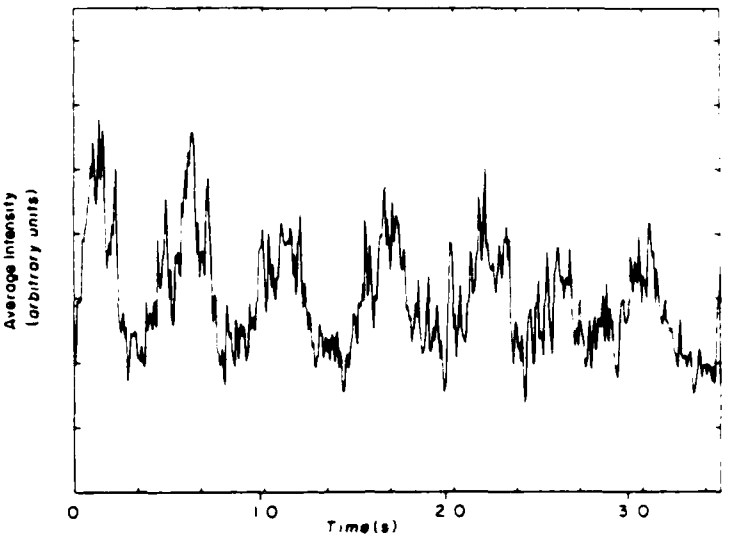

Fig. 11. The intensity integrated along the position axis is plotted as a function of time for $z/D = 0.50$. The full 3.5 s time history is plotted (with every two frames averaged), showing approximately seven puffing cycles.

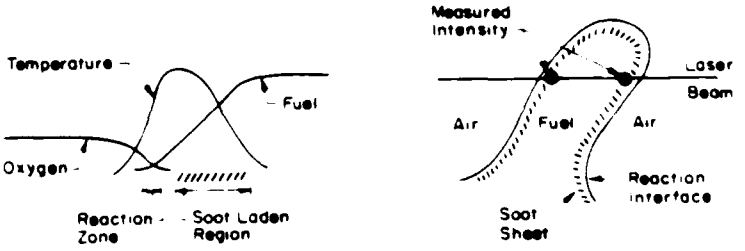

Fig. 12. The left sketch shows schematically the location of soot within a laminar diffusion flamelet. The right sketch indicates the regions where scattered laser radiation originates when a flamelet is swept past the laser beam.

The conditional soot intermittency for the $z/D = 0.2$ case is plotted in Fig. 13 (upper curve) and is nearly constant across the flame. There is an indication of a dip near the center (pixel 117) as well as some residual structure further out along the radius, but the curve lies predominantly between 45 and 55%. For $z/D = 0.5$ (Fig. 14, upper curve), the conditional soot intermittency lies near 40% except near the center (pixel 260), where the peaks to about 70%. Figure 13 is typical of all stations less than $z/D = 0.35$, while Fig. 14 is typical for axial stations $z/D = 0.35$ and greater. The peak in Fig. 14 indicates that there is some difference in structure between the center and edges of the soot distribution for larger z/D values, which we believe may be related to the connecting strands of soot between puffs. Nevertheless, the falling off of the simple soot intermittency toward the edges is not present in the conditional soot intermittency for any of our data.

The puff shape, then, primarily determines the simple soot intermittency curve, and the conditional soot intermittency is generally uniform within the flame edges and has a value near 40% (neglecting dips or peaks on the centerline). The flame sheets may or may not be as discontinuous as the soot sheets, but one might expect that the puff shape modulates the fraction of time that flame sheets are encountered also.

This study raises several questions. In the

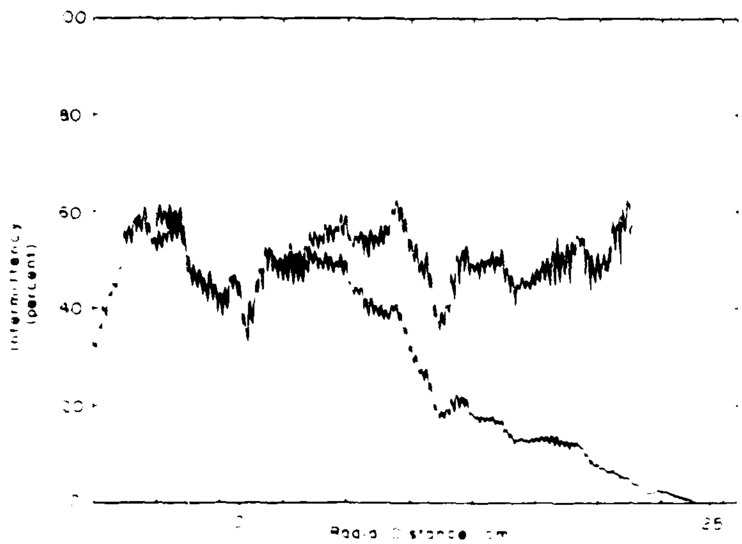

Fig. 13. Soot intermittency (i.e. fraction of time soot is present) is plotted versus position for $x/D = 0.20$. The lower curve was calculated using a threshold value of 1.5–2.0 times the rms noise level. Conditional soot intermittency (upper curve) can be seen to be more nearly constant. Unreliable data near the extreme edges of the figure are not plotted for the conditional intermittency. The horizontal axis is as in Figs. 9c and 9d.

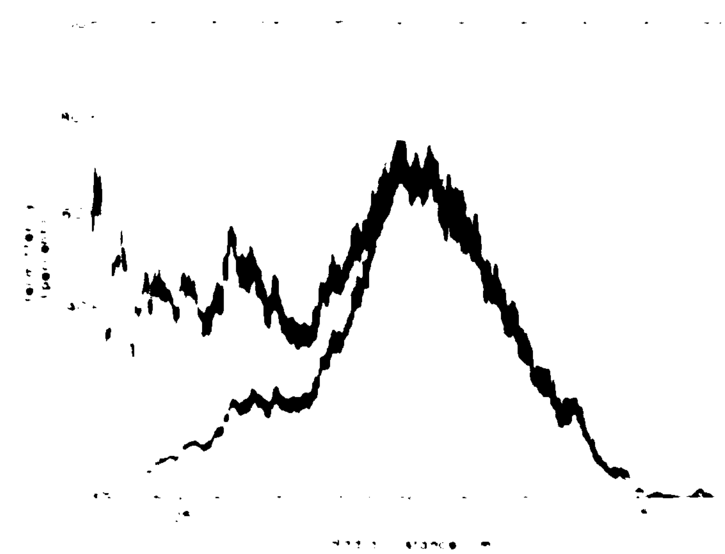

[illegible]

particular flames studied, the soot was found primarily in thin sheets. The entire flame was in the buoyancy-dominated range and was a (nonpremixed) diffusion flame. If one is led to surmise that the combustion is occurring on flame sheets in this flame, a supposition that perhaps must be supported by further experimentation, the question arises as to how general such a result might be. Do momentum-dominated diffusion flames also form soot sheets and does the combustion occur in flame sheets in these flames? Greater differences might be expected with premixed combustion since a fuel oxidizer interface does not exist and soot production is usually quite low.

To answer these questions, a means of measuring the combustion reaction interface itself must be used. Two dimensional data (r-t or r-z) must be acquired to elucidate the structure and connectivity of the reaction zones. It may be necessary to work in a nonsooting flame (such as hydrogen flames) in measuring flame sheets directly to avoid interference with the soot particles or their luminosity.

CONCLUSIONS

It has been shown how the scattering of laser light by soot particles may be used to determine soot distributions in diffusion flames. With some caveats, the soot located directed adjacent to a flame sheet can be thought of as marking flame sheets, although cases may exist where a flame sheet occurs in the absence of adjacent soot or, in other diffusion flames of other fuels, soot may exist in the absence of a flamelet.

The technique described here was used to study the structure of large buoyant diffusion flames. A [illegible] plane of the flame was scanned in time in order to obtain two-dimensional r-t diagrams of the soot structure. The results show that the flame sheets exist as highly wrinkled but continuous surfaces near the burner where strain rates are relatively small, but they appear to become discontinuous at larger distances. These soot discontinuities suggest that the strain here might be sufficient to [illegible] the flame sheets or at least suppress [illegible]. The decrease in the thickness of [illegible] with increasing height above the burner is also consistent with an increase in strain rate.

The puffing character of these flames was readily apparent in the data and was found to be quasi-periodic with a frequency of about 0.5 $\sqrt{g/D}$.

Plots of soot intermittency indicate that the soot is present most frequently near the burner axis and drops to zero near the edges. By determining the instantaneous flame boundary, the conditional soot intermittency can be analyzed. Plots of the conditional soot intermittency indicate that the soot sheets occupy about 40–60% of the instantaneous volume within the outer boundaries of the flame uniformly across the flame. These data support a model of the flame made up of flame sheets distributed approximately uniformly within the confines of the quasi-periodic pufflike structures. This model indicates that the surface of the stoichiometric mixture ratio also winds throughout the puffs, even crossing the centerline.

The authors thank Prof. P. Dimotakis for suggesting the soot-scattering imaging technique, Prof. E. Zukoski for useful discussions on buoyancy-dominated flames, and both for critical reading of and suggestions on the manuscript. This work was sponsored by the Gas Research Institute under grant number 5083-260-0878. The linear camera and computer data-acquisition system used in this investigation were developed under the sponsorship of the Air Force Office of Scientific Research with primary contributions from Dr. Daniel B. Lang under contract number F49620-79-C-0159 and grant number AFOSR-83-0213.

REFERENCES

1. Thomas, P. H., Baldwin, R., and Heselden, A. J. M., *Tenth Symposium (International) on Combustion*, The Combustion Institute, Pittsburgh, 1964, pp. 983–996.
2. Zukoski, E. E., Cetegen, B. M., and Kubota, T., *Twentieth Symposium (International) on Combustion*, The Combustion Institute, Pittsburgh, 1984, pp. 361–366.
3. Keyser, A. J. R., Bilger, R. W., and Kent, J. H., *Combust. Flame* 46:105–108 (1982).

4 Zukoski, E. E., Kubota, T., and Cetegen, B., *Fire Safety J.* 3:107–121 (1980–81).
5 Bevler, C. L., Ph.D. Thesis, Harvard Univ., Cambridge, MA, 1983.
6 Cetegen, B. M., Zukoski, E. E., and Kubota, T., *Comb. Sci. and Tech.* 39:305–331 (1984).
7 Markstein, G. H., Tech. Rept. J.I.OMONI BU, Factory Mutual Research Corp., Norwood, MA, 1983.
8 Koochesfahani, M. M., and Dimotakis, P. E., *AIAA J.* 23:1700–1707 (1985).
9 Tsuji, H., and Yamaoka, I., *Thirteenth Symposium (International) on Combustion*, The Combustion Institute, Pittsburgh, 1970, pp. 723–731.
10 Vandsburger, U., Kennedy, I., and Glassman, I., *Comb. Sci. and Tech.* 39:263–285 (1984).
11 Glassman, I., and Yaccarino, P., *Eighteenth Symposium (International) on Combustion*, The Combustion Institute, Pittsburgh, 1981, pp. 1175–1183.
12 Kennedy, I. M., *Phys. Fluids* 28:3515–3524 (1985).

Received 5 May 1986; revised 24 July 1986

Appendix D

A Model for Reactions in Turbulent Jets: Effects of Reynolds, Schmidt, and Damköhler Numbers

James E. BROADWELL

GRADUATE AERONAUTICAL LABORATORIES
CALIFORNIA INSTITUTE OF TECHNOLOGY

1 May 1987

To be presented at the United States-France Joint Workshop
on Turbulent Reactive Flows

6-10 July 1987 at Rouen, FRANCE

Sponsored by
NATIONAL SCIENCE FOUNDATION
and
CENTRE NATIONAL DE LA RECHERCHE SCIENTIFIQUE

A MODEL FOR REACTIONS IN TURBULENT JETS: EFFECTS OF REYNOLDS, SCHMIDT, AND DAMKÖHLER NUMBERS

James E. Broadwell

Graduate Aeronautical Laboratories
California Institute of Technology

1 May 1987

ABSTRACT

Data from several recent experiments on mixing and chemical reactions in turbulent shear layers and jets is discussed in some detail and used to formulate a picture of the path from the freestream to the molecularly mixed state. A model is proposed which incorporates the essential steps in this path and which appears to provide a framework for understanding the major effects of Reynolds, Schmidt, and Damköhler numbers on the chemical reaction. A simplified version of the model reproduces the observed Reynolds number dependence of nitric oxide production in turbulent fuel jets.

INTRODUCTION

It is a tenet of classical turbulence theory that in the limit of Reynolds number approaching infinity, dissipation is independent of Reynolds number and takes place at the Kolmogorov scale. The same assumptions concerning scalar mixing are the basis for a model of molecular mixing in shear layers and jets that has been under development for some time, Broadwell and Breidenthal (1982), Broadwell and Mungal (1986,1987). The approach was suggested by the experiments that revealed large scale organized motions in shear layers and jets, primarily those of Brown and Roshko (1974), Konrad (1976), and Breidenthal (1982) in shear layers and of Dimotakis, Papantoniou and Miake-Lye (1983), in jets. In the shear layer, these experiments and the computations of Corcos and Sherman (1976) showed that instabilities lead to concentrated regions of vorticity and that free stream fluids enter the layer in streams with dimensions of order of the layer thickness, δ. It is a basic postulate in the model that in the limit $Re \to \infty$, no mixing takes place until the scale of these entering streams is reduced, by inviscid motions, to the Kolmogorov scale, $\lambda_K \sim \delta/Re^{3/4}$, where Re is the Reynolds number. When the scale of the concentration fluctuations in the streams reaches λ_K, it is shown by arguments given later that the time required for diffusion to "homogenize" the mixture is negligible compared to the time to reach λ_K from δ, i.e. compared to δ/U, where U is a characteristic large scale velocity. The quantity, or volume fraction, of molecularly mixed fluid so formed is, therefore, independent of both the Reynolds number, and the Schmidt number, Sc. In this limit then, the rate of molecular mixing is a constant as is the rate of entrainment into the layer.

When the Reynolds number is finite, but such that $(Re\,Sc)^{1/2} \gg 1$, diffusion layers form at the boundaries of the entering streams and, because their thickness, λ_T, scales with the large scale variables, U and δ it is given by

$$\lambda_T \sim \delta/(Sc\,Re)^{1/2} \sim \delta/Pe^{1/2}$$

where Pe is a Peclet number. Since the surface area per unit volume, S, of these diffusion sheets scales only with δ^{-1}, their fractional volume ($S \cdot \lambda_\gamma$) is proportional to $Pe^{-1/2}$.

In this case, also, when all scales in the entering stream are reduced to the Kolmogorov scale the mixture is homogenized as before. In this Lagrangian description of the path from the free stream to the molecularly mixed state, the same quantity of fluid is involved whatever the Reynolds number. Therefore, the fractional volume of mixed fluid produced by diffusion at the Kolmogorov scale is independent of the Reynolds number. The diffusion at the scale λ_γ causes mixing that is "early" or upstream, in the Eulerian viewpoint.

The above described picture of shear layer mixing is, by the same argument, applicable to jets, in which case the entering stream of reservoir fluid mixes at a constant rate with jet fluid. Differences between the two flows emerge only when chemical reactions are considered.

At any axial station in either shear layers or jets, then, the molecularly mixed volume fraction, V_m, can be written,

$$V_m = A + B/(Sc\,Re)^{1/2} \qquad \begin{matrix} Re \gg 1 \\ (Sc\,Re)^{1/2} \gg 1 \\ Re \gg (\ln Sc)^2 \end{matrix} \qquad (1)$$

in which A is the average volume fraction generated when the entrained fluid reaches the scale λ_K and B is the average non-dimensional surface area per unit volume, i.e., S measured in terms of δ. The notation Sc Re is used instead of Pe because of the need to state the conditions of applicability of the model. The origin of the restriction, $Re \gg (\ln Sc)^2$ is discussed later.

In the above referenced discussions of the model, the diffusion layers were called strained laminar flames. Connection is made with the preceding discussion by noting that if these layers are in equilibrium

with the local large scale strain [illegible], their thickness is proportional to $D\varepsilon^{-1/2}$ and the expression above results. See Carrier, Fendell, and Marble (1975) for a discussion of these flames. D is the diffusion coefficient. When $Sc = \nu/D$, λ is the Taylor scale, a fact brought to our attention by H. W. Liepmann who points out that they are, in the mathematical sense, internal boundary layers.

The discussion so far has been concerned only with molecular mixing with no restrictions on the nature of the chemical reactions. In particular, reaction rates of any magnitude can be considered. This flexibility, also a characteristic of the coherent flame model, Marble and Broadwell (1977), may be useful in interpreting the recently measured finite kinetic effects in hydrogen flames, Dibble and Magre (1987), and in studying lift-off and blow-out of fuel jets.

With regard to the Taylor diffusion layers, notice that in the jet they form between newly entrained reservoir fluid and jet fluid, i.e. fluid that is, or was, "turbulent". For them to persist it appears to be necessary for the small scale turbulent motions in the jet fluid to have been destroyed, by momentum diffusion, when the concentration variations were destroyed. In the shear layer, this picture is consistent with the observations of Coles (1983) and Hussain (1983), that turbulence is generated in the braids and dissipated in the cores of the vortices. Furthermore, if the small scale motion is dissipated, the vortices would be left in solid-body-like rotation, evidence for which is reported by Wygnanski and Fiedler (1979). In both shear layers and jets, the motions are unsteady on the largest spatial and temporal scales in the flow. These unsteady motions, as illustrated by the flame length fluctuations observed by Dahm and Dimotakis (1985), for instance, make possible, if not plausible, the idea that the small scale motions and concentration fluctuations are successively generated and destroyed in the jet fluid as it moves along the axis.

While, as just stated, large scale unsteadiness is an inherent feature of the flows being considered, the model attempts to deal only with their averaged consequences. In addition, in most of the discussion that follows, the density will be taken to be constant. The

modifications that are needed when the jet and reservoir fluid have different densities, or when heat release is considered, are discussed after the basic ideas are presented.

THE HIGH REYNOLDS NUMBER LIMIT

In the above cited references to earlier work on the model, an upper limit for the time required for diffusion to homogenize the fluids at the Kolmogorov scale was estimated from the time to diffuse across that scale, i.e., from $\lambda_K^2/D \sim (R/u)\, Sc/Re^{1/2}$ where R is the jet radius and u the axial velocity. Batchelor (1959) shows that local straining reduces λ_K to $R/(Re^{3/4}Sc^{1/2})$ in a time $(R/u)\ (1/Re^{1/2})\ \ln Sc$, a result brought to the author's attention by P. E. Dimotakis. Since the time for diffusion across the smaller scale is only $(R/u)/Re^{1/2}$, the larger time $(1/Re^{1/2})\ln Sc$ is controlling and is the restriction given relative to Equation (1).

When the conditions, $Re \gg 1$, $(Sc\, Re)^{1/2} \gg 1$, and $Re \gg (\ln Sc)^2$ are satisfied, it is a simplification to consider the scales to be divisible into the three separate categories:

$$R,\ R/Re^{1/2} \text{ and } R/Re^{3/4},$$

and to assume instantaneous mixing at the scale λ_K.

Consider first the limiting case $Re \to \infty$ for any fixed Schmidt number, in which case mixing takes place only at λ_K. (Note that the requirement $Re > (\ln Sc)^2$ precludes the case $Sc \to \infty$ for fixed Reynolds number. It seems clear, intuitively, that the mixed volume fraction goes to zero in this limit.)

A critical check on the model in the high Reynolds number limit is whether or not the mixing rate is independent of Re and Sc. Very little evidence is available concerning this point, but the experiments of

Breidenthal (1981) and Koochesfahani and Dimotakis (1986) in the same facility and over a limited Reynolds number range, $10^4 < Re < 10^5$, show that for Sc ~ 600, there is no dependence on Re. These results suggest that Sc Re > 10^7 is sufficient for the limiting condition to apply. In gases, Sc ~ 1, at Re ~ 10^5, however, Mungal, Hermanson, and Dimotakis (1985) find Reynolds number effects; 10^5 is apparently not high enough.

Indirect support for the proposed mixing mechanisms in the high Reynolds number limit is in the composition and spatial distribution of the molecularly mixed fluid. If there is a delay, after entrainment, during which the fluids are distributed by large scale motion throughout the shear layer or the jet, the mixed fluid composition should be independent of the lateral coordinate in shear layers and of the radius in axi-symmetric jets.

Konrad (1976) noted the approximate flatness, in his gas shear layer, of the mixed fluid composition and, in fact, this observation was one of the motivations of the present model. The most remarkable results, however, are those obtained in shear layers in water (Sc - 600) and Re - $2 \cdot 10^4$ by Koochesfahani and Dimotakis (1986).
Figure 1 shows their mean mixed fluid composition deduced from chemical reaction experiments that eliminated probe resolution errors. (They show, incidentally, the rigorous requirements for accurate measurements of this quantity by conventional instrumentation). We see that there is no indication whatever of a lateral gradient. It is a convenient and useful additional approximation for modeling, used the following, to assume that the mixed composition has a single value, but what is to be noted here is lateral distribution. It is difficult to escape the conclusion that the fluids are distributed throughout the layer before they mix.

The picture is not as simple for jets. Dahm and Dimotakis (1985), again in experiments in water in the Re range 10^3 - 10^4, conclude from laser sheet photographs and composition profiles that there are large region of nearly uniform composition but that they are so arranged that radial scans sometimes intersected more than one. Figure 2 contains samples of this measurement. More data is needed but the few results

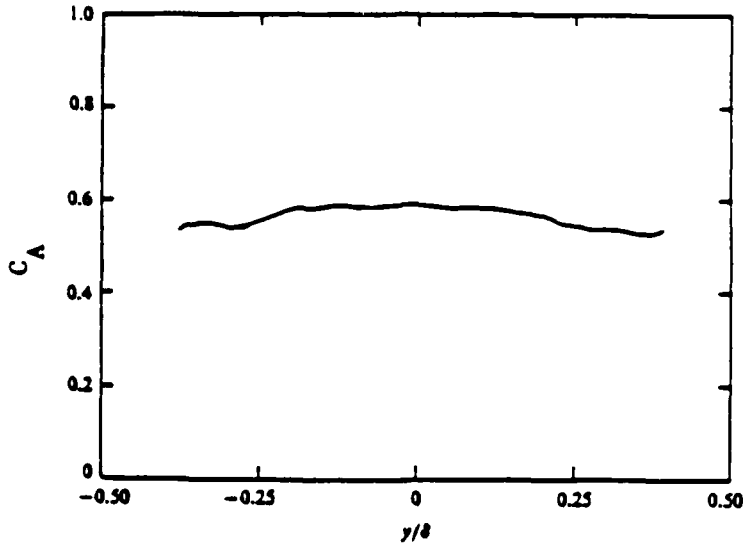

Figure 1. Dependence on lateral coordinate, y/δ, of average concentration of mixed fluid. C_A denotes high speed fluid. Koochesfahani and Dimotakis (1986).

are in accord with the notion that large scale motions distribute reservoir fluid throughout the jet before it mixes molecularly. Such motions are dramatically illustrated in high speed laser sheet images of Long (1987). Likewise, temperature-time traces in a plane jet, Antonia et al (1986), have been shown by them to be evidence of large scale motions.

JET MODEL OF THE LIMIT $Sc\,Re \to \infty$, $Re \gg 1$, $Re \gg (\ln Sc)^2$

To put the above description in approximate quantitative form, we consider only the far field where the jet spreads linearly and similarity in the velocity distribution, $u(x/d_o, \eta)$ has been attained.

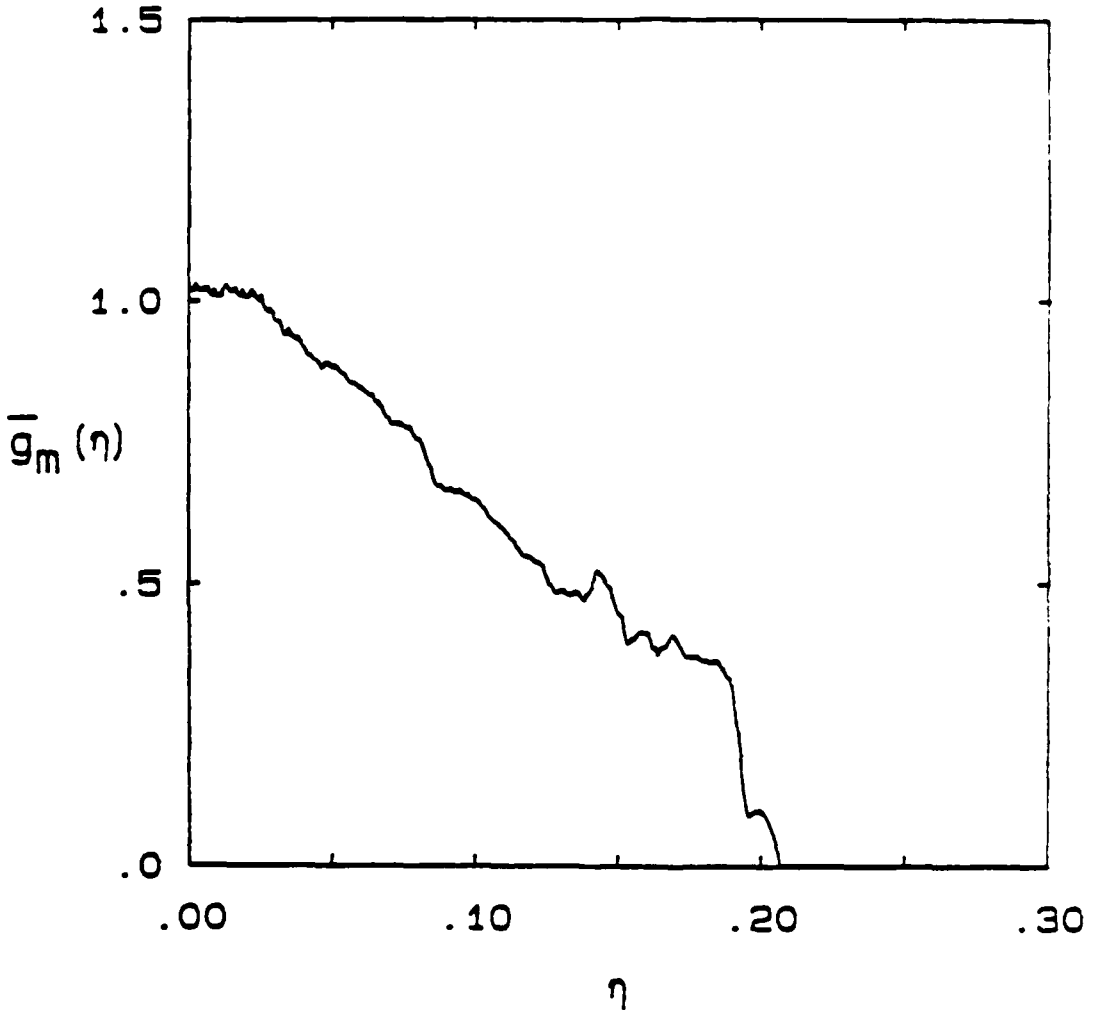

Figure 3. Mean radial profile of mixed fluid concentration x/d_o = 300, Re = 5000. Dahm (1985).

Here, x is the axial distance, d_o, the jet nozzle diameter, R, the local jet radius, and $\eta = r/R$. Likewise the molecularly mixed fraction, α, is taken to depend only on η. Recall that the justification for the independence of α from x is that the entrained fluid reaches the Kolmogorov scale and mixes after it moves downstream a distance that scales only with the radius at which it was entrained.

The connection between α and the rate, v_h, at which reservoir fluid "enters" the molecularly mixed flux is

$$v_h = 2\pi \frac{d}{dx} R^2 \int \alpha(\eta)\, u(x/d_o, \eta)\, \eta\, d\eta \qquad (2)$$

Let

$$R = C_1^{1/2} x \text{ and } u = (u_o d_o/x)\, g(\eta)\,. \qquad (3)$$

Then,

$$v_h = 2\pi\, C_1\, u_o\, d_o\, E \qquad (4)$$

where $E = \int \alpha(\eta)\, g(\eta)\, \eta\, d\eta\,.$ (5)

The independence of α from x implies, therefore, that the molecularly mixed fluid flux rises linearly with x as does the total jet flux. As is well known, the latter result follows simply from the conservation equations; the numerical rate has been measured by Ricou and Spalding (1961).

In the shear layer, as was noted above, the mean concentration in this limit is independent of the lateral coordinate. If, in addition, the concentration is taken to have a single value, then the integral $\int \alpha(\eta)\, d\eta$, the average mixed volume fraction, can be determined from chemical reaction experiments to be 0.28. (See Broadwell and Mungal, 1986.) Dahm (1985) computed the mean mixed concentration from profiles like those in Figure 1, finding, of course, a radial variation in this quantity, Figure 3. Such variation, as well as probe resolution

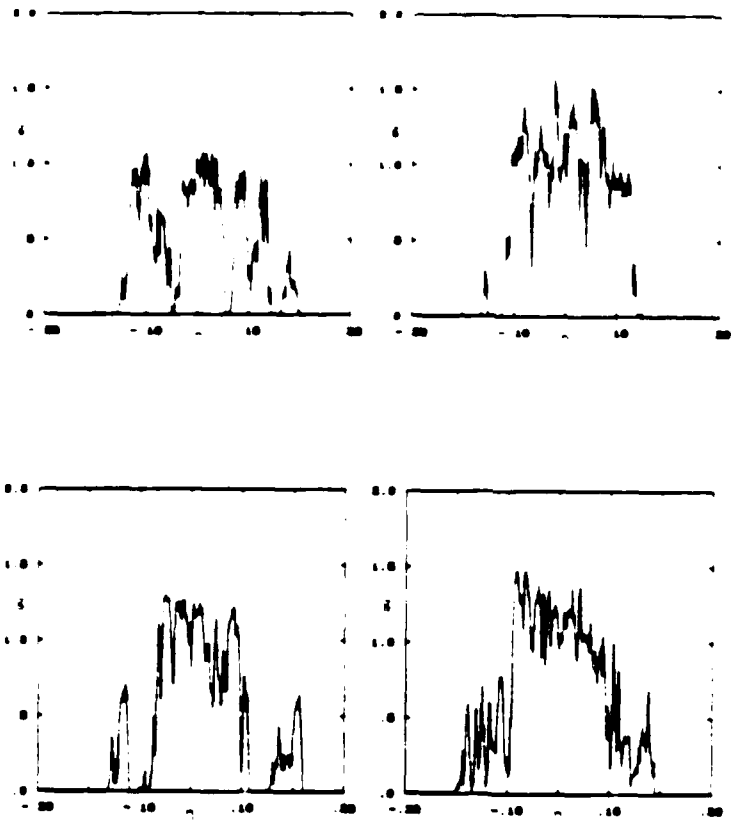

Figure 2. Representative instantaneous radial profiles of concentration in the jet, x/d_o = 300, Re = 5000. Dahm and Dimotakis (1985).

questions, makes the accuracy of the determination of the corresponding value for the jet questionable. It is instructive nevertheless, to use the approximate expressions derived from the data of Dahm for the mean mixed jet fluid concentration, $\bar{F}_m$, and the mean concentration, $\bar{F}$, approximated by the equations

$$\bar{F}_m = 3.2\, d_0/x \qquad (6)$$

$$\bar{F} = 1.7\, d_0/x$$

to find

$$A = \int \alpha(\eta)\, \eta\, d\eta = 0.5 .$$

This value, twice that in the shear layer, is in approximate accord with that found by Waddell in his use of acid-base reactions in water to study mixing in jets, Hottel (1953). (This early work provided the starting point for the liquid shear layer and jet experiments discussed above.)

With the assumption that the mixed fluid composition is independent of η and has a single value, the fuel conservation equation becomes

$$2\pi \frac{d}{dx} (C_F)_h R^2 \int \alpha(\eta)\, u(x,\eta)\, \eta\, d\eta = -2\pi k\, (C_F)_h\, (C_O)_h R^2 \int \alpha(\eta)\, \eta\, d\eta$$

The oxidizer, carried in the reservoir fluid, is governed by

$$2\pi \frac{d}{dx} (C_O)_h R^2 \int \alpha(\eta) u(x,\eta)\, \eta\, d\eta = -2\pi k\, (C_F)_h\, (C_O)_h R^2 \int \alpha(\eta)\, \eta\, d\eta + \dots$$

where $(C_F)_h$ and $(C_O)_h$ denote the fuel and oxidizer concentrations in the mixed fluid, $(C_O)_\infty$ is the reservoir oxidizer concentration, and k is the reaction rate coefficient for the reaction:

$$O + F \xrightarrow{k} P$$

in which the stoichiometric ratio [illegible] definiteness, the reaction has been [illegible]

AD-A186 141 CHEMICAL REACTIONS IN TURBULENT MIXING FLOWS(U) 2/2
CALIFORNIA INST OF TECH PASADENA GRADUATE AERONAUTICAL
LABS P E DIMOTAKIS ET AL. 01 JUN 87 AFOSR-TR-87-1160
UNCLASSIFIED $AFOSR-83-0213 F/G 20/4 NL

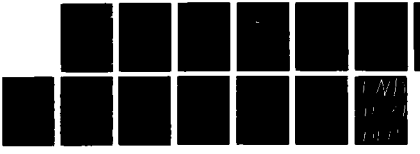

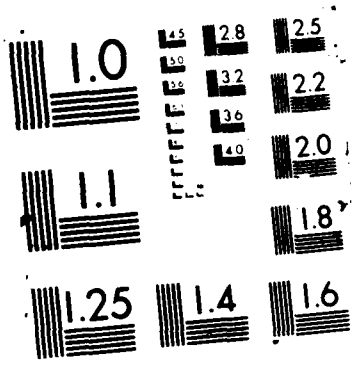
1.0
1.1
1.25
1.4
1.6
1.8
2.0
2.2
2.5
2.8
3.2
3.6
4.0
4.5

binary reaction with a constant rate coefficient. As will be seen, this simpification can be dropped when numerical computations and complex reactions are considered.

Introducing the variables $C^*_O = (C_O)_h/(C_O)_\infty$, $C^*_F = (C_F)_h/(C_F)_i$, and $z = x/d_o$, where $(C_F)_i$ in the initial fuel concentration, and using Equations (2)-(5), we can write Equations (7) and (8) in the form

$$\frac{d}{dz}(z\,C^*_F) = -Da\,z^2\,C^*_F\,C^*_O \tag{9}$$

$$\frac{d}{dz}(z\,C^*_O) = -Da\,\phi\,z^2\,C^*_F\,C^*_O + 1 \tag{10}$$

in which ϕ is the equivalence ratio, $(C_F)_i/(C_O)_\infty$, and Da the Damköhler number defined by

$$Da = \frac{A(C_O)_\infty\,k\,d_o}{E\,u_o}$$

and $A = \int \alpha(\eta)\,\eta\,d\eta$.

When there is no reaction, Da = 0, Equation (9) yields

$$C^*_F = c/z = 3.2/z \tag{11}$$

where the constant is taken from Equation (6).

Since $(C^*_F + C^*_H) = 1$ for Da = 0,

$$C^*_F = 1 - 3.2/z$$

Multiplication of Equation (9) by ϕ and subtraction from Equation (10) yields

$$\frac{d}{dz}\left[z\,(C^*_O - \phi\,C^*_F\right] = 1,$$

from which we find,

$$(C^*_O - \phi\,C^*_F) = \frac{z-3.2\,(\phi+1)}{z}$$

in which the constant comes from Equation (11). For $Da \to \infty$, $C_0^* \to 0$ in the flame; therefore

$$C_F^* = \frac{3.2(\phi+1)-z}{\phi z}$$

and the flame ends, $C^*_F = 0$, at

$$z_e = 3.2\,(\phi+1) \qquad (12)$$

Since Equation (12) is valid for any form of the reaction term, as long as $Da \to \infty$, it may be compared with the "flame length" measurements of Waddell and of Dahm et al (1984) for reactions in water where $R_e \sim 10^3 - 10^4$ and $Sc\,Re \sim 10^6 - 10^7$.

The experimental results are shown in Figures 4 and 5, the first establishing the independence of z_e from Reynolds number for $Re > 3000$, and the second the linear dependence of z_e on ϕ. Since in the experiments z_e was taken to be the axial location of the last indication of any unreacted jet fluid and since the flame length fluctuations are large, it is understandable that the measured lengths are much larger than that given by Equation (12). The important point, however, is that the linear dependence of z_e on ϕ in the experiment is consistent with the Equation (12), and hence consistent with the assumption that α is independent of axial distance.

FINITE REYNOLD NUMBER JET

At Reynolds numbers for which the jet is turbulent but low enough for the Taylor layers or strained flames to make significant contributions to the molecular mixing, the procedure is as follows. To simplify the notation, the Schmidt number will be taken to be unity in this section.

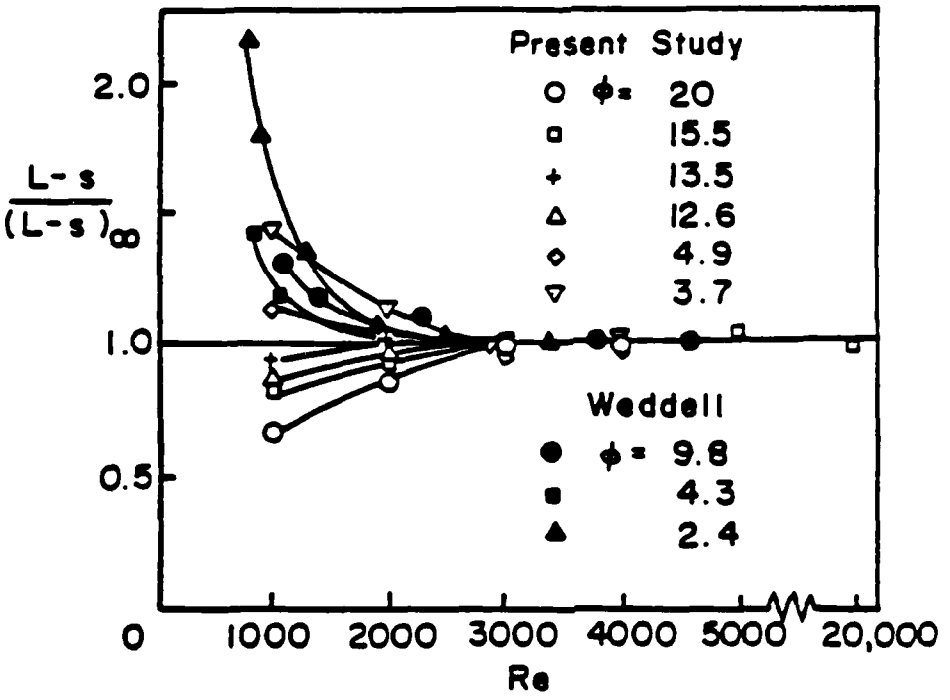

Figure 4. Mean turbulent flame length normalized by its asymptotic value versus Reynolds number and equivalence ratio. Dahm et al. (1984).

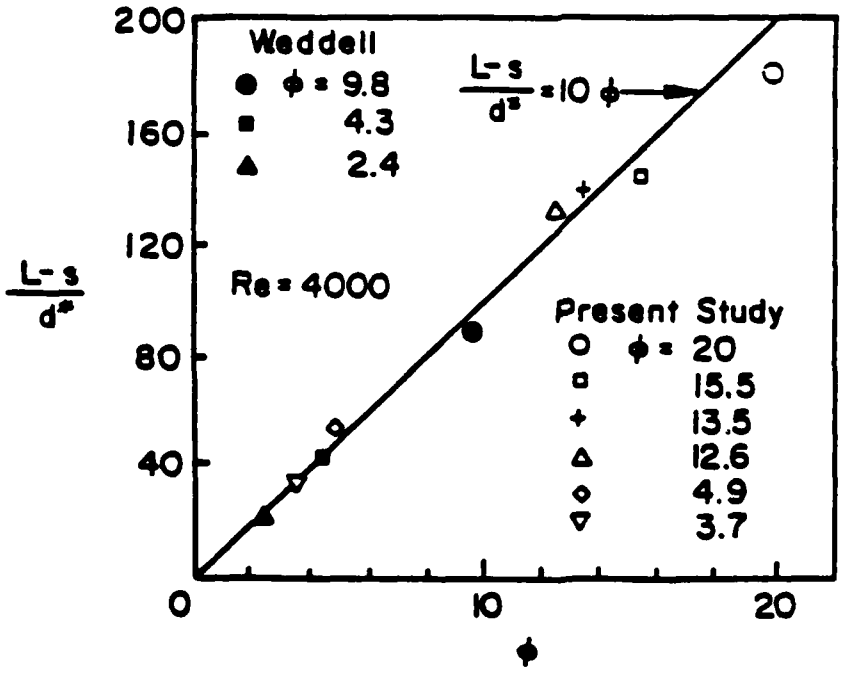

Figure 5. Mean turbulent flame length at high Reynolds number versus equivalence ratio. Dahm et al. (1984).

Recognizing that the strained flames form between the newly entrained reservoir fluid and the continuously reacted jet fluid, we may sketch the process as shown in Figure 6. The equality of

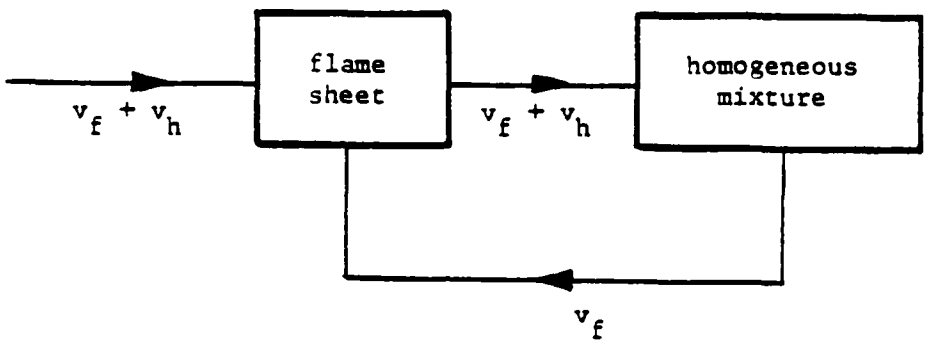

Figure 6. Schematic diagram for reactions in the jet model.

the net volume flux to the flame sheets, v_f, from the homogeneous mixture and the free stream comes from the assumption of constant molecular transport properties, an assumption leading to sheets constituted of equal amounts of fluid from the two streams. Notice that the net flux to the homogeneous mixture, v_h, is unchanged; the presence of the flame sheets only changes the constituents in the entering stream. The fluid in the flame sheets at any axial station becomes part of the homogeneous fluid further downstream.

The net volume addition to the flame sheets, v_f, can be written

$$v_f = 2\pi \frac{d}{dx} R^2 \int \frac{\beta(\eta)}{R} \cdot \frac{b R}{Re^{1/2}} u \eta d\eta \qquad (13)$$

in which $\beta(\eta)/R$ is the flame sheet area per unit volume and the sheet thickness is taken to be that of a strained flame in equilibrium with the large scale strain u/R, i.e.

$$\lambda_r = b\,(D/\varepsilon)^{1/2} = b\,(DR/u)^{1/2} = b\,R/(Re)^{1/2}$$

where b is a constant of order one (See Carrier, Fendell, and Marble, 1975.) With Equations (3), Equation (13) becomes

$$v_f = 2\pi\, C_1\, u_o\, d_o\, F/Re^{1/2} \qquad (14)$$

where

$$F = b \int \beta(n)\, g(n)\, n\, d\, n\,.$$

As before

$$v_h = 2\pi\, C_1\, u_o\, d_o\, E \qquad (3)$$

and

$$E = \int \alpha(n)\, g(n)\, n\, d\, n$$

With the help of Equations (3) and (14), fuel and oxidizer conservation equations similar to Equations (9) and (10) can be written for both the flame sheets and the homogeneous mixture. Now, however, the flame sheet chemical reactions must be treated numerically even for the simple reaction considered in the preceding section. The proposed scheme for solution, currently being carried out for a simple reaction, is to consider at each integration step, the flame sheet properties to be those of a strained flame in equilibrium with the local strain, u/R, and to use either numerical solutions, such as those of Dixon-Lewis et al (1984), or approximations to them. One side of the flame is pure reservoir fluid and the other the fluid of changing composition from the homogeneous mixture.

In the absence of such solutions, however, several useful conclusions can be drawn from the nature of the model. First, since the flame ends when all the fuel is consumed in both regions, and since the addition rate to the homogeneous mixture is unaffected by the flame sheets, the flame length is independent of Reynolds number in this case also. The same argument shows the independence from Schmidt number.

Experimental information on this point is discussed later.

Julian Tishkoff called this paradox to our attention, i.e., the apparent contradiction between the influence of Reynolds and Schmidt numbers on molecular mixing and the dependence of flame length from these parameters. The arguments just given appear to resolve the paradox: the upstream molecular mixing in the strained flames influences the mixing rate but does not reduce the distance required for every element of jet fluid to be mixed with ϕ parts of reservoir fluid.

Next, the model provides a basis for understanding the dependence of the nitric oxide production rate on Reynolds number. The experiments of Bilger and Beck (1974) on hydrogen-air flames and of Peters and Donnerhack (1981) on methane-air showed that when the effect of residence time was removed, there remained an effect of Reynolds number; the amount produced appeared to decline approximately with $Re^{1/2}$. Since NO is produced by a slow chemical reaction when the temperature is high, in the model it appears in the flame sheets only at small x/d_o, where, in the absence of radiation, the adiabatic flame temperature is reached. The forward NO reactions stop and NO may be destroyed when the flame sheet material returns to the homogeneous mixture. Near the end of the flame NO is produced in both regions. As Equation (14) illustrates explicitly, the flame sheet NO production also depends on $1/Re^{1/2}$ and the model, therefore, has a mechanism for explaining the experimental results.

To examine these ideas in more detail, an approximate calculation was carried out for both fuels with a full set of kinetic equations. A representative list of the reactions and species can be found in Heap, et al (1976), and the actual updated set used in the calculations in Bowman and Corley (in press).

For the model computation, Tyson, Kau and Broadwell (1982), the strained flame "reactor" was considered to contain a homogeneous mixture like that generated at the Kolmogorov scale, but v_f from the homogeneous mixture was varied to maintain a stoichiometric mixture in the flames and thus to yield the adiabatic flame temperature reached in strained

flames. The constant fixing the flow rate, v_h, was inferred, as described above, from the flame length data of Waddell (seee Hottel, 1953) and the remaining constant chosen to match the model to the data at one point. Approximate account was taken of radiation in both flames.

The model-experiment comparison for the hydrogen flame is shown in Figure 7. Only the NO emission index was measured for the methane flame and while the agreement, with the same constants, in that case is equally good, the Reynolds number range for the high Froude number runs was limited. In fact, the Reynolds numbers of both experiments are so low that the good quantitative agreement between the model predictions and the experiments is likely only fortuitous. The qualitative trend with $1/Re^{1/2}$, however, is clear in the model and, having been observed in different experiments in two gases, seems believable. There are plans to repeat the experiment and to make a more complete model calculation.

A more straight-forward check of the ability of the model to deal with molecular effects is a comparison of model predictions with experiment of the differences between gas and water reactions, Mungal and Dimotakis (1984). The satisfactory agreement in that case as well not only gives more confidence in the model but lends credence to the idea that nitric oxide production in flames is, indeed, Reynolds number dependent.

EFFECTS OF DENSITY CHANGE

In the discussion so far the density has been taken to be constant. However, Ricou and Spalding (1961) show that when the jet density, ρ_j, differs from that in the reservoir, ρ_∞, the ratio of the total jet flux to the initial value is

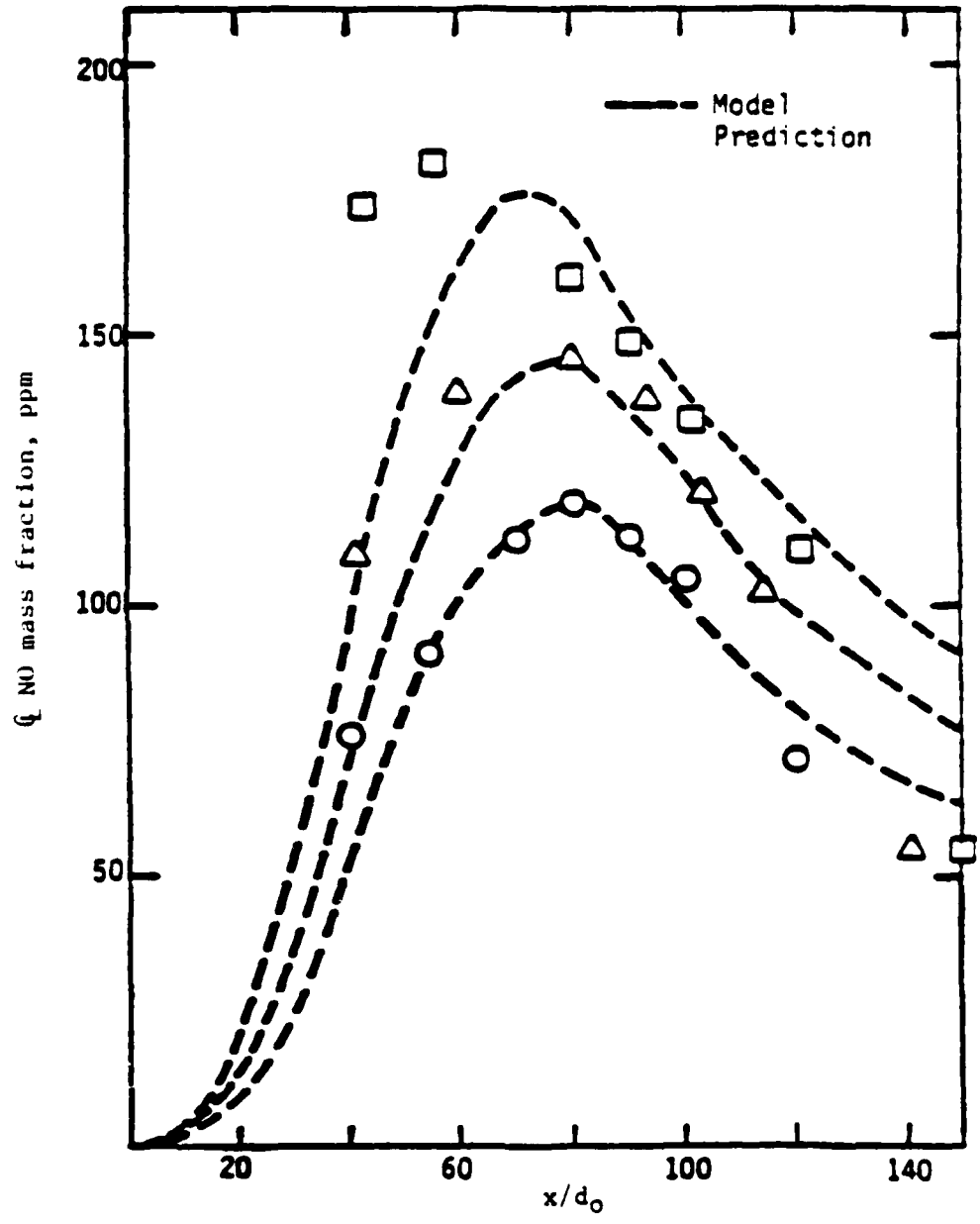

Figure 7. Comparison of calculated nitric oxide concentration with measurements for hydrogen-air flame. □, Re = 1,540; △, Re = 4,350; ○, Re = 12,300. (Froude number ~$6 \cdot 10^5$. Data from Bilger and Beck (1974). From Tyson, et al. (1982).

$$m/m_o = c(x/d_o)\,(\rho_\infty/\rho_j)^{1/2} \qquad (15)$$

Since this relation is consistent with the idea that the entrainment is controlled by the jet momentum, it may be expected to hold when the jet is reactive. Avery and Faeth (1974) develop a theory for such jets and with it are able to correlate the flame lengths of a remarkable variety of reactants by a relationship of the form of Equation (15) in which d_o is replaced by $d^* = d_o(\rho_\infty/\rho_j)^{1/2}$. Dahm & Dimotakis (1985) present their data together with that collected by Avery and Faeth in this form as shown in Figure 8.

The results in this figure are explained by the present model if the distance after entrainment for the jet and reservoir fluid to reach the Kolmogorov scale continues to depend, in this case also, only on the local jet radius. The arguments leading to Equation (11) appear to be valid in this more general situation.

DAMKÖHLER NUMBER EFFECTS

Experiments by Mungal and Frieler (1984) on the hydrogen-fluorine reaction is a shear layer cover the Damköhler number the range from zero to mixing limited conditions. In this flow and for their fixed high equivalence ratio, an integral treatment of the strained flame allows a complete analytical solution of the model equations. Figure 9 shows a comparison of the solution with the experimental results (Broadwell, Mungal, 1986). The constants A and B in the model equations had been determined from earlier experiments (Mungal and Dimotakis, 1984) on the fast reaction in this flow and from the experiments in water (Koochesfahani & Dimotakis, 1986). In the figure Da is defined as $k(C_H)_\infty\, x/\bar{u}$ where $k(C_H)_\infty$ is the reaction rate coefficient, x the distance of the measuring station from the splitter plate, and $\bar{u}$ the mean shear

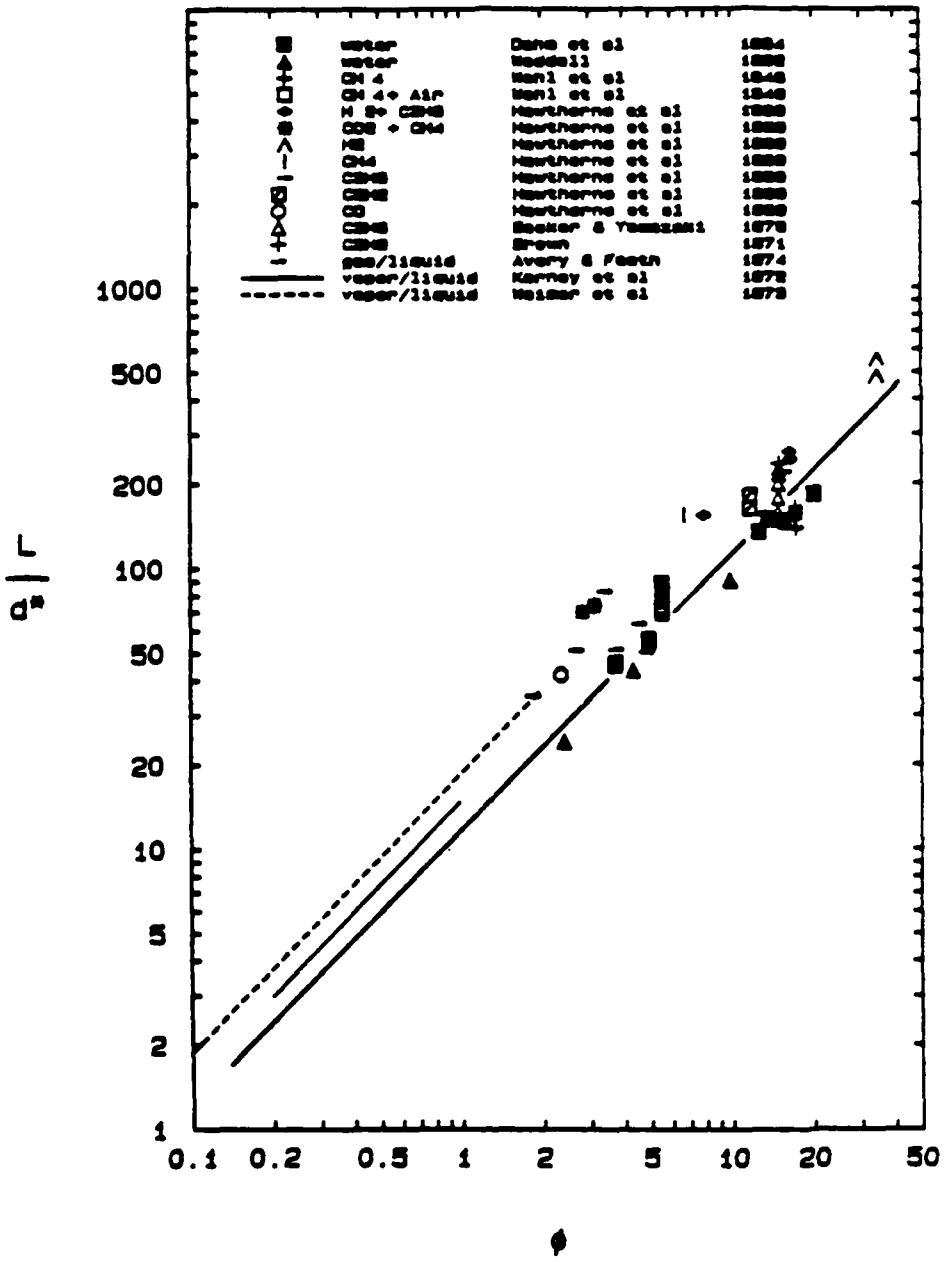

Figure 8. Mean flame length versus equivalence ratio for various reacting jets. Dahm (1985).

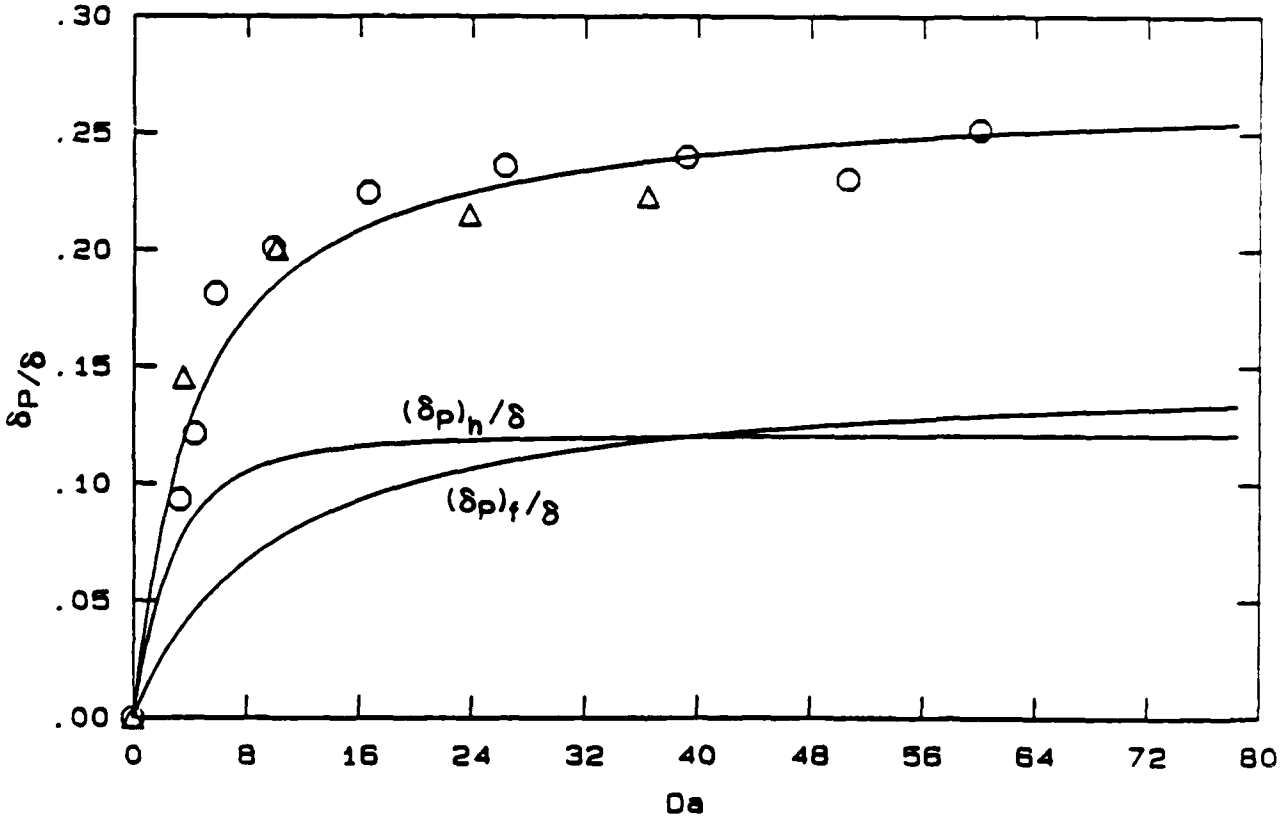

Figure 9. Dependence in shear layer of product on Damköhler number, $Da = k(C_H)_\infty x/\bar{u}$. δ_p, total product thickness; $(\delta_p)_f$, flame sheet product; $(\delta_p)_h$, homogeneous mixture product; δ, shear layer thickness. The symbols are experimental data from Mungal and Frieler (1985) for two different velocities at the same velocity ratio.

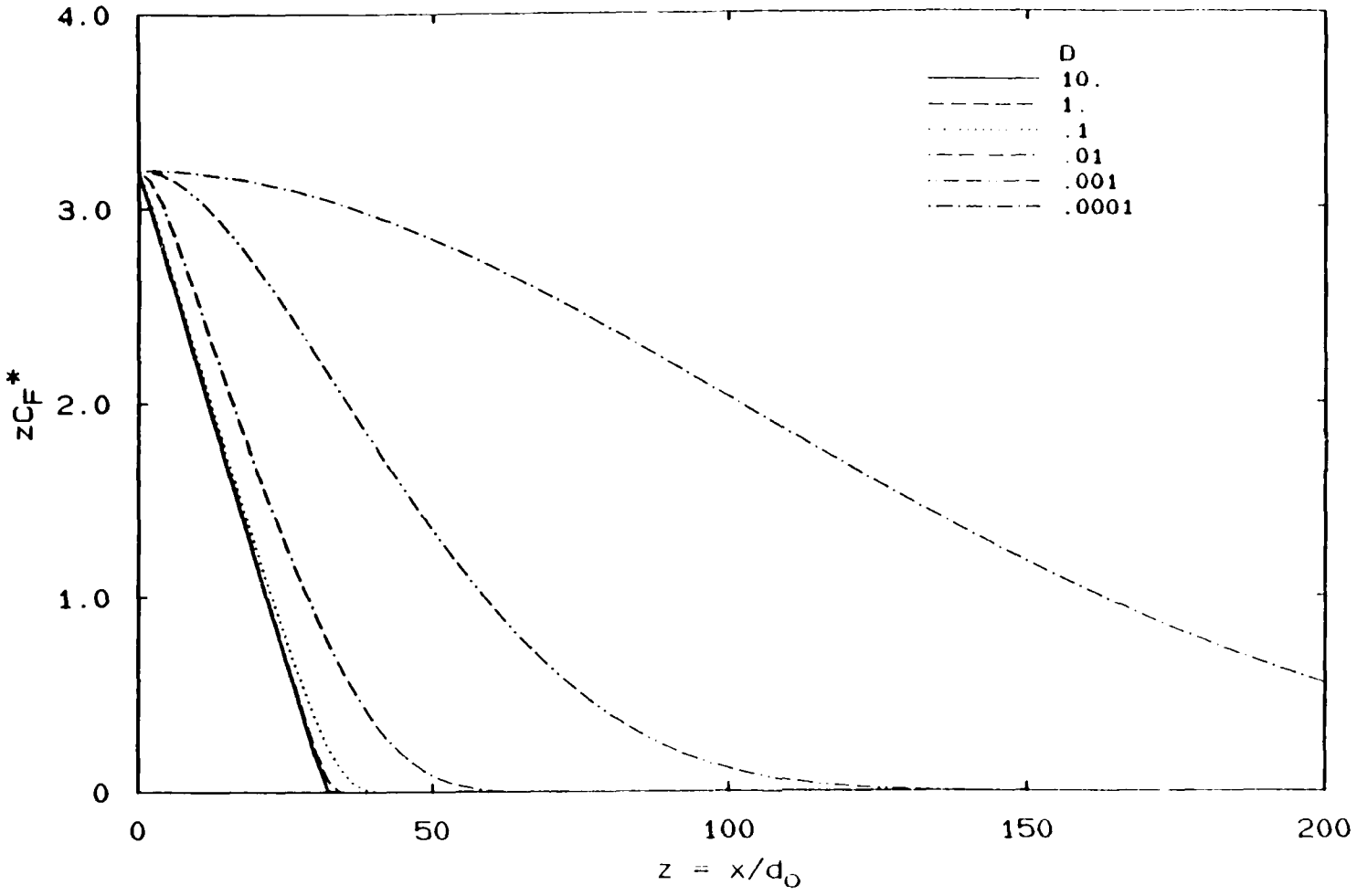

Figure 10. Dependence of fuel concentration on axial distance for various Damköhler numbers. Equivalence Ratio, ϕ, = 10.

layer velocity. The ordinate δ_p/δ is a non-dimensional measure of the amount of product at this station. The separate contributions of the flame sheets $(\delta_p)_f$ and the homogeneous zones $(\delta_p)_h$ are shown, with the latter seen to reach its limiting value more quickly.

In the jet, the varying jet fluid composition appears to preclude a similar integral treatment of the flame sheets. Hence, only the high Reynolds number situation, described by Equations (9) and (10), has been considered. C. F. Frieler (private communication) notes that an analytical solution of these equations is possible but that it is of such complexity that numerical results, which he has also kindly provided, are more useful. These are shown in Figure 10, in which we see that the limiting concentration distribution is attained for Da > 1 compared to Da > 10 in the shear layer. The decline in jet velocity with distance must be responsible for this difference as well as for the non-linear influence of Da on the jet solution. The flame length for Da → ∞, i.e. > 1, is 32 in agreement with Equation (11).

CONCLUDING REMARKS

As has been pointed out in the foregoing, an implication of this analysis is that extremely high values of the parameter Sc Re are required to eliminate explicit molecular effects on molecular mixing. For a Schmidt number of unity, it appears that Reynolds numbers of the order of 10^6 - 10^7 are necessary. This would mean that most laboratory combustion experiments are significantly influenced by "low Reynolds number" effects and that analyses neglecting them are likely to be inadequate. These observations may also have some bearing on the discussion of fluid mechanics at high Reynolds number as noted in the Introduction.

With regard to flame sheets, the present analysis emphasizes the notion that the fuel side consists of fuel mixed with a linearly rising amount of products, from x/d_o - 10, and that the flame sheet concept is appropriate for any Damköhler number provided the Peclet number is sufficiently high. The proposed model is simple enough that output from fairly elaborate strained flame calculations should be able to be incorporated fairly easily. Since there is no limitation on the Damköhler number, the same sort of calculations may help clarify the mechanisms controlling lift-off and blow-off.

ACKNOWLEDGEMENTS

This paper is extracted from a summary report on mixing and reactions in shear layers and jets that is in preparation in collaboration with Godfrey M. Mungal. His assistance as well as that of the author's GALCIT colleagues is gratefully acknowledged. The ideas of Roddam Narasimha and Anatol Roshko concerning the volume fraction in which dissipation occurs helped greatly to clarify the relationship between dissipation and scalar mixing. The author also thanks Werner Dahm and Manooch Koochesfahani for permission to use figures from their theses and for many instructive discussions of their work.

We wish to acknowledge support for this work by the Air Force Office of Scientific Research under Contract No. F49602-79-C-0159 and Grant No. AFOSR-83-0213, the Office of Naval Research under Contract No. 00014-85-k-0646, and the Gas Research Institute under Grant No. 5083-260-0878.

REFERENCES

ANTONIA, R. A., CHAMBERS, A. J., BRITZ, D. and BROWNE, L. W. B. [1986] "Organized structures in a turbulent plane jet: topology and contribution to momentum and heat transport", J. Fluid Mech. 172, 211-229.

AVERY, J. F. and FAETH, G. M. [1974] "Combustion of a Submerged Gaseous Oxidizer Jet in a Liquid Metal", 15th Annual Combustion Institute, 501-512.

BATCHELOR, G. K. [1959] "Small-scale variation of convected quantities like temperature in turbulent fluid. Part 1. General discussion and the case of small conductivity", J. Fluid Mech. 5, 113-133

BILGER, R. W. and BECK, R. E. [1974] "Further experiments on turbulent jet diffusion flames", Fifteenth Symposium (International) on Combustion (The Combustion Institute), 541.

BOWMAN, C. T. and CORLEY, T. C. [in press] "Chapter II", EPA Project Decade Monograph, Ed. A. F. Sarofim, T. Lester, G. B. Martin, W. S. Lanier.

BREIDENTHAL, R. E. [1981] "Structure in turbulent mixing layers and wakes using a chemical reaction", J. Fluid Mech. 109, 1.

BROADWELL, J. E. [1982] "A Model of Turbulent Diffusion Flames and Nitric Oxide Generation. Part I", TRW Document No. 38515-6001-UT-00, EERC Final Report, PO No. 18889.

BROADWELL, J. E. and BREIDENTHAL, R. E. [1982] "A Simple Model of Mixing and Chemical Reaction in a Turbulent Shear Layer", J. Fluid Mech. 125, 397-410.

BROADWELL, J. E. and MUNGAL, M. G. [1986] "The Effects of Damköhler number in a turbulent shear layer", GALCIT Report FM86-01.

BROADWELL, J. E. AND MUNGAL, G. M. [1987] "Molecular Mixing and Chemical Reactions in Turbulent Shear Layers and Jets", GALCIT Report in preparation.

BROWN, G. L. and ROSHKO, A. [1974] "On Density Effects and Large Structure in Turbulent Mixing Layers", J. Fluid Mech. 64(4), 775-816.

CARRIER, G. F., FENDELL, F. E. and MARBLE, F. E. [1975] "The Effect of Strain on Diffusion Flames", SIAM J. Appl. Math. 28(2), 463-500.

COLES, D. [1983] "On one mechanism of turbulence production in coherent structures", Turbulence and Chaotic Phenomenon in Fluids. Ed. T. Tatsumi, IUTAM Elsevier Science Pub. B. V., 397-402.

CORCOS, G. M. and SHERMAN, F. S. [1976] "Vorticity Concentration and the Dynamics of Unstable Free Shear Layers", J. Fluid Mech. 73(2), 241-264.

DAHM, W. J. A. [1985] Experiments on Entrainment, Mixing and Chemical Reactions in Turbulent Jets at Large Schmidt Numbers, California Institute of Technology, Ph. D. thesis.

DAHM, W. J. A. and DIMOTAKIS, P. E. [1985] "Measurements of Entrainment and Mixing in Turbulent Jets", AIAA 23rd Aerospace Sciences Meeting 14-17 January 1985 (Reno, Nevada), AIAA Paper No. 85-0056.

DAHM, W. J. A., DIMOTAKIS, P. E. and BROADWELL, J. E. [1984] "Non-premixed turbulent jet flames", AIAA 22nd Aerospace Sciences Meeting (Reno, Nevada), AIAA Paper No. 84-0369.

DIBBLE, R. and MAGRE, P [1987] "Finite chemical Kinetics Effects in a Subsonic Turbulent Hydrogen Flame", Presented at AIAA 25th Aerospace Sciences Meeting (Reno, Nevada) 12-15 January 1987, SAND87-8601.

DIMOTAKIS, P. E., MIAKE-LYE, R. C., and PAPANTONIOU, D. A. [1983] "Structure and Dynamics of Round Turbulent Jets", Fluid Dynamics Transactions, 11, 47-76.

DIXON-LEWIS, G., DAVID, T., GASKELL, P. H., FUKUTANI, F., JINNO, H., MILLER, J. A., KEE, B. J., SMOOKE, M. D., PETERS, N., EFFELSBERG, E., WARNATZ, J. AND BEHRENDT, F. [1984] "Calculation of the structure and extinction limit of a mathane-air counterflow diffusion flame in the forward stagnation region of a porous cylinder", from: Twentieth Symposium (International) on Combustion/The Combustion Institute, 1893-1904.

HEAP, M. P., TYSON, T. J., CICHANOWICZ, J. E., GERSHMAN, R., and KAU, C. J. [1976] "Environmental Aspects of Low Btu Gas Combustion", 16th Symposium (International) on Combustion, 535-545.

HOTTEL, H. C. [1953] "Burning in Laminar and Turbulent Fuel Jets", 4th (International) Symposium on Combustion (The Williams and Wilkins Co.), 97-113.

HUSSAIN, A. K. M. F. [1983] "Coherent structures and incoherent turbulence", Turbulence and Chaotic Phenomenon in Fluids, Ed. T. Tatsumi, IUTAM, Elsevier Science Pub. B. V., 453-460.

KONRAD, J. H. [1976] An Experimental Investigation of Mixing in Two-Dimensional Turbulent Shear Flows with Applications to Diffusion-Limited Chemical Reactions, Ph.D. Thesis, California Institute of Technology, and Project SQUID Technical Report

CIT-8-PU (December 1976).

KOOCHESFAHANI, M. M. and DIMOTAKIS, P. E. [1986] "Mixing and chemical reactions in a turbulent liquid mixing layer", J. Fluid Mech. 170, 83-112.

LONG, M. B. [1987] "Measurement of the topology of large scale structure in reacting flow", These proceedings.

MARBLE, F. E. and BROADWELL, J. E. [1977] "The Coherent Flame Model for Turbulent Chemical Reactions", Project SQUID Technical Report TRW-9-PU.

MUNGAL, M. G. and DIMOTAKIS, P. E. [1984] "Mixing and combustion with low heat release in a turbulent mixing layer", J. Fluid Mech. 148, 349-382.

MUNGAL, M. G, HERMANSON, J. C. and DIMOTAKIS, P. E. [1985] "Reynolds Number Effects on Mixing and Combustion in a Reacting Shear Layer", AIAA J. 23(9), 1418-1423.

MUNGAL, M. G. and FRIELER, C. E. [1985] "Chemical reactions in a turbulent mixing layer: The effects of the reaction rate coefficient - Part I", GALCIT report FM85-01 (31-Dec-85).

PETERS, N. and DONNERHACK, S. [1981] "Structure and Similarity of Nitric Oxide Production in Turbulent Diffusion Flames", Eighteenth Symposium (International) on Combustion (The Combustion Institute), 33-42.

RICOU, F. P. and SPALDING, D. B. [1961] "Measurements of Entrainment by Axisymmetrical Turbulent Jets", J. Fluid Mech. 11, 21-32.

TYSON, T. J., KAU, C. J., and BROADWELL, J. E. [1982] "A Model of Turbulent Diffusion Flames and Nitric Oxide Generation. Part II" Energy & Environmental Res. Corp. (June 1982) Report.

WYGNANSKI, I. and FIEDLER, H. E. [1970] "The Two Dimensional Mixing Region", J. Fluid Mech. 41(2), 327-361.

END

12-87

DTIC